Argonne NATIONAL LABORATORY

ANL-10/22

YALINA-Booster Subcritical Assembly Pulsed-Neutron Experiments: Data Processing and Spatial Corrections

Nuclear Engineering Division

About Argonne National Laboratory
Argonne is a U.S. Department of Energy laboratory managed by UChicago Argonne, LLC under contract DE-AC02-06CH11357. The Laboratory's main facility is outside Chicago, at 9700 South Cass Avenue, Argonne, Illinois 60439. For information about Argonne, see www.anl.gov.

Availability of This Report
This report is available, at no cost, at http://www.osti.gov/bridge. It is also available on paper to the U.S. Department of Energy and its contractors, for a processing fee, from:

U.S. Department of Energy
Office of Scientific and Technical Information
P.O. Box 62
Oak Ridge, TN 37831-0062
phone (865) 576-8401
fax (865) 576-5728
reports@adonis.osti.gov

Disclaimer
This report was prepared as an account of work sponsored by an agency of the United States Government. Neither the United States Government nor any agency thereof, nor UChicago Argonne, LLC, nor any of their employees or officers, makes any warranty, express or implied, or assumes any legal liability or responsibility for the accuracy, completeness, or usefulness of any information, apparatus, product, or process disclosed, or represents that its use would not infringe privately owned rights. Reference herein to any specific commercial product, process, or service by trade name, trademark, manufacturer, or otherwise, does not necessarily constitute or imply its endorsement, recommendation, or favoring by the United States Government or any agency thereof. The views and opinions of document authors expressed herein do not necessarily state or reflect those of the United States Government or any agency thereof, Argonne National Laboratory, or UChicago Argonne, LLC.

ANL-10/22

YALINA-Booster Subcritical Assembly Pulsed-Neutron Experiments: Data Processing and Spatial Corrections

by
Y. Cao and Y. Gohar
Nuclear Engineering Division, Argonne National Laboratory

August 2010

August 2010 ANL-10/22

YALINA-Booster Subcritical Assembly Pulsed-Neutron Experiments: Data Processing and Spatial Corrections

By

Yan Cao and Yousry Gohar

Nuclear Engineering Division
Argonne National Laboratory
9700 South Cass Avenue
Argonne, IL 60439

Work supported by the
Office of Global Nuclear Material Threat Reduction
U.S. Department of Energy
Under Contract to DE-AC02-06CH11357

YALINA-Booster Subcritical Assembly Pulsed-Neutron Experiments: Data Processing and Spatial Corrections

Table of Contents

Page

1. INTRODUCTION 2
2. PULSED-NEUTRON EXPERIMENTS 2
3. PROCESSING OF THE PULSED-NEUTRON EXPERIMENTAL DATA ... 3
   - A. REACTIVITY ρ 3
   - B. PROMPT DECAY CONSTANT α 5
   - C. PERFORMANCE OF THE SHORT AND THE LONG HE-3 DETECTORS 6
4. SPATIAL CORRECTIONS 7
   - A. BELL'S CORRECTION FACTOR - THEORY 7
   - B. BELL'S CORRECTION FACTOR – RESULTS 9
   - C. BELL'S CORRECTION FACTOR – ERRORS 10
5. SUMMARY 11

REFERENCES 12

APPENDIX 13

YALINA-Booster Subcritical Assembly Pulsed-Neutron Experiments: Data Processing and Spatial Corrections

List of Figures

Page

FIGURE 1. FUEL LOADING OF YALINA-BOOSTER CONFIGURATION WITH 1141 EK-10 FUEL RODS 7

FIGURE 2. FUEL LOADING OF YALINA-BOOSTER CONFIGURATION WITH 1185 EK-10 FUEL RODS 8

FIGURE 3. X-Y CROSS-SECTIONAL VIEW OF THE YALINA-BOOSTER ASSEMBLY, DIMENSIONS IN MM 9

FIGURE 4. OBTAINED REACTIVITIES FOR YANLINA CONFIGURATION WITH 36% ENRICHED URANIUM IN THE FAST ZONE AND 1185 EK-10 FUEL RODS IN THE THERMAL ZONE AS FUNCTION OF THE FITTING INTERVALS FOR THE DELAYED NEUTRON BACKGROUND OF EC1B, EC2B, AND EC3B CHANNELS 10

FIGURE 5. OBTAINED REACTIVITIES FOR YALINA CONFIGURATION WITH 36% ENRICHED URANIUM IN THE FAST ZONE AND 1185 EK-10 FUEL RODS IN THE THERMAL ZONE AS A FUNCTION OF THE FITTING INTERVALS FOR THE DELAYED NEUTRON BACKGROUND FOR EC5T CHANNEL 10

FIGURE 6. OBTAINED REACTIVITIES FOR YALINA CONFIGURATION WITH 36% ENRICHED URANIUM IN THE FAST ZONE AND 1185 EK-10 FUEL RODS IN THE THERMAL ZONE AS A FUNCTION OF THE FITTING INTERVALS FOR THE DELAYED NEUTRON BACKGROUND FOR EC6T CHANNEL 11

FIGURE 7. OBTAINED REACTIVITIES FOR YALINA CONFIGURATION WITH 36% ENRICHED URANIUM IN THE FAST ZONE AND 1185 EK-10 FUEL RODS IN THE THERMAL ZONE AS A FUNCTION OF THE FITTING INTERVALS FOR THE DELAYED NEUTRON BACKGROUND FOR EC7T CHANNEL 11

FIGURE 8. OBTAINED REACTIVITIES FOR YALINA CONFIGURATION WITH 36% ENRICHED URANIUM IN THE FAST ZONE AND 1185 EK-10 FUEL RODS IN THE THERMAL ZONE AS A FUNCTION OF THE FITTING INTERVALS FOR THE DELAYED NEUTRON BACKGROUND FOR MC5 CHANNEL 12

FIGURE 9. OBTAINED REACTIVITIES FOR YALINA CONFIGURATION WITH 36% ENRICHED URANIUM IN THE FAST ZONE AND 1185 EK-10 FUEL RODS IN THE THERMAL ZONE AS A FUNCTION OF THE FITTING INTERVALS FOR THE DELAYED NEUTRON BACKGROUND FOR EC8R CHANNEL 12

FIGURE 10. OBTAINED REACTIVITIES FOR YALINA CONFIGURATION WITH 36% ENRICHED URANIUM IN THE FAST ZONE AND 1185 EK-10 FUEL RODS IN THE THERMAL ZONE AS A FUNCTION OF THE FITTING INTERVALS FOR THE DELAYED NEUTRON BACKGROUND FOR EC9R CHANNEL 13

FIGURE 11. UNCORRECTED AND SPATIALLY CORRECTED REACTIVITIES FROM THE PULSED-NEUTRON EXPERIMENTS FOR YALINA CONFIGURATION WITH 90% ENRICHED FUEL IN THE FAST ZONE AND 1141 EK-10 FUEL RODS IN THE THERMAL ZONE..... 13

FIGURE 12. UNCORRECTED AND SPATIALLY CORRECTED REACTIVITIES FROM THE PULSED-NEUTRON EXPERIMENTS FOR YALINA CONFIGURATION WITH 36% ENRICHED FUEL IN THE FAST ZONE AND 1185 EK-10 FUEL RODS IN THE THERMAL ZONE..... 14

FIGURE 13. UNCORRECTED AND SPATIALLY CORRECTED REACTIVITIES FROM THE PULSED-NEUTRON EXPERIMENTS FOR YALINA CONFIGURATION WITH 21% ENRICHED FUEL IN THE FAST ZONE AND 1185 EK-10 FUEL RODS IN THE THERMAL ZONE WITH CR OUT IN DEC-03-2009..... 14

FIGURE 14. PROMPT NEUTRON DECAY CONSTANT α AS A FUNCTION OF THE FITTING INTERVALS FOR EC1B, EC2B, AND EC3B CHANNELS FOR YALINA CONFIGURATION WITH 36% ENRICHED FUEL IN THE FAST ZONE AND 1185 EK-10 FUEL RODS IN THE THERMAL ZONE..... 15

FIGURE 15. PROMPT NEUTRON DECAY CONSTANT α AS A FUNCTION OF THE FITTING INTERVALS FOR EC5T CHANNEL FOR YALINA CONFIGURATION WITH 36% ENRICHED FUEL IN THE FAST ZONE AND 1185 EK-10 FUEL RODS IN THE THERMAL ZONE..... 15

FIGURE 16. PROMPT NEUTRON DECAY CONSTANT α AS A FUNCTION OF THE FITTING INTERVALS FOR EC6T CHANNEL FOR YALINA CONFIGURATION WITH 36% ENRICHED FUEL IN THE FAST ZONE AND 1185 EK-10 FUEL RODS IN THE THERMAL ZONE..... 16

FIGURE 17. PROMPT NEUTRON DECAY CONSTANT α AS A FUNCTION OF THE FITTING INTERVALS FOR EC7T CHANNEL FOR YALINA CONFIGURATION WITH 36% ENRICHED FUEL IN THE FAST ZONE AND 1185 EK-10 FUEL RODS IN THE THERMAL ZONE..... 16

FIGURE 18. PROMPT NEUTRON DECAY CONSTANT α AS A FUNCTION OF THE FITTING INTERVALS FOR MC5 CHANNEL FOR YALINA CONFIGURATION WITH 36% ENRICHED FUEL IN THE FAST ZONE AND 1185 EK-10 FUEL RODS IN THE THERMAL ZONE..... 17

FIGURE 19. PROMPT NEUTRON DECAY CONSTANT α AS A FUNCTION OF THE FITTING INTERVALS FOR EC8R CHANNEL FOR YALINA CONFIGURATION WITH 36% ENRICHED FUEL IN THE FAST ZONE AND 1185 EK-10 FUEL RODS IN THE THERMAL ZONE..... 17

FIGURE 20. PROMPT NEUTRON DECAY CONSTANT α AS A FUNCTION OF THE FITTING INTERVALS FOR EC9R CHANNEL FOR YALINA CONFIGURATION WITH 36% ENRICHED FUEL IN THE FAST ZONE AND 1185 EK-10 FUEL RODS IN THE THERMAL ZONE..... 18

FIGURE 21. PROMPT DECAY CONSTANT α OBTAINED FROM THE PULSED-NEUTRON EXPERIMENT OF YALINA CONFIGURATION WITH 90% ENRICHED URANIUM FUEL IN THE FAST ZONE AND 1141 EK-10 FUEL RODS IN THE THERMAL ZONE..... 18

FIGURE 22. PROMPT DECAY CONSTANT α OBTAINED FROM THE PULSED-NEUTRON EXPERIMENT OF YALINA CONFIGURATION WITH 36% ENRICHED URANIUM FUEL IN THE FAST ZONE AND 1185 EK-10 FUEL RODS IN THE THERMAL ZONE 19

FIGURE 23. PROMPT DECAY CONSTANT α OBTAINED FROM THE PULSED-NEUTRON EXPERIMENT OF YALINA CONFIGURATION WITH 21% ENRICHED URANIUM FUEL IN THE FAST ZONE AND 1185 EK-10 FUEL RODS IN THE THERMAL ZONE WITH CR OUT 19

FIGURE 24. LINEAR FIT OF THE PULSED NEUTRON EXPERIMENT RECORDED BY LONG HE-3 DETECTOR IN EC1B CHANNEL OF YALINA CONFIGURATION WITH 90% ENRICHED FUEL IN THE FAST ZONE AND 1141 EK-10 FUEL RODS IN THE THERMAL ZONE IN BATCH 0.1 20

FIGURE 25. LINEAR FIT OF THE PULSED NEUTRON EXPERIMENT RECORDED BY LONG HE-3 DETECTOR IN EC2B CHANNEL OF YALINA CONFIGURATION WITH 90% ENRICHED FUEL IN THE FAST ZONE AND 1141 EK-10 FUEL RODS IN THE THERMAL ZONE IN BATCH 0.1 20

FIGURE 26. LINEAR FIT OF THE PULSED NEUTRON EXPERIMENT RECORDED BY LONG HE-3 DETECTOR IN EC3B CHANNEL OF YALINA CONFIGURATION WITH 90% ENRICHED FUEL IN THE FAST ZONE AND 1141 EK-10 FUEL RODS IN THE THERMAL ZONE IN BATCH 0.1 21

FIGURE 27. LINEAR FIT OF THE PULSED NEUTRON EXPERIMENT RECORDED BY LONG HE-3 DETECTOR IN EC2B CHANNEL OF YALINA CONFIGURATION WITH 90% ENRICHED FUEL IN THE FAST ZONE AND 1141 EK-10 FUEL RODS IN THE THERMAL ZONE IN BATCH 0.1 21

FIGURE 28. LINEAR FIT OF THE PULSED NEUTRON EXPERIMENT RECORDED BY SMALL HE-3 DETECTOR IN EC1B CHANNEL OF YALINA CONFIGURATION WITH 90% ENRICHED FUEL IN THE FAST ZONE AND 1141 EK-10 FUEL RODS IN THE THERMAL ZONE IN BATCH 0.2 22

FIGURE 29. LINEAR FIT OF THE PULSED NEUTRON EXPERIMENT RECORDED BY SMALL HE-3 DETECTOR IN EC2B CHANNEL OF YALINA CONFIGURATION WITH 90% ENRICHED FUEL IN THE FAST ZONE AND 1141 EK-10 FUEL RODS IN THE THERMAL ZONE IN BATCH 0.2 22

FIGURE 30. LINEAR FIT OF THE PULSED NEUTRON EXPERIMENT RECORDED BY SMALL HE-3 DETECTOR IN EC3B CHANNEL OF YALINA CONFIGURATION WITH 90% ENRICHED FUEL IN THE FAST ZONE AND 1141 EK-10 FUEL RODS IN THE THERMAL ZONE IN BATCH 0.2 23

FIGURE 31. LINEAR FIT OF THE PULSED NEUTRON EXPERIMENT RECORDED BY LONG HE-3 DETECTOR IN EC6T CHANNEL OF YALINA CONFIGURATION WITH 90% ENRICHED FUEL IN THE FAST ZONE AND 1141 EK-10 FUEL RODS IN THE THERMAL ZONE IN BATCH 0.3 23

FIGURE 32. LINEAR FIT OF THE PULSED NEUTRON EXPERIMENT RECORDED BY SMALL HE-3 DETECTOR IN EC6T CHANNEL OF YALINA CONFIGURATION WITH 90% ENRICHED FUEL IN THE FAST ZONE AND 1141 EK-10 FUEL RODS IN THE THERMAL ZONE IN BATCH 0.4 24

FIGURE 33. LINEAR FIT OF THE PULSED NEUTRON EXPERIMENT RECORDED BY LONG HE-3 DETECTOR IN EC8R CHANNEL OF YALINA CONFIGURATION WITH 90% ENRICHED FUEL IN THE FAST ZONE AND 1141 EK-10 FUEL RODS IN THE THERMAL ZONE IN BATCH 0.3 24

FIGURE 34. LINEAR FIT OF THE PULSED NEUTRON EXPERIMENT RECORDED BY SMALL HE-3 DETECTOR IN EC8R CHANNEL OF YALINA CONFIGURATION WITH 90% ENRICHED FUEL IN THE FAST ZONE AND 1141 EK-10 FUEL RODS IN THE THERMAL ZONE IN BATCH 0.4 25

FIGURE 35. LINEAR FIT OF THE PULSED NEUTRON EXPERIMENT RECORDED BY SMALL HE-3 DETECTOR IN EC5T CHANNEL OF YALINA CONFIGURATION WITH 36% ENRICHED FUEL IN THE FAST ZONE AND 1185 EK-10 FUEL RODS IN THE THERMAL ZONE IN BATCH 0.1 25

FIGURE 36. LINEAR FIT OF THE PULSED NEUTRON EXPERIMENT RECORDED BY LONG HE-3 DETECTOR IN MC5 CHANNEL OF YALINA CONFIGURATION WITH 36% ENRICHED FUEL IN THE FAST ZONE AND 1185 EK-10 FUEL RODS IN THE THERMAL ZONE IN BATCH 0.1 26

FIGURE 37. LINEAR FIT OF THE PULSED NEUTRON EXPERIMENT RECORDED BY SMALL HE-3 DETECTOR IN EC6T CHANNEL OF YALINA CONFIGURATION WITH 36% ENRICHED FUEL IN THE FAST ZONE AND 1185 EK-10 FUEL RODS IN THE THERMAL ZONE IN BATCH 0.1 26

FIGURE 38. LINEAR FIT OF THE PULSED NEUTRON EXPERIMENT RECORDED BY LONG HE-3 DETECTOR IN MC5 CHANNEL OF YALINA CONFIGURATION WITH 36% ENRICHED FUEL IN THE FAST ZONE AND 1185 EK-10 FUEL RODS IN THE THERMAL ZONE IN BATCH 0.2 27

FIGURE 39. LINEAR FIT OF THE PULSED NEUTRON EXPERIMENT RECORDED BY SMALL HE-3 DETECTOR IN EC7T CHANNEL OF YALINA CONFIGURATION WITH 36% ENRICHED FUEL IN THE FAST ZONE AND 1185 EK-10 FUEL RODS IN THE THERMAL ZONE IN BATCH 0.2 27

FIGURE 40. LINEAR FIT OF THE PULSED NEUTRON EXPERIMENT RECORDED BY SMALL HE-3 DETECTOR IN EC8R CHANNEL OF YALINA CONFIGURATION WITH 36% ENRICHED FUEL IN THE FAST ZONE AND 1185 EK-10 FUEL RODS IN THE THERMAL ZONE IN BATCH 0.2 28

FIGURE 41. LINEAR FIT OF THE PULSED NEUTRON EXPERIMENT RECORDED BY LONG HE-3 DETECTOR IN MC5 CHANNEL OF YALINA CONFIGURATION WITH 36% ENRICHED FUEL IN THE FAST ZONE AND 1185 EK-10 FUEL RODS IN THE THERMAL ZONE IN BATCH 0.3 28

FIGURE 42. LINEAR FIT OF THE PULSED NEUTRON EXPERIMENT RECORDED BY SMALL HE-3 DETECTOR IN EC7T CHANNEL OF YALINA CONFIGURATION WITH 36% ENRICHED FUEL IN THE FAST ZONE AND 1185 EK-10 FUEL RODS IN THE THERMAL ZONE IN BATCH 0.3 29

FIGURE 43. LINEAR FIT OF THE PULSED NEUTRON EXPERIMENT RECORDED BY SMALL HE-3 DETECTOR IN EC8R CHANNEL OF YALINA CONFIGURATION WITH 36% ENRICHED FUEL IN THE FAST ZONE AND 1185 EK-10 FUEL RODS IN THE THERMAL ZONE IN BATCH 0.3 29

FIGURE 44. LINEAR FIT OF THE PULSED NEUTRON EXPERIMENT RECORDED BY LONG HE-3 DETECTOR IN MC5 CHANNEL OF YALINA CONFIGURATION WITH 36% ENRICHED FUEL IN THE FAST ZONE AND 1185 EK-10 FUEL RODS IN THE THERMAL ZONE IN BATCH 0.4 30

FIGURE 45. LINEAR FIT OF THE PULSED NEUTRON EXPERIMENT RECORDED BY SMALL HE-3 DETECTOR IN EC5T CHANNEL OF YALINA CONFIGURATION WITH 36% ENRICHED FUEL IN THE FAST ZONE AND 1185 EK-10 FUEL RODS IN THE THERMAL ZONE IN BATCH 0.4 30

FIGURE 46. LINEAR FIT OF THE PULSED NEUTRON EXPERIMENT RECORDED BY SMALL HE-3 DETECTOR IN EC6T CHANNEL OF YALINA CONFIGURATION WITH 36% ENRICHED FUEL IN THE FAST ZONE AND 1185 EK-10 FUEL RODS IN THE THERMAL ZONE IN BATCH 0.4 31

FIGURE 47. LINEAR FIT OF THE PULSED NEUTRON EXPERIMENT RECORDED BY LONG HE-3 DETECTOR IN MC5 CHANNEL OF YALINA CONFIGURATION WITH 36% ENRICHED FUEL IN THE FAST ZONE AND 1185 EK-10 FUEL RODS IN THE THERMAL ZONE IN BATCH 0.5 31

FIGURE 48. LINEAR FIT OF THE PULSED NEUTRON EXPERIMENT RECORDED BY LONG HE-3 DETECTOR IN EC5T CHANNEL OF YALINA CONFIGURATION WITH 36% ENRICHED FUEL IN THE FAST ZONE AND 1185 EK-10 FUEL RODS IN THE THERMAL ZONE IN BATCH 0.5 32

FIGURE 49. LINEAR FIT OF THE PULSED NEUTRON EXPERIMENT RECORDED BY SMALL HE-3 DETECTOR IN EC6T CHANNEL OF YALINA CONFIGURATION WITH 36% ENRICHED FUEL IN THE FAST ZONE AND 1185 EK-10 FUEL RODS IN THE THERMAL ZONE IN BATCH 0.5 32

FIGURE 50. LINEAR FIT OF THE PULSED NEUTRON EXPERIMENT RECORDED BY LONG HE-3 DETECTOR IN MC5 CHANNEL OF YALINA CONFIGURATION WITH 36% ENRICHED FUEL IN THE FAST ZONE AND 1185 EK-10 FUEL RODS IN THE THERMAL ZONE IN BATCH 0.6 33

FIGURE 51. LINEAR FIT OF THE PULSED NEUTRON EXPERIMENT RECORDED BY LONG HE-3 DETECTOR IN EC6T CHANNEL OF YALINA CONFIGURATION WITH 36% ENRICHED FUEL IN THE FAST ZONE AND 1185 EK-10 FUEL RODS IN THE THERMAL ZONE IN BATCH 0.6 33

FIGURE 52. LINEAR FIT OF THE PULSED NEUTRON EXPERIMENT RECORDED BY SMALL HE-3 DETECTOR IN EC7T CHANNEL OF YALINA CONFIGURATION WITH 36% ENRICHED FUEL IN THE FAST ZONE AND 1185 EK-10 FUEL RODS IN THE THERMAL ZONE IN BATCH 0.6 34

FIGURE 53. LINEAR FIT OF THE PULSED NEUTRON EXPERIMENT RECORDED BY SMALL HE-3 DETECTOR IN EC5T CHANNEL OF YALINA CONFIGURATION WITH 36% ENRICHED FUEL IN THE FAST ZONE AND 1185 EK-10 FUEL RODS IN THE THERMAL ZONE IN BATCH 0.7 34

FIGURE 54. LINEAR FIT OF THE PULSED NEUTRON EXPERIMENT RECORDED BY LONG HE-3 DETECTOR IN EC7T CHANNEL OF YALINA CONFIGURATION WITH 36% ENRICHED FUEL IN THE FAST ZONE AND 1185 EK-10 FUEL RODS IN THE THERMAL ZONE IN BATCH 0.7 35

FIGURE 55. LINEAR FIT OF THE PULSED NEUTRON EXPERIMENT RECORDED BY LONG HE-3 DETECTOR IN MC5 CHANNEL OF YALINA CONFIGURATION WITH 36% ENRICHED FUEL IN THE FAST ZONE AND 1185 EK-10 FUEL RODS IN THE THERMAL ZONE IN BATCH 0.7 35

FIGURE 56. LINEAR FIT OF THE PULSED NEUTRON EXPERIMENT RECORDED BY LONG HE-3 DETECTOR IN MC5 CHANNEL OF YALINA CONFIGURATION WITH 36% ENRICHED FUEL IN THE FAST ZONE AND 1185 EK-10 FUEL RODS IN THE THERMAL ZONE IN BATCH 0.8 36

FIGURE 57. LINEAR FIT OF THE PULSED NEUTRON EXPERIMENT RECORDED BY LONG HE-3 DETECTOR IN EC8R CHANNEL OF YALINA CONFIGURATION WITH 36% ENRICHED FUEL IN THE FAST ZONE AND 1185 EK-10 FUEL RODS IN THE THERMAL ZONE IN BATCH 0.8 36

FIGURE 58. LINEAR FIT OF THE PULSED NEUTRON EXPERIMENT RECORDED BY SMALL HE-3 DETECTOR IN EC9R CHANNEL OF YALINA CONFIGURATION WITH 36% ENRICHED FUEL IN THE FAST ZONE AND 1185 EK-10 FUEL RODS IN THE THERMAL ZONE IN BATCH 0.8 37

FIGURE 59. LINEAR FIT OF THE PULSED NEUTRON EXPERIMENT RECORDED BY LONG HE-3 DETECTOR IN MC5 CHANNEL OF YALINA CONFIGURATION WITH 36% ENRICHED FUEL IN THE FAST ZONE AND 1185 EK-10 FUEL RODS IN THE THERMAL ZONE IN BATCH 0.9 37

FIGURE 60. LINEAR FIT OF THE PULSED NEUTRON EXPERIMENT RECORDED BY SMALL HE-3 DETECTOR IN EC8R CHANNEL OF YALINA CONFIGURATION WITH 36% ENRICHED FUEL IN THE FAST ZONE AND 1185 EK-10 FUEL RODS IN THE THERMAL ZONE IN BATCH 0.9 38

FIGURE 61. LINEAR FIT OF THE PULSED NEUTRON EXPERIMENT RECORDED BY LONG HE-3 DETECTOR IN EC9R CHANNEL OF YALINA CONFIGURATION WITH 36% ENRICHED FUEL IN THE FAST ZONE AND 1185 EK-10 FUEL RODS IN THE THERMAL ZONE IN BATCH 0.9 38

FIGURE 62. LINEAR FIT OF THE PULSED NEUTRON EXPERIMENT RECORDED BY LONG HE-3 DETECTOR IN MC5 CHANNEL OF YALINA CONFIGURATION WITH 36% ENRICHED FUEL IN THE FAST ZONE AND 1185 EK-10 FUEL RODS IN THE THERMAL ZONE IN BATCH 1.0 39

FIGURE 63. LINEAR FIT OF THE PULSED NEUTRON EXPERIMENT RECORDED BY SMALL HE-3 DETECTOR IN EC6T CHANNEL OF YALINA CONFIGURATION WITH 36% ENRICHED FUEL IN THE FAST ZONE AND 1185 EK-10 FUEL RODS IN THE THERMAL ZONE IN BATCH 1.0 39

FIGURE 64. LINEAR FIT OF THE PULSED NEUTRON EXPERIMENT RECORDED BY LONG HE-3 DETECTOR IN EC3B CHANNEL OF YALINA CONFIGURATION WITH 36% ENRICHED FUEL IN THE FAST ZONE AND 1185 EK-10 FUEL RODS IN THE THERMAL ZONE IN BATCH 1.0 40

FIGURE 65. LINEAR FIT OF THE PULSED NEUTRON EXPERIMENT RECORDED BY LONG HE-3 DETECTOR IN MC5 CHANNEL OF YALINA CONFIGURATION WITH 36% ENRICHED FUEL IN THE FAST ZONE AND 1185 EK-10 FUEL RODS IN THE THERMAL ZONE IN BATCH 1.1 40

FIGURE 66. LINEAR FIT OF THE PULSED NEUTRON EXPERIMENT RECORDED BY LONG HE-3 DETECTOR IN EC2B CHANNEL OF YALINA CONFIGURATION WITH 36% ENRICHED FUEL IN THE FAST ZONE AND 1185 EK-10 FUEL RODS IN THE THERMAL ZONE IN BATCH 1.1 41

FIGURE 67. LINEAR FIT OF THE PULSED NEUTRON EXPERIMENT RECORDED BY SMALL HE-3 DETECTOR IN EC5T CHANNEL OF YALINA CONFIGURATION WITH 36% ENRICHED FUEL IN THE FAST ZONE AND 1185 EK-10 FUEL RODS IN THE THERMAL ZONE IN BATCH 1.1 41

FIGURE 68. LINEAR FIT OF THE PULSED NEUTRON EXPERIMENT RECORDED BY LONG HE-3 DETECTOR IN MC5 CHANNEL OF YALINA CONFIGURATION WITH 36% ENRICHED FUEL IN THE FAST ZONE AND 1185 EK-10 FUEL RODS IN THE THERMAL ZONE IN BATCH 1.2 42

FIGURE 69. LINEAR FIT OF THE PULSED NEUTRON EXPERIMENT RECORDED BY LONG HE-3 DETECTOR IN EC1B CHANNEL OF YALINA CONFIGURATION WITH 36% ENRICHED FUEL IN THE FAST ZONE AND 1185 EK-10 FUEL RODS IN THE THERMAL ZONE IN BATCH 1.2 42

FIGURE 70. LINEAR FIT OF THE PULSED NEUTRON EXPERIMENT RECORDED BY SMALL HE-3 DETECTOR IN EC7T CHANNEL OF YALINA CONFIGURATION WITH 36% ENRICHED FUEL IN THE FAST ZONE AND 1185 EK-10 FUEL RODS IN THE THERMAL ZONE IN BATCH 1.2 43

FIGURE 71. LINEAR FIT OF THE PULSED NEUTRON EXPERIMENT RECORDED BY DAQ SYSTEM WITH LONG HE-3 DETECTOR IN EC1B CHANNEL OF YALINA CONFIGURATION WITH 21% ENRICHED FUEL IN THE FAST ZONE AND 1185 EK-10 FUEL RODS IN THE THERMAL ZONE IN BATCH 0.1 IN DEC-03-2009 43

FIGURE 72. LINEAR FIT OF THE PULSED NEUTRON EXPERIMENT RECORDED BY DAQ SYSTEM WITH LONG HE-3 DETECTOR IN EC5T CHANNEL OF YALINA CONFIGURATION WITH 21% ENRICHED FUEL IN THE FAST ZONE AND 1185 EK-10 FUEL RODS IN THE THERMAL ZONE IN BATCH 0.1 IN DEC-03-2009 44

FIGURE 73. LINEAR FIT OF THE PULSED NEUTRON EXPERIMENT RECORDED BY MCS WITH LONG HE-3 DETECTOR IN EC5T CHANNEL OF YALINA CONFIGURATION WITH 21% ENRICHED FUEL IN THE FAST ZONE AND 1185 EK-10 FUEL RODS IN THE THERMAL ZONE IN BATCH 0.1 IN DEC-03-2009 44

FIGURE 74. LINEAR FIT OF THE PULSED NEUTRON EXPERIMENT RECORDED BY DAQ SYSTEM WITH LONG HE-3 DETECTOR IN EC2B CHANNEL OF YALINA CONFIGURATION WITH 21% ENRICHED FUEL IN THE FAST ZONE AND 1185 EK-10 FUEL RODS IN THE THERMAL ZONE IN BATCH 0.2 IN DEC-03-2009 45

FIGURE 75. LINEAR FIT OF THE PULSED NEUTRON EXPERIMENT RECORDED BY DAQ SYSTEM WITH LONG HE-3 DETECTOR IN EC6T CHANNEL OF YALINA CONFIGURATION WITH 21% ENRICHED FUEL IN THE FAST ZONE AND 1185 EK-10 FUEL RODS IN THE THERMAL ZONE IN BATCH 0.2 IN DEC-03-2009 45

FIGURE 76. LINEAR FIT OF THE PULSED NEUTRON EXPERIMENT RECORDED BY MCS WITH LONG HE-3 DETECTOR IN EC6T CHANNEL OF YALINA CONFIGURATION WITH 21% ENRICHED FUEL IN THE FAST ZONE AND 1185 EK-10 FUEL RODS IN THE THERMAL ZONE IN BATCH 0.2 IN DEC-03-2009 46

FIGURE 77. LINEAR FIT OF THE PULSED NEUTRON EXPERIMENT RECORDED BY DAQ SYSTEM WITH LONG HE-3 DETECTOR IN EC3B CHANNEL OF YALINA CONFIGURATION WITH 21% ENRICHED FUEL IN THE FAST ZONE AND 1185 EK-10 FUEL RODS IN THE THERMAL ZONE IN BATCH 0.3 IN DEC-03-2009 46

FIGURE 78. LINEAR FIT OF THE PULSED NEUTRON EXPERIMENT RECORDED BY DAQ SYSTEM WITH LONG HE-3 DETECTOR IN EC7T CHANNEL OF YALINA CONFIGURATION WITH 21% ENRICHED FUEL IN THE FAST ZONE AND 1185 EK-10 FUEL RODS IN THE THERMAL ZONE IN BATCH 0.3 IN DEC-03-2009 47

FIGURE 79. LINEAR FIT OF THE PULSED NEUTRON EXPERIMENT RECORDED BY MCS WITH LONG HE-3 DETECTOR IN EC7T CHANNEL OF YALINA CONFIGURATION WITH 21% ENRICHED FUEL IN THE FAST ZONE AND 1185 EK-10 FUEL RODS IN THE THERMAL ZONE IN BATCH 0.3 IN DEC-03-2009 47

FIGURE 80. LINEAR FIT OF THE PULSED NEUTRON EXPERIMENT RECORDED BY DAQ SYSTEM WITH LONG HE-3 DETECTOR IN EC8R CHANNEL OF YALINA CONFIGURATION WITH 21% ENRICHED FUEL IN THE FAST ZONE AND 1185 EK-10 FUEL RODS IN THE THERMAL ZONE IN BATCH 0.4 IN DEC-03-2009 48

FIGURE 81. LINEAR FIT OF THE PULSED NEUTRON EXPERIMENT RECORDED BY DAQ SYSTEM WITH LONG HE-3 DETECTOR IN EC9R CHANNEL OF YALINA CONFIGURATION WITH 21% ENRICHED FUEL IN THE FAST ZONE AND 1185 EK-10 FUEL RODS IN THE THERMAL ZONE IN BATCH 0.4 IN DEC-03-2009 48

FIGURE 82. LINEAR FIT OF THE PULSED NEUTRON EXPERIMENT RECORDED BY DAQ SYSTEM WITH LONG HE-3 DETECTOR IN MC3 CHANNEL OF YALINA CONFIGURATION WITH 21% ENRICHED FUEL IN THE FAST ZONE AND 1185 EK-10 FUEL RODS IN THE THERMAL ZONE IN BATCH 0.5 IN DEC-03-2009 49

FIGURE 83. LINEAR FIT OF THE PULSED NEUTRON EXPERIMENT RECORDED BY DAQ SYSTEM WITH LONG HE-3 DETECTOR IN MC4 CHANNEL OF YALINA CONFIGURATION WITH 21% ENRICHED FUEL IN THE FAST ZONE AND 1185 EK-10 FUEL RODS IN THE THERMAL ZONE IN BATCH 0.5 IN DEC-03-2009 49

FIGURE 84. THE DETECTOR COUNT RATIO OF THE HE-3 LONG DETECTOR TO THE SMALL DETECTOR AT EC1B, EC2B, EC3B AND EC9R POSITIONS IN THE YALINA CONFIGURATION WITH 21% ENRICHED FUEL IN THE FAST ZONE AND 1185 EK-10 FUEL RODS IN THE THERMAL ZONE IN DEC-17-2009..... 50

FIGURE 85. THE DETECTOR COUNT RATIO OF THE HE-3 LONG DETECTOR TO THE SMALL DETECTOR AT EC9R IN THE YALINA CONFIGURATION WITH 36% ENRICHED FUEL IN THE FAST ZONE AND 1185 EK-10 IN THE THERMAL ZONE..... 50

FIGURE 86. THE DETECTOR COUNT RATIO OF THE HE-3 LONG DETECTOR TO THE SMALL DETECTOR AT EC6T AND EC8R IN THE YALINA CONFIGURATION WITH 90% ENRICHED FUEL IN THE FAST ZONE AND 1141 EK-10 FUEL RODS IN THE THERMAL ZONE..... 51

FIGURE 87. THE MONTE CARLO SIMULATED DETECTOR RESPONSES OF A U-235 LONG DETECTOR OR A HE-3 LONG DETECTOR AT EC1B IN THE YALINA 1141 CONFIGURATION 51

FIGURE 88. THE REACTIVITY OBTAINED FROM THE PULSED-NEUTRON EXPERIMENT FOR THE YALINA CONFIGURATION WITH 36% ENRICHED URANIUM FUELS IN THE FAST ZONE AND DIFFERENT EK-10 FUEL RODS IN THE THERMAL ZONE 52

FIGURE 89. THE PROMPT DECAY CONSTANTS OBTAINED FROM THE PULSED-NEUTRON EXPERIMENT FOR THE YALINA CONFIGURATION WITH 36% ENRICHED URANIUM FUELS IN THE FAST ZONE AND DIFFERENT EK-10 FUEL RODS IN THE THERMAL ZONE 52

FIGURE 90. LINEAR FIT OF THE PULSED NEUTRON EXPERIMENT RECORDED BY SMALL HE-3 DETECTOR IN EC5T CHANNEL OF YALINA CONFIGURATION WITH 36% ENRICHED FUEL IN THE FAST ZONE AND 802 EK-10 FUEL RODS IN THE THERMAL ZONE 53

FIGURE 91. LINEAR FIT OF THE PULSED NEUTRON EXPERIMENT RECORDED BY SMALL HE-3 DETECTOR IN EC6T CHANNEL OF YALINA CONFIGURATION WITH 36% ENRICHED FUEL IN THE FAST ZONE AND 802 EK-10 FUEL RODS IN THE THERMAL ZONE 53

FIGURE 92. LINEAR FIT OF THE PULSED NEUTRON EXPERIMENT RECORDED BY SMALL HE-3 DETECTOR IN EC5T CHANNEL OF YALINA CONFIGURATION WITH 36% ENRICHED FUEL IN THE FAST ZONE AND 854 EK-10 FUEL RODS IN THE THERMAL ZONE 54

FIGURE 93. LINEAR FIT OF THE PULSED NEUTRON EXPERIMENT RECORDED BY SMALL HE-3 DETECTOR IN EC6T CHANNEL OF YALINA CONFIGURATION WITH 36% ENRICHED FUEL IN THE FAST ZONE AND 854 EK-10 FUEL RODS IN THE THERMAL ZONE 54

FIGURE 94. LINEAR FIT OF THE PULSED NEUTRON EXPERIMENT RECORDED BY SMALL HE-3 DETECTOR IN EC5T CHANNEL OF YALINA CONFIGURATION WITH 36% ENRICHED FUEL IN THE FAST ZONE AND 905 EK-10 FUEL RODS IN THE THERMAL ZONE 55

FIGURE 95. LINEAR FIT OF THE PULSED NEUTRON EXPERIMENT RECORDED BY SMALL HE-3 DETECTOR IN EC6T CHANNEL OF YALINA CONFIGURATION WITH 36% ENRICHED FUEL IN THE FAST ZONE AND 905 EK-10 FUEL RODS IN THE THERMAL ZONE 55

FIGURE 96. LINEAR FIT OF THE PULSED NEUTRON EXPERIMENT RECORDED BY SMALL HE-3 DETECTOR IN EC5T CHANNEL OF YALINA CONFIGURATION WITH 36% ENRICHED FUEL IN THE FAST ZONE AND 953 EK-10 FUEL RODS IN THE THERMAL ZONE 56

FIGURE 97. LINEAR FIT OF THE PULSED NEUTRON EXPERIMENT RECORDED BY SMALL HE-3 DETECTOR IN EC6T CHANNEL OF YALINA CONFIGURATION WITH 36% ENRICHED FUEL IN THE FAST ZONE AND 953 EK-10 FUEL RODS IN THE THERMAL ZONE 56

FIGURE 98. LINEAR FIT OF THE PULSED NEUTRON EXPERIMENT RECORDED BY SMALL HE-3 DETECTOR IN EC5T CHANNEL OF YALINA CONFIGURATION WITH 36% ENRICHED FUEL IN THE FAST ZONE AND 1013 EK-10 FUEL RODS IN THE THERMAL ZONE 57

FIGURE 99. LINEAR FIT OF THE PULSED NEUTRON EXPERIMENT RECORDED BY SMALL HE-3 DETECTOR IN EC6T CHANNEL OF YALINA CONFIGURATION WITH 36% ENRICHED FUEL IN THE FAST ZONE AND 1013 EK-10 FUEL RODS IN THE THERMAL ZONE 57

FIGURE 100. LINEAR FIT OF THE PULSED NEUTRON EXPERIMENT RECORDED BY SMALL HE-3 DETECTOR IN EC5T CHANNEL OF YALINA CONFIGURATION WITH 36% ENRICHED FUEL IN THE FAST ZONE AND 1105 EK-10 FUEL RODS IN THE THERMAL ZONE 58

FIGURE 101. LINEAR FIT OF THE PULSED NEUTRON EXPERIMENT RECORDED BY SMALL HE-3 DETECTOR IN EC6T CHANNEL OF YALINA CONFIGURATION WITH 36% ENRICHED FUEL IN THE FAST ZONE AND 1105 EK-10 FUEL RODS IN THE THERMAL ZONE 58

FIGURE 102. LINEAR FIT OF THE PULSED NEUTRON EXPERIMENT RECORDED BY SMALL HE-3 DETECTOR IN EC5T CHANNEL OF YALINA CONFIGURATION WITH 36% ENRICHED FUEL IN THE FAST ZONE AND 1141 EK-10 FUEL RODS IN THE THERMAL ZONE 59

FIGURE 103. LINEAR FIT OF THE PULSED NEUTRON EXPERIMENT RECORDED BY SMALL HE-3 DETECTOR IN EC6T CHANNEL OF YALINA CONFIGURATION WITH 36% ENRICHED FUEL IN THE FAST ZONE AND 1141 EK-10 FUEL RODS IN THE THERMAL ZONE 59

FIGURE 104. LINEAR FIT OF THE PULSED NEUTRON EXPERIMENT RECORDED BY SMALL HE-3 DETECTOR IN EC5T CHANNEL OF YALINA CONFIGURATION WITH 36% ENRICHED FUEL IN THE FAST ZONE AND 1177 EK-10 FUEL RODS IN THE THERMAL ZONE 60

FIGURE 105. LINEAR FIT OF THE PULSED NEUTRON EXPERIMENT RECORDED BY SMALL HE-3 DETECTOR IN EC6T CHANNEL OF YALINA CONFIGURATION WITH 36% ENRICHED FUEL IN THE FAST ZONE AND 1177 EK-10 FUEL RODS IN THE THERMAL ZONE 60

FIGURE 106. LINEAR FIT OF THE PULSED NEUTRON EXPERIMENT RECORDED BY SMALL HE-3 DETECTOR IN EC5T CHANNEL OF YALINA CONFIGURATION WITH 36% ENRICHED FUEL IN THE FAST ZONE AND 1185 EK-10 FUEL RODS IN THE THERMAL ZONE 61

FIGURE 107. LINEAR FIT OF THE PULSED NEUTRON EXPERIMENT RECORDED BY SMALL HE-3 DETECTOR IN EC6T CHANNEL OF YALINA CONFIGURATION WITH 36% ENRICHED FUEL IN THE FAST ZONE AND 1185 EK-10 FUEL RODS IN THE THERMAL ZONE 61

YALINA-Booster Subcritical Assembly Pulsed-Neutron Experiments: Data Processing and Spatial Corrections

List of Tables

Page

TABLE I. PULSED NEUTRON EXPERIMENTS FOR YALINA CONFIGURATION WITH 90% ENRICHED URANIUM FUEL IN FAST ZONE AND 1141 EK-10 FUEL RODS IN THERMAL ZONE 14

TABLE II. PULSED NEUTRON EXPERIMENTS FOR YALINA CONFIGURATION WITH 36% ENRICHED URANIUM FUEL IN FAST ZONE AND 1185 EK-10 FUEL RODS IN THERMAL ZONE 15

TABLE III. PULSED NEUTRON EXPERIMENTS FOR YALINA CONFIGURATION WITH 21% ENRICHED URANIUM FUEL IN FAST ZONE AND 1185 EK-10 FUEL RODS IN THERMAL ZONE, AND CONTROL ROD IN THE OUTSIDE OF THE REACTOR 16

TABLE IV. PULSED NEUTRON EXPERIMENTAL DATA FOR YALINA CONFIGURATION WITH 90% ENRICHED URANIUM FUEL IN FAST ZONE AND 1141 EK-10 FUEL RODS IN THERMAL ZONE 18

TABLE V. PULSED NEUTRON EXPERIMENTAL DATA FOR YALINA CONFIGURATION WITH 36% ENRICHED URANIUM FUEL RODS IN FAST ZONE AND 1185 EK-10 FUEL RODS IN THERMAL ZONE 19

TABLE VI. PULSED NEUTRON EXPERIMENTAL DATA FOR YALINA CONFIGURATION WITH 21% ENRICHED URANIUM FUEL IN FAST ZONE AND 1185 EK-10 FUEL RODS IN THERMAL ZONE 20

TABLE VII. MEASURED REACTIVITIES OF YALINA CONFIGURATIONS WITH 90% ENRICHED URANIUM FUEL IN THE FAST ZONE AND 1141 EK-10 FUEL RODS IN THE THERMAL ZONE, AND 36% AND 21% ENRICHED URANIUM FUEL IN FAST ZONE AND 1185 EK-10 FUEL RODS IN THERMAL ZONE 1

TABLE VIII. MEASURED PROMPT DECAY CONSTANTS OF YALINA CONFIGURATIONS 2

TABLE IX. SPATIAL CORRECTIONS FOR THE PULSED NEUTRON EXPERIMENTAL DATA FOR YALINA CONFIGURATION WITH 90% ENRICHED URANIUM FULE IN FAST ZONE AND 1141 EK-10 FUEL RODS IN THERMAL ZONE MEASURED WITH HE-3 DETECTORS (β^{MCNP} = 759.4 ± 5 PCM) 3

TABLE X. SPATIAL CORRECTIONS FOR THE PULSED NEUTRON EXPERIMENTAL DATA WITH D-D SOURCE NEUTRONS AND HE-3 DETECTORS IN YALINA CONFIGURATION WITH 36% ENRICHED URANIUM FUEL IN FAST ZONE AND 1185 EK-10 FUEL RODS IN THERMAL ZONE 4

TABLE XI. SPATIAL CORRECTIONS FOR THE PULSED NEUTRON EXPERIMENTAL DATA WITH D-D SOURCE NEUTRONS AND HE-3 DETECTORS IN YALINA CONFIGURATION WITH 21% ENRICHED URANIUM FUEL IN FAST ZONE AND 1185 EK-10 FUEL RODS IN THERMAL ZONE IN DEC-03-2009 (ρ^{MCNP} = -5.175 $, β^{MCNP} = 720.8 ± 1.4 PCM) .. 5

TABLE XII. SPATIAL CORRECTION FACTORS FOR THE U-235 DETECTORS IN THE YALINA CONFIGURATION WITH 36% ENRICHED FUEL IN FAST ZONE AND 1185 OR 802 EK-10 FUEL RODS IN THERMAL ZONE 6

YALINA-Booster Subcritical Assembly Pulsed-Neutron Experiments: Data Processing and Spatial Corrections

Abstract

The YALINA-Booster experiments and analyses are part of the collaboration between Argonne National Laboratory of USA and the Joint Institute for Power & Nuclear Research – SOSNY of Belarus for studying the physics of accelerator driven systems for nuclear energy applications using low enriched uranium. The YALINA-Booster subcritical assembly is utilized for studying the kinetics of accelerator driven systems with its highly intensive D-T or D-D pulsed neutron source. In particular, the pulsed neutron methods are used to determine the reactivity of the subcritical system. This report examines the pulsed-neutron experiments performed in the YALINA-Booster facility with different configurations for the subcritical assembly. The 1141 configuration with 90% U-235 fuel and the 1185 configuration with 36% or 21% U-235 fuel are examined. The Sjöstrand area-ratio method is utilized to determine the reactivities of the different configurations. The linear regression method is applied to obtain the prompt neutron decay constants from the pulsed-neutron experimental data.

The reactivity values obtained from the experimental data are shown to be dependent on the detector locations inside the subcritical assembly and the types of detector used for the measurements. In this report, Bell's spatial correction factors are calculated based on a Monte Carlo model to remove the detector dependences. The large differences between the reactivity values given by the detectors in the fast neutron zone of the YALINA-Booster are reduced after applying the spatial corrections. In addition, the estimated reactivity values after the spatial corrections are much less spatially dependent.

YALINA-Booster Subcritical Assembly Pulsed-Neutron Experiments: Data Processing and Spatial Corrections

1. Introduction

The YALINA-Booster is a research subcritical assembly constructed in Belarus [1]. It operates with k_{eff} < 0.98, and it can be driven by a Cf-252 neutron source, a Deuterium-Deuterium or a Deuterium-Tritium neutron source. The subcritical assembly has a fast neutron zone at the center surrounded by a thermal neutron zone and a graphite reflector zone. The external neutrons are multiplied in the fast neutron zone, and neutrons are leaking out into the thermal neutron zone and into the reflector. A "valve" zone, which consists of an inner layer of metallic natural uranium rods and an outer layer of boron carbide rods, separates the fast and the thermal neutron zones. Therefore, thermal neutrons are prevented from entering into the fast neutron zone, and the fast and the thermal neutron zones are only coupled by fast neutrons.

The YALINA-Booster experiments and analyses are part of the collaboration between Argonne National Laboratory of USA and the Joint Institute for Power & Nuclear Research – SOSNY of Belarus for studying the physics of accelerator driven systems for nuclear energy applications using low enriched uranium. In addition, the YALINA benchmark project is part of the IAEA coordinated project "*Low Enriched Uranium Fuel Utilization in Accelerator Driven Sub-Critical Assembly Systems*", which converts HEU (Highly Enriched Uranium) fuels in the fast neutron zone to low enriched uranium fuels, i.e., 36% then 21% enriched uranium fuel. The YALINA benchmark project is also part of the IAEA activities "*Analytical and Experimental Analysis of Accelerator Driven Systems*" to study the ADS (Accelerator Driven System). In the original YALINA subcritical assembly, the HEU fuel with 90% U-235 is utilized in the fast neutron zone, and the reactivity of the subcritical assembly is adjusted by varying the number of EK-10 fuel rods in the thermal neutron zone. The polyethylene is utilized as the neutron moderator in the thermal neutron zone. With the highly intensive pulsed neutron sources and the fast and thermal neutron zones, the YALINA subcritical assembly are utilized to study the neutron kinetics in a subcritical system, in particular, to verify the pulsed neutron methods in determining the reactivity of a subcritical system.

This report documents the pulsed-neutron experiments performed in the YALINA-Booster with 90%, 36% or 21% enriched fuel rods loaded in the fast neutron zone. The fuel loading maps for the 1141 and 1185 configurations are shown in Figure 1 and Figure 2. The Sjöstrand area-ratio method is utilized to determine the reactivity of each subcritical configuration. The linear regression method is applied to obtain the prompt neutron decay constants of the subcritical assembly configurations. The obtained reactivity values from the area-ratio method are known to be dependent on the detector locations (spatial dependence) and also on the type of detectors (spectral dependence) [2]. In this report, correction factors are calculated based on Monte Carlo models to remove the detector dependences.

2. Pulsed-Neutron Experiments

In a pulsed neutron experiment for measuring the reactivity of a subcritical assembly, several neutron detectors are placed at different experimental channels monitoring the decay of the neutron fluxes resulted from short neutron pulses injected into the subcritical assembly. In the YALINA project, the neutron pulse consists of D-T or D-D neutrons and it is repeated every 0.02 s. The neutron fluxes in the subcritical assembly are recorded mainly by the He-3 neutron detectors at several experimental channels. Figure 3 shows all the experimental channels in the YALINA assembly, EC1B, EC2B, EC3B and EC4B in the fast neutron zone, EC5T, EC6T, and EC7T in the thermal neutron zone, MC5 and MC6 in the polythene moderator, and EC8R, EC9R in the graphite reflector.

In order to apply the area-ratio method for measuring the assembly reactivity, the detector responses are recorded from thousands of repetitive neutron pulses after the delayed neutron level reaches an equilibrium status. Table I, Table II and Table III document the detailed experiments performed in the YALINA-Booster with 90%, 36%, and 21% enriched uranium fuels in the booster, respectively. In the YALINA configuration with 36% enriched fuel, one long He-3 detector (25 cm) and one short He-3 small detector (1 cm) are simultaneously loaded into the subcritical assembly at different experimental channels and a long He-3 detector is always placed in MC5 experimental channel. In total, 12 batches of experimental data were obtained for this configuration. To identify each set of the experimental data, they are labeled “0.1” to “1.2” while plotting the experimental data as shown in the latter figures. Among all the measurements, the best detector counting statistics is always found when the detector is placed in the thermal neutron zone or in the moderator, e.g., EC5T, and EC6T. The detectors in the fast neutron zone usually register much lower counts. In addition, the detector counting width is 2 μs, except that it is 1 μs for the measurement made in the EC8R reflector channel in batch 0.3. Similarly, separate sets of pulsed-neutron experimental data are also recorded for the 90% enriched uranium fuel configuration using different detectors. A couple of experiments are made with 21% enriched fuel configuration. Each set of these experimental data is also labeled as shown in Table I and Table III. In addition, pulsed-neutron experiments are also performed when the core configuration was changed from 90% enriched uranium fuels to 36% enriched uranium fuels with different number of EK-10 loaded in the assembly. Detail analysis of those data will be included in the Appendix.

3. Processing of the Pulsed-Neutron Experimental Data

A. Reactivity ρ

In the area-ratio method, the reactivity of the subcritical reactor ρ in unit of dollars is the negative ratio of the prompt neutron area $\boldsymbol{A_p}$ to the delayed neutron area $\boldsymbol{A_d}$ obtained in a pulsed neutron experiment [3]:

$$\rho(\$) = \frac{\rho}{\beta} = -\frac{A_p}{A_d}. \tag{1}$$

In the experiment, the neutron pulse period is small compared with the delayed neutron decay constants, and the delayed neutrons in the subcritical assembly reach an

equilibrium status after thousands of neutron pulses repeated. Thus, a constant delayed neutron background can be observed in the detector response, and its value can be obtained by averaging the detector counts within a fitting interval while the prompt neutrons vanish in the assembly. For each set of experimental data, the delayed neutron area $\boldsymbol{A_d}$ is calculated to be the integration of the delayed neutron background over the pulse period, and the prompt neutron area $\boldsymbol{A_p}$ is the result of subtracting the delayed neutron area from the total neutron area.

The experimental data obtained from the YALINA configuration with the 36% enriched uranium fuel were used to examine different fitting intervals for the delayed neutron background. The fitted value is sensitive to the fitting interval. Figures 4 through 10 show the obtained reactivity values as a function of the low fitting boundary for the 36 sets of experimental data. As shown in these figures, for most of the experimental data, the differences between the maximum and the minimum reactivity are less than 3% by varying the fitting intervals, except it is about 6% for the experiment data obtained in EC7T and EC8R channels in batch ".2", 3.4% in EC8R channel in batch ".9", 16% for EC2B channel in batch "1.1", and "25%" for EC1B channel in batch "1.2". In addition, for the experimental data with the 3% variation, the obtained reactivity values from the different channels agree with each other within the error bars when the low fitting boundary is larger than 0.012 s, except for EC5T channel in batch "0.1" and EC8R channel in batch ".8". The estimated statistical error increases when the fitting interval is small. Therefore, the delayed neutron background was obtained with the fitting interval starting from 0.012 s till the end of the pulse for all the experimental data. The estimated error in the reactivity value is calculated based on a simple error propagation method, and only the statistical errors in the detector counts are considered.

Figure 12 plots the reactivity values obtained for the YALINA configuration with 36% enriched fuel. The data points obtained with the Long He-3 detector are labeled with "L" in the figure. The number of interval on the x axis corresponds to the number of the experimental channels and the 12 vertical lines in each interval correspond to the 12 batch of experiments data (0.1 to 1.2), respectively. The reactivity values obtained from EC1B, EC2B, and EC3B channels are more than 60%, 50%, and 20% larger than the average value from the 36 sets of experimental data, respectively. In addition, the reactivity values from EC1B and EC2B channels have slightly larger standard deviations due to the large counting statistical errors. Overall, the reactivity values obtained from EC6T, EC7T, MC5, EC8R and EC9R channels in the thermal neutron zone and in the reflector are more consistent with each other. The absolute reactivity value measured with the long He-3 detectors is about 0.3$~0.5$ smaller than with the short detectors at position EC5T. Also, the use of the long detectors in EC6T, EC7T, EC8R and EC9R channels results in smaller reactivity values relative to the average value. This observation will be discussed latter with more details.

The experimental data obtained from the YALINA 90% and 21% configurations are also analyzed following a similar procedure. The fitting interval all starts from 0.012 s to obtain consistent delayed neutron backgrounds. Tables IV through VI list the calculated reactivities for the three configurations. Figures 11 and 13 show the reactivities from different experimental channels measured for the 90% and 21% U-235 configurations, respectively. For the 21% configuration, only the datasets which were obtained with long

He-3 detectors in December 03, 2009 are plotted. The spatial dependence of the measured reactivity on the measurement location and the detector type are similar in the three configurations. In addition, Table VII compares the reactivities obtained by the long and the short detectors respectively. For the 36% configuration, the reactivities obtained with the short He-3 detectors are the average value of all the measurements at the same detector position. From the comparison, all the pulsed-neutron experiments with the long He-3 detectors tend to give smaller reactivities than with the short He-3 detectors, especially for the pulsed neutron experiments performed on December 17, 2009 using the 21% configuration, the differences are more than 50% at each detector position.

B. Prompt decay constant α

The detector counts due to the prompt neutrons can be obtained at each time bin by subtracting the delayed neutron background from the total counts. Assuming that the prompt neutron flux in the subcritical decays exponentially:

$$\phi_p(r,E,t) = \phi(r,E)e^{-\alpha t}, \tag{2}$$

the prompt decay constant α can be obtained through the least square fitting method [4].

Similar to the linear fit of the delayed neutron background, the fitted parameter α is also sensitive to the fitting interval of the linear regression method. Figures 14 through 20 show the fitted α as a function of the starting fitting point of 0.001 seconds to 0.0038 seconds with a fixed time interval of 0.001 seconds. The fitting was done for the 36 sets of the pulse neutron experimental data recorded in YALINA configuration with 36% enriched fuel. The fitting error gradually increases as the low boundary of the fitting interval increases, due to the exponential decay of the neutron population. The linear fit of the experimental data from EC3B channel results in very consistent α's for a wide range of fitting interval. The linear fits of the experimental data obtained from EC1B and EC2B channels are also results in consistent α's if the lower boundary of the fitting interval is less than 2 ms. As the lower boundary of the fitting interval continually increases, the obtained α's become invalid because of the low counts.

For the experimental channels in the thermal neutron zone, i.e., EC5T, EC6T, EC7T, and MC5, the fitted α's are almost independent of the fitting interval, except for the EC5T channel of batch "1.1", EC6T channel of batch "1.0", and EC7T of batch "1.2", which have large statistical errors. The linear fitting is also invalid for the EC9R channel of batch ".9" due to the low neutron counts. In a pulsed neutron experiment, after the neutron pulse is turned off, the detector responses of the reflector channels (EC8R and EC9R) have a rapid increase in the first few ms before the detector responses start to decrease, due to the buildup of the thermal neutrons in the subcritical assembly. Therefore, the fitted parameter α at those positions are much smaller in the first 2 or 3 ms as shown in Figures 17 and 18, which indicate the fitting interval for the prompt decay constants should avoid this region.

In order to obtain the decay constant using as much experimental data as possible, the linear regression is performed in an interval of [0.0015 to 0.0045] seconds for all the experimental data obtained at EC3B, EC5T, EC6T, EC7T and MC5 channels, since

Figures 14 through 18 have demonstrated that the fitted α is not sensitive to the fitting interval. The fitting interval is [0.0015 0.003] for EC1B and EC2B channels, and [0.0025 0.0045] for EC8R and EC9R channels. The detail linear fittings of all the sets of the experimental data analyzed are shown in Figures 24 through 83. The fitted parameter αs are plotted in Figures 21 to 23 for the YALINA three configurations. The corresponding calculated ratio of Chi-square (Chi2) to its Degreed of Freedom (DoF) represents the fitting quality are plotted in the same figure. For the 21% configuration, Figure 23 shows the prompt decay constants with Chi2/DoF ratio smaller than 1.2. In contrast to the strong spatial dependence of the reactivity obtained from the use of the area method as shown in Figures 11 to 13, the decay constants show much less spatial dependence. Specifically, for the experimental data obtained from the three YALINA configurations with 90%, 36% and 21% enriched fuel, the experimental prompt decay constants varies within ±3%, ±4%, ±7% from the average value, except for the EC8R experimental channel in batch ".9" for the 36%, the EC9R channel in batch 0.3, the EC3B channel in batch 0.3, which Chi2/DoF deviate from 1.0 significantly.

Overall, the 36 sets of experimental data of the 36% configuration result in the average reactivity ρ of -4.36 $, and the average decay constant α of - 663.4 s^{-1}. Similar analyses performed for the experimental data of the 90% and 21% configurations. The average reactivity ρ is -3.34 $, and the average decay constant α is -601.4 s^{-1} for the 90% configuration. The corresponding values for the 21% configuration from the experimental dataset of December 03, 2009 are -6.46 $ and -807.7 s^{-1}, respectively. The calculated Chi-square (Chi2), the ratio to its Degreed of Freedom (DoF), and the derived ρ and α, and their associated errors are all listed in Tables IV through VI for all the experimental data in the three configurations.

C. Performance of the short and the long He-3 detectors

Due to the low counts of the short He-3 detectors in the YALINA-Booster fast neutron zone, the long He-3 detector is often used to perform the pulsed-neutron experiment. However, as shown in Table VII, the long He-3 detector always tends to give smaller reactivity values than the short He-3 detector at the same detector position in the same configuration. As listed in Table VIII and shown in Figures 22 to 24, the prompt decay constants obtained with the short and the long detectors are close to each other and are independent of the type of detector size. These trigger further examination of the experimental data obtained with the long detector.

According to the area-ratio method, the reactivity ρ is the negative ratio of the prompt neutron area to the delayed neutron area. The delayed neutron area is obtained from the integration of the constant delayed neutron background. The ratio of the counts from the long and the short detectors at each time bin for the same detector position should reach a constant value within few tens μs after the neutron pulse turned off. Figure 84 shows this ratio of the detector counts for each time bin (2 μs) in the 21% configuration. Compared with the asymptotic ratio corresponding to the delayed neutrons, the ratios are much smaller within the first 0.3 ms for EC1B and EC2B and within the first 1.9 ms for EC3B. The maximum number of counts is more than five thousands for these three channels. EC9R channel has the smallest calculated ratio at about 1 ms when the number of counts exceeds 10000. The counts drop below 5000 at 4 ms and Figure 84 shows a significant

reduction in the ratio before this time. Additionally, Figure 85 shows the calculated ratio of the counts of EC8R channel of the 36% configuration, where the maximum count is ~5000. Figure 86 plots the ratios for EC6T and EC8R channels for the 90% configuration, where the maximum counts are 14534 and 6118 for EC6T and EC8R channels, respectively.

Figures 84 to 86 show that the ratio at the beginning of the pulse from the prompt neutrons is same as the ratio at the end of the pulse from the delayed neutrons when the counts are less than a few thousand. However, the ratio drops significantly if the counting rate increases. It indicates a significant deduction of the prompt neutron area recorded by the long detector, so the reactivity ρ obtained from the experiment with the long detector is also reduced. This deduction is very likely due to the dead time associated with the detector and the counting system, which leads to significant count loss when the counting is high. Figure 13 shows that the pulsed neutron experiment results of December 03, 2009 with counts less than a few thousand performed with the long He-3 detector for the 21% configuration. In order to obtain accurate reactivity measurements with high counting rates, a detector system with a fast response is suggested, or proper correction has to be made for the experimental data.

4. Spatial Corrections

A. Bell's correction factor - theory

The reactivities obtained in the YALINA pulsed neutron experiment show strong spatial dependences for the detector locations. In particular for the measurements performed in the EC1B, EC2B, and EC3B in the booster zone, spatial corrections have to be applied in order to yield a reliable estimation of the actual reactivity value of the subcritical configuration. Among many of the spatial correction methods, the spatial correction method suggested in Bell's book can be implemented straightforward [3]:

$$f^{cal} = \left[\frac{\rho^{cal}}{\beta^{cal}}\right] \times \left[-\frac{A_d}{A_p}\right]^{cal} = \left[\frac{\rho^{cal}}{\beta^{cal}}\right] \times \left[-\frac{A_t - A_p}{A_p}\right]^{cal}. \tag{3}$$

Using a numerical model of the subcritical assembly, each parameter in the correction factor f can be obtained by numerical calculations. The multiplication factor k_{eff} of the numerical model can be given by a criticality calculation [5]:

$$\rho^{cal} = 1 - \frac{1}{k_{eff}}. \tag{4}$$

The effective delayed neutron fraction β can be approximated very well with the prompt method [6]:

$$\beta^{cal} = 1 - \frac{k_p}{k_{eff}}, \tag{5}$$

where k_p is the prompt neutron multiplication factor and can be obtained from a criticality calculation without the delayed neutrons. According to Bell, the prompt- and delayed-neutron areas also can be determined by performing two steady-state fixed-source calculations [3]. The neutron flux in the assembly satisfies the time-dependent Boltzmann equations (with one-group delayed neutrons assumed):

$$\frac{1}{v}\frac{\partial\phi(r,E,t)}{\partial t}+\mathbf{L}(r,E)\phi(r,E,t)=(1-\beta)\chi_p(E)\int\mathbf{F}(r,E')\phi(r,E',t)dE' + \chi_d\lambda C(r,t)+Q(r,E,t), \tag{6}$$

$$\frac{\partial C(r,t)}{\partial t}+\lambda C(r,t)=\beta\int\mathbf{F}(r,E)\phi(r,E,t)dE, \tag{7}$$

where **L** and **F** operators are the neutron destruction and the neutron fission operators respectively, and Q is the external pulsed neutron source. Since the prompt neutrons decay very quickly within the pulse period, the neutron flux ϕ_p due to the prompt neutrons also satisfies the reduced transport equation:

$$\frac{1}{v}\frac{\partial\phi_p(r,E,t)}{\partial t}+\mathbf{L}(r,E)\phi_p(r,E,t)=(1-\beta)\chi_p(E)\int\mathbf{F}(r,E')\phi_p(r,E',t)dE' + Q(r,E,t). \tag{8}$$

The neutron areas observed at each detector position can be explicitly represented as:

$$A_t(r)=\int_0^T dt\int dE\Sigma_d(r,E)\phi(r,E,t)=\int dE\Sigma_d(r,E)\int_0^T dt\phi(r,E,t) = \left\langle\Sigma_d(r,E),\Phi_t(r,E)\right\rangle_E, \tag{9}$$

$$A_p(r)=\int_0^T dt\int dE\Sigma_d(r,E)\phi_p(r,E,t)=\int dE\Sigma_d(r,E)\int_0^T dt\phi_p(r,E,t) = \left\langle\Sigma_d(r,E),\Phi_p(r,E)\right\rangle_E. \tag{10}$$

In the pulsed neutron experiment, because of the delayed neutron equilibrium status reached in the assembly, by integrating the neutron fluxes over the pulse period *T*, the time-dependent Boltzmann equations (6) – (8) are reduced to two steady state equations:

$$\mathbf{L}(r,E)\Phi(r,E)=\chi(E)\int\mathbf{F}(r,E')\Phi(r,E')dE'+Q(r,E), \tag{11}$$

$$\mathbf{L}(r,E)\Phi_p(r,E)=(1-\beta)\chi_p(E)\int\mathbf{F}(r,E')\Phi_p(r,E')dE'+Q(r,E), \tag{12}$$

where, χ is the total fission neutron spectrum and Q is the pulsed neutron source integrated over the pulse period. The neutron areas are then equivalent to the reaction rates of the above two steady state equations recorded by the detectors, and can be calculated directly from the numerical model.

B. Bell's correction factor – results

Previous Monte Carlo analyses of the 90% configuration have been performed with a detailed model [7]. This Monte Carlo model with small modifications is utilized to simulate the 36% and the 21% configurations. In the Monte Carlo simulation, a small cylindrical isotropic neutron source with mono-energy of 2.45 or 14.1 MeV is utilized to simulate the D-D or the D-T neutrons. The neutron detecting channels are empty, and the neutron detectors are not simulated explicitly in the model. The prompt- and delayed-neutron areas at each detector location are obtained by tallying the neutron fluxes in the detecting channel, and multiplied with the detector cross sections through the FM card available in MCNPX. In the actual experiment, the He-3 detectors may have an active length of 1 or 25 cm. In the Monte Carlo simulation, the average neutron fluxes are tallied in the detecting channel in a cylindrical volume centered at the middle plane of the configuration and with the cylinder length 1 or 25 cm reflecting the detector actual active length.

The calculated k_{eff} from the numerical simulations are 0.97968, 0.97499 and 0.96404 for the 90%, the 36% and the 21% configurations, respectively. The standard deviation is less than 4 pcm for all calculations. The calculated k_p is 0.97224, 0.96754 and 0.95705 for the 90%, the 36% and the 21% configurations, respectively. The standard deviations are 3 pcm, 4 pcm, 4 pcm, respectively for the three configurations. Thus, the effective delayed neutron fraction β is approximately 759.4 pcm, 764.1 pcm, 720.8 pcm, with standard deviations of ~5 pcm, and the calculated reactivity of the numerical models are -2.73 $, -3.34 $, and -5.17 $ respectively. Tables IX through Table XI list the calculated correction factors at each detector position, and the reactivities after the spatial corrections for the three configurations.

The spatial corrections are first made for the experimental data obtained for the 90% configuration. As shown in Table IX and Figure 11, the large discrepancies between the measured reactivities in the fast neutron zone with short He-3 detectors are eliminated by the spatial corrections. The average reactivity after the spatial corrections is -3.20$, which is slightly smaller than the average value without spatial corrections. The reactivities obtained in the fast neutron zone with the long He-3 detectors are suspected as discussed in previous section. Thus, no spatial corrections made for these experimental points. For this YALINA configuration, Monte Carlo numerical simulations were also performed to calculate the spatial correction factors through a direct numerical simulation of the detector responses with neutron pulses [8], and deterministic simulation using Bell's method [9]. Table IX shows that the correction factors obtained from these simulations agree with the Monte Carlo calculated correction factors of this work within the standard deviations.

For detector positions with multiple measurements in the 36% configuration, the averaged values of the measured reactivities are calculated, and the spatial correction factors are applied upon the averaged values. The spatial corrections are made separately for the short and the long detectors used in the experiments. The spatial correction factors

are calculated from the Monte Carlo model. Now, the absolute value of reactivity obtained at positions EC1B, EC2B and EC3B channels after the spatial correction is close to the average value. Overall, as shown in Figure 12, the spatial dependences in the measured reactivities have been greatly reduced with the spatial corrections. The 3.41 $ difference between EC1B and EC7T channels with the long He-3 detectors is reduced to 0.92$, and the 0.86$ difference between EC5T and EC8R channels with the short He-3 detectors is reduced to 0.31$. The average reactivity after the spatial correction is -4.35 $ with the long detectors, and -4.33$ with the short detectors. However, the maximum deviations from the averages are still about 13.6% for the long He-3 detector at EC1B channel and 5.3% for the short detector at EC7T channel.

Spatial corrections are only made for the experimental data corresponding to the experimental dataset obtained in December 03, 2009 for the 21% configuration. As shown in Table XI and Figure 13, the spatial dependences of the reactivity have been reduced in the fast neutron zone. After spatial corrections, the 4.7 $ difference between the reactivity obtained at EC1B and the average value of all the experimental data is reduced to be 0.79$.

The spatial dependences of the measured reactivities using the area-ratio method were analyzed and theoretically explained in the work of Cao and Lee [10]. The spatial corrections are function of the experimental conditions, i.e., the characteristics of the external neutron source, the neutron detector, and the subcritical assembly. Small differences were observed between the spatial correction factors for the measurements with D-T and D-D neutron sources. According to the calculated correction factors shown in Table XII, the measured reactivity obtained by He-3 neutron detectors have less spatial dependence relative to the values by U-235 fission chambers. Figure 87 confirms that the He-3 detector is less sensitive to the fast neutrons in the EC1B experimental channel of the fast neutron zone. In addition, the spatial effects will also be enhanced in deep subcritical systems. For the 36% configuration with different number of EK-10 fuel rods in the thermal neutron zone, the spatial correction factors further deviate from 1.0 as the subcriticality level increases as shown Table XII.

C. Bell's correction factor – errors

In the above calculation of the correction factor *f*, if it is assumed that the Monte Carlo calculations of the total neutron area $\mathbf{A}_t$, the prompt neutron area $\mathbf{A}_p$, the prompt neutron multiplication factor k_p and the multiplication factor *k* are independent of each other, the associated error of the calculated *f* due to the statistical errors in the Monte Carlo calculations can then be estimated using the error propagation method:

$$\frac{\sigma_f^2}{f^2} = \frac{(k_p - 1)^2 k^2}{(k - k_p)^2 (k-1)^2}\left[\frac{\sigma_k^2}{k^2}\right] + \frac{k_p^2}{(k-k_p)^2}\left[\frac{\sigma_{k_p}^2}{k_p^2}\right] + \left[\frac{A_t/A_p}{1 - A_t/A_p}\right]^2 \times \left[\frac{\sigma_{A_t}^2}{A_t^2} + \frac{\sigma_{A_p}^2}{A_p^2}\right]$$

$$= \frac{(k_p - 1)^2 k^2}{(k - k_p)^2 (k-1)^2} \left[\frac{\sigma_k^2}{k^2} \right] + \frac{k_p^2}{(k - k_p)^2} \left[\frac{\sigma_{k_p}^2}{k_p^2} \right] + (\rho - 1)^2 \times \left[\frac{\sigma_{A_t}^2}{A_t^2} + \frac{\sigma_{A_p}^2}{A_p^2} \right]. \quad (13)$$

It is evident that the error is dependent on the reactivity of the subcritical reactor. When the absolute value of ρ is large (i.e. deep subcritical system), the error increases, even when the neutron areas estimated by the Monte Carlo methods are very accurate compared to a subcritical assembly with K_{eff} close to 1 with the same standard deviations. This can be easily understood by inspecting Equations (3) and (4), which involve calculating the difference between the total neutron area $\mathbf{A}_t$ and the prompt neutron area $\mathbf{A}_p$, and the difference between k_p and k. As the delayed neutrons become less important in a subcritical assembly, the differences between the systems with or without delayed neutrons become smaller, and it is more difficult to calculate accurately the difference by Monte Carlo methods. Variance reduction technique such as correlated sampling or weight window may be used to help calculate the correction factors for deep subcritical system. In Table XII, the weight window is applied to calculate *f* for the 36% configuration with 802 EK-10 fuel rods in the thermal zone.

5. Summary

The area-ratio method has been successfully applied to derive the reactivity of the YALINA-Booster configurations with 90%, 36% and 21% enriched uranium fuels. The Monte Carlo model of this subcritical assembly is utilized to calculate the spatial correction factors for each experimental channel. The spatial effects in estimating the reactivity by the area-ratio method using different experimental channels have been greatly reduced. The reactivity of this YALINA-Booster configuration with 21%, 36% and 90% enriched fuels is determined to be -6.17 $, -4.34 $ and -3.20 $, respectively, after the spatial corrections.

In addition, the analysis of the spatial correction factors with different pulsed-neutron experimental conditions suggest that if good counting statistics can be obtained, the reactivity measured with a He-3 detector will exhibit less spatial dependence than a U-235 fission chamber detector. The measurement will also be more reliable with detectors loaded in the thermal neutron zone or in the reflector, which are away from the external neutron source for both type of detectors. Additionally, the spatial effects are manifested in measuring the reactivity of a deep subcritical system using the area-ratio method. Spatial corrections have to be made especially for those experiments with detectors placed near the external source in order to obtain a meaningful estimation of the actual reactivity.

References

[1] V. Bournos, A. Fokov, Y. Fokov, H. Kiyavitskaya, B. Martsynkevich, C. Routkovskaia, Y. Gohar, C-M Persson, and W. Gudowski, "YALINA-Booster Benchmark Specifications for the IAEA Coordinated Research Projects on Analytical and Experimental Benchmark Analysis on Accelerator Driven Systems and Low Enriched Uranium Fuel Utilization in Accelerator-Driven Sub-Critical Assembly Systems," (2008).

[2] M. Carta, A. D'Angelo, V. Peluso, G. Aliberti, G. Imel, V. Kulik, G. Palmiotti, J. Lebrat, Y. Rugama, C. Destouches, E. Gonzalez-Romero, D. Villamarin, S. Dulla, F. Gabrielli, P. Ravetto, and M. Salvatores, "Reactivity assessment and Spatial Time-Effects from the MUSE-Kinetics Experiments," *Proceedings of the PHYSOR 2004: The Physics of Fuel Cycles and Advanced Nuclear Systems –Global Developments* (2004).

[3] Ilka Antcheva, Olivier Couet, Ed., "ROOT-An Object-Oriented Data Analysis Framework: The ROOT Users Guide 5.24," (2009).

[4] G. I. Bell and S. Glasstone, *Nuclear Reactor Theory*, Van Nostrand Reinhold Company (1970).

[5] Denise B. Pelowitz, Ed., "MCNPX User's Manual Version 2.6.0," LA-CP-07-1473, (2008).

[6] R. K. Meulekamp and S C. van der Marck, "Calculating the Effective Delayed Neutron Fraction with Monte Carlo," *Nucl. Sci. Eng.*, **152**, 142-148 (2006).

[7] A. Talamo and Y. Gohar, "Monte Carlo Modeling and Analyses of YALINA-Booster Subcritical Assembly Part I: Analytical Models and Main Neutron Parameters," Argonne National Laboratory, ANL-NE-08/31 (2008).

[8] A. Talamo, Y. Gohar and C. Rabiti, "Monte Carlo Modeling and Analyses of YALINA-Booster Subcritical Assembly Part II: Pulsed Neutron Source," Argonne National Laboratory, ANL-08/33 (2008).

[9] G. Aliberti, Private Communication.

[10] Y. Cao and J. C. Lee, "Spatial Corrections for Pulsed-Neutron Reactivity Measurements," To be published in *Nucl. Sci. Eng.*, (2010).

Appendix

In the YALINA-Booster, after replacing the 90% enriched uranium fuels with the 36% enriched uranium fuels, the number of EK-10 fuel rods in the thermal zone was increased gradually to reach k_{eff} of ~0.98. During this loading process, the pulsed-neutron experiment was performed to determine the reactivity of the assembly, with two He-3 detectors located at EC5T and EC6T channels. The subcriticality and the prompt decay constants of the assembly as a function of the number of EK-10 fuel rods loaded into the thermal zone are shown in Figures 88 and 89.

Figures 90 through 107 display the fitting of each set of the experimental data, in which the fitting interval for the delayed neutron background starts at 0.012 s if the pulsed period ***T*** is larger than that, otherwise starts at 0.006 s. The fitting interval for the prompt neutron decay constants is [0.0015 s to 0.0045 s] for ***T*** **>** 0.012s, and [0.001 s to 0.002 s] otherwise. Overall, the prompt decay constants obtained from the measurements of EC5T and EC6T channels agree with each other for every configuration. The absolute reactivity value obtained from EC5T channel is always larger than that from EC6T channel, except at the configuration with 953 EK-10 fuel rods. The analysis of the experimental data obtained by EC5T at this configuration show a large standard deviation of 0.32 $. The standard deviations for other reactivities are all much less than 0.1 $.

Table I. Pulsed Neutron Experiments for YALINA configuration with 90% enriched uranium fuel in fast zone and 1141 EK-10 fuel rods in thermal zone

Exp Date	Batch channel	Neutron Source	Pulse *f* (HZ)	Detector type /Exp Channel
07/2006	0.1	(D,D)	50.0	He-3L / EC1B
	0.1	(D,D)	50.0	He-3L / EC2B
	0.1	(D,D)	50.0	He-3L / EC2B
	0.1	(D,D)	50.0	He-3L / EC3B
02/2008	0.2	(D,T)	50.0	He-3S / EC1B
	0.2	(D,T)	50.0	He-3S / EC2B
	0.2	(D,T)	50.0	He-3S / EC3B
12/2007	0.3	(D,D)	50.0	He-3L / EC6T
	0.3	(D,D)	50.0	He-3L / EC8R
	0.4	(D,D)	50.0	He-3S / EC6T
	0.4	(D,D)	50.0	He-3S / EC8R

Table II. Pulsed Neutron Experiments for YALINA configuration with 36% enriched uranium fuel in fast zone and 1185 EK-10 fuel rods in thermal zone

Exp Date	Batch channel	Neutron Source	Pulse *f* (HZ)	Detector type /Exp Channel
02/11/2009	0.1	(D,D)	50.0	He-3S / EC5T
	0.1	(D,D)	50.0	He-3S / EC6T
	0.1	(D,D)	50.0	He-3L / MC5
	0.2	(D,D)	50.0	He-3S / EC7T
	0.2	(D,D)	50.0	He-3S / EC8R
	0.2	(D,D)	50.0	He-3L / MC5
02/12/2009	0.3	(D,D)	50.0	He-3S / EC7T
	0.3	(D,D)	50.0	He-3S / EC8R
	0.3	(D,D)	50.0	He-3L / MC5
	0.4	(D,D)	50.0	He-3S / EC5T
	0.4	(D,D)	50.0	He-3S / EC6T
	0.4	(D,D)	50.0	He-3L / MC5
03/05/2009	0.5	(D,D)	50.0	He-3L / EC5T
	0.5	(D,D)	50.0	He-3S / EC6T
	0.5	(D,D)	50.0	He-3L / MC5
	0.6	(D,D)	50.0	He-3L / EC6T
	0.6	(D,D)	50.0	He-3S / EC7T
	0.6	(D,D)	50.0	He-3L / MC5
	0.7	(D,D)	50.0	He-3S / EC5T
	0.7	(D,D)	50.0	He-3L / EC7T
	0.7	(D,D)	50.0	He-3L / MC5
	0.8	(D,D)	50.0	He-3L / EC8R
	0.8	(D,D)	50.0	He-3S / EC9R
	0.8	(D,D)	50.0	He-3L / MC5
	0.9	(D,D)	50.0	He-3S / EC8R
	0.9	(D,D)	50.0	He-3L / EC9R
	0.9	(D,D)	50.0	He-3L / MC5
03/09/2009	1.0	(D,D)	50.0	He-3L / EC3B
	1.0	(D,D)	50.0	He-3S / EC6T
	1.0	(D,D)	50.0	He-3L / MC5
	1.1	(D,D)	50.0	He-3L / EC2B
	1.1	(D,D)	50.0	He-3S / EC5T
	1.1	(D,D)	50.0	He-3L / MC5
	1.2	(D,D)	50.0	He-3L / EC1B
	1.2	(D,D)	50.0	He-3S / EC7T
	1.2	(D,D)	50.0	He-3L / MC5

Table III. Pulsed Neutron Experiments for YALINA configuration with 21% enriched uranium fuel in fast zone and 1185 EK-10 fuel rods in thermal zone, and control rod in the outside of the reactor

Exp Date	Batch channel	Neutron Source	Data Acquisition	Detector type /Exp Channel
12/3/2009	0.1	(D,D)/CR out	DAQ	He-3L / EC1B
	0.1	(D,D) /CR out	DAQ	He-3L / EC5T
	0.1	(D,D) /CR out	MCS32	He-3L / EC5T
	0.2	(D,D) /CR out	DAQ	He-3L / EC2B
	0.2	(D,D) /CR out	DAQ	He-3L / EC6T
	0.2	(D,D) /CR out	MCS32	He-3L / EC6T
	0.3	(D,D) /CR out	DAQ	He-3L/ EC3B
	0.3	(D,D) /CR out	DAQ	He-3L/ EC7T
	0.3	(D,D) /CR out	MCS32	He-3L/ EC7T
	0.4	(D,D) /CR out	DAQ	He-3L/ EC8R
	0.4	(D,D) /CR out	DAQ	He-3L/ EC9R
	0.4	(D,D) /CR out	MCS32	He-3L/ EC9R
	0.5	(D,D) /CR out	DAQ	He-3L/ MC3
	0.5	(D,D) /CR out	DAQ	He-3L/ MC4
	0.5	(D,D) /CR out	MCS32	He-3L/ MC4
12/17/2009	0.1	(D,T) /CR out	DAQ	He-3L / EC1B
	0.1	(D,T) /CR out	MCS32	He-3L / EC2B
	0.1	(D,T) /CR out	DAQ	He-3L / EC2B
	0.2	(D,T) /CR out	DAQ	He-3L / EC3B
	0.2	(D,T) /CR out	DAQ	He-3L / EC9R
	0.2	(D,T) /CR out	MCS32	He-3L / EC9R
	0.3	(D,T) /CR out	DAQ	He-3S / EC3B
	0.3	(D,T) /CR out	MCS32	He-3S / EC3B
	0.3	(D,T) /CR out	DAQ	He-3S / EC9R
	0.4	(D,T) /CR out	DAQ	He-3S / EC1B
	0.4	(D,T) /CR out	DAQ	He-3S / EC2B
	0.4	(D,T) /CR out	MCS32	He-3S / EC2B
12/18/2009	0.1	(D,T) /CR out	DAQ	He-3S / EC1B
	0.1	(D,T) /CR out	DAQ	KNT31 / EC2B
	0.1	(D,T) /CR out	MCS32	He-3S / EC5T
03/23/2010	0.1	(D,T) /CR out	DAQ	He-3S / EC6T
	0.2	(D,T) /CR out	DAQ	He-3S/EC6TCd
	0.2	(D,T) /CR out	DAQ	He-3S / EC7T
	0.3	(D,T) /CR in	DAQ	He-3S/EC6TCd
	0.3	(D,T) /CR in	DAQ	He-3S / EC7T

03/26/2010	0.1	(D,T) /CR in	MCS32	KNT31 / EC1B
	0.1	(D,T) /CR in	DAQ	He-3S/EC6TCd
	0.1	(D,T) /CR in	DAQ	He-3S / EC7T
	0.2	(D,T) /CR out	MCS32	KNT31 / EC1B
	0.2	(D,T) /CR out	DAQ	He-3S/EC6TCd
	0.2	(D,T) /CR out	DAQ	He-3S / EC7T
	0.3a	(D,T) /CR out	DAQ	He-3S / EC6T
	0.3a	(D,T) /CR out	DAQ	He-3S/EC7TCd
	0.3b	(D,T) /CR out	DAQ	He-3S / EC6T
	0.3b	(D,T) /CR out	DAQ	He-3S/EC7TCd
	0.4a	(D,T) /CR in	DAQ	He-3S / EC6T
	0.4a	(D,T) /CR in	DAQ	He-3S/EC7TCd
	0.4b	(D,T) /CR in	DAQ	He-3S / EC6T
	0.4b	(D,T) /CR in	DAQ	He-3S/EC7TCd
	0.6	(D,T) /CR in	DAQ	KNT31/EC3B
	0.6	(D,T) /CR in	DAQ	He-3S/EC7TCd
	0.7	(D,T)) /CR out	DAQ	KNT31 / EC3B
	0.7	(D,T)) /CR out	DAQ	He-3S/EC7TCd
03/29/2010	0.4	(D,T) /CR out	DAQ	KNT31 / EC3B
	0.4	(D,T) /CR out	MCS32	He-3S /EC6T
	0.4	(D,T) /CR out	DAQ	He-3S/EC7TCd
	0.5	(D,T) /CR in	DAQ	KNT31/MC2
	0.5	(D,T) /CR in	MCS32	He-3S / MC3
	0.5	(D,T) /CR in	DAQ	He-3S/MC4Cd

Table IV. Pulsed Neutron Experimental data for YALINA configuration with 90% enriched uranium fuel in fast zone and 1141 EK-10 fuel rods in thermal zone

Config.	Batch	Det.	ρ ($)	Δρ ($)	α (1/s)	Δα (1/s)	Chi2	DoF	Chi2/ DoF
1141	0.1	EC1B_L	-3.50	0.007	-603.9	2.45	752	747	1.01
	0.1	EC2B_L	-3.22	0.006	-597.3	2.18	693	747	0.93
	0.1	EC2B_L	-3.29	0.006	-601.0	2.16	718	747	0.96
	0.1	EC3B_L	-3.20	0.007	-605.2	1.15	1490	1497	0.995
	0.2	EC1B_S	-4.03	0.02	-613.5	7.19	794	747	1.06
	0.2	EC2B_S	-3.80	0.02	-614.2	6.27	711	747	0.95
	0.2	EC3B_S	-3.23	0.006	-583.7	1.13	1521	1497	1.02
	0.3	EC6T_L	-2.73	0.003	-566.9	0.57	2457	1497	1.64
	0.3	EC8R_L	-3.08	0.004	-589.6	1.56	1024	997	1.03
	0.4	EC6T_S	-3.44	0.01	-624.0	1.77	1586	1497	1.06
	0.4	EC8R_S	-3.29	0.02	-616.0	5.31	1045	997	1.05
Average	---	---	-3.34	---	-601.4	---	---	---	---

Table V. Pulsed Neutron Experimental data for YALINA configuration with 36% enriched uranium fuel rods in fast zone and 1185 EK-10 fuel rods in thermal zone

Config.	Batch #	Det.	ρ ($)	Δρ ($)	α (1/s)	Δα (1/s)	DoF	Chi2/ DoF
1185	0.1	EC5T_S	-4.67	0.02	-671.9	2.5	1497	0.98
	0.1	EC6T_S	-3.93	0.01	-659.7	2.1	1497	0.97
	0.1	MC5_L	-3.86	0.01	-673.3	0.8	1497	1.02
	0.2	EC7T_S	-4.02	0.02	-659.1	1.8	1497	1.04
	0.2	EC8R_S	-3.81	0.02	-649.5	5.0	997	0.94
	0.2	MC5_L	-3.81	0.01	-671.2	0.8	1497	1.03
	0.3	EC7T_S	-4.00	0.01	-664.5	1.5	1497	0.98
	0.3	EC8R_S	-3.90	0.02	-641.2	4.3	1997	1.04
	0.3	MC5_L	-4.29	0.00	-670.2	0.5	1497	1.08
	0.4	EC5T_S	-4.77	0.01	-672.7	1.5	1497	0.98
	0.4	EC6T_S	-4.09	0.01	-662.3	1.3	1497	1.08
	0.4	MC5_L	-4.24	0.00	-674.2	0.5	1497	0.97
	0.5	EC5T_L	-4.34	0.01	-665.1	0.9	1497	0.98
	0.5	EC6T_S	-4.33	0.03	-660.1	3.8	1497	1.04
	0.5	MC5_L	-4.30	0.01	-686.1	1.2	1497	1.01
	0.6	EC6T_L	-3.88	0.01	-658.2	0.8	1497	1.05
	0.6	EC7T_S	-4.24	0.03	-667.6	4.4	1497	1.10
	0.6	MC5_L	-4.27	0.01	-682.9	1.2	1497	1.00
	0.7	EC5T_S	-4.93	0.03	-669.1	4.2	1497	1.07
	0.7	EC7T_L	-3.77	0.01	-654.7	0.8	1497	0.95
	0.7	MC5_L	-4.25	0.01	-682.5	1.1	1497	1.07
	0.8	EC8R_L	-3.80	0.01	-647.6	2.1	997	0.97
	0.8	EC9R_S	-4.16	0.08	---	---	---	---
	0.8	MC5_L	-4.18	0.01	-672.2	1.1	1497	1.00
	0.9	EC8R_S	-4.01	0.04	-615.4	10.6	997	1.17
	0.9	EC9R_L	-4.06	0.01	-649.4	3.4	997	1.02
	0.9	MC5_L	-4.19	0.01	-668.9	1.0	1497	1.02
	1.0	EC3B_L	-5.15	0.03	-671.6	3.5	1497	1.08
	1.0	EC6T_S	-4.24	0.03	-647.9	3.8	1497	1.06
	1.0	MC5_L	-4.19	0.01	-675.5	1.0	1497	1.02
	1.1	EC2B_L	-6.53	0.08	-663.4	16.3	747	1.15
	1.1	EC5T_S	-4.97	0.03	-655.0	3.9	1497	1.05
	1.1	MC5_L	-4.21	0.01	-673.6	0.9	1497	0.97
	1.2	EC1B_L	-7.18	0.11	-646.1	20.6	747	1.15
	1.2	EC7T_S	-4.10	0.03	-643.4	4.4	1497	1.09
	1.2	MC5_L	-4.20	0.01	-672.9	1.1	1497	1.02
Average	---	---	-4.36	---	-662.8	---	---	---

Table VI. Pulsed Neutron Experimental data for YALINA configuration with 21% enriched uranium fuel in fast zone and 1185 EK-10 fuel rods in thermal zone

Config.	Batch	Det.	ρ ($)	Δρ ($)	α (1/s)	Δα (1/s)	DoF	Chi2/ DoF
(12/03/ 09)	0.1	EC1B	-11.83	0.19	-781.8	20.1	747	1.19
	0.1	EC5T_MCS	-6.37	0.01	-833.5	1.3	1497	1.00
	0.1	EC5T	-6.37	0.01	-833.4	1.2	1497	0.97
	0.2	EC2B	-9.92	0.15	-795.6	18.8	747	1.20
	0.2	EC6T	-5.47	0.01	-836.2	1.1	1497	1.05
	0.2	EC6T_MCS	-5.47	0.01	-836.4	1.1	1497	1.01
	0.3	EC3B	-7.48	0.06	-810.2	4.8	1497	1.09
	0.3	EC7T_MCS	-5.31	0.01	-830.6	1.2	1497	0.92
	0.3	EC7T	-5.30	0.01	-830.4	1.2	1497	0.98
	0.4	EC8R	-5.11	0.01	-802.5	3.1	997	1.04
	0.4	EC9R_MCS	-5.47	0.03	-786.9	4.9	997	1.06
	0.4	EC9R	-5.44	0.03	-786.1	4.9	997	1.08
	0.5	MC3	-5.46	0.04	-772.9	7.2	997	1.05
	0.5	MC4	-5.52	0.04	-770.8	7.2	997	1.03
(12/17/ 09)	0.1	EC2BL_MCS	-5.63	0.03	-794.3	6.6	747	1.06
	0.1	EC1BL	-6.04	0.01	-792.0	2.8	747	0.96
	0.1	EC2BL	-5.68	0.01	-797.0	2.6	747	0.95
	0.2	EC3B_L	-4.22	0.01	-750.5	0.7	1497	1.56
	0.2	EC9R_L_MCS	-2.95	0.00	-602.1	0.8	997	3.85
	0.3	EC3B_MCS	-6.98	0.03	-815.7	2.7	1497	0.99
	0.3	EC3B_s	-6.92	0.03	-817.2	2.7	1497	0.99
	0.3	EC9R_s	-5.41	0.01	-767.8	2.6	997	1.10
	0.4	EC1B_s	-9.28	0.08	-794.8	11.5	747	1.17
	0.4	EC2B_s_MCS	-8.58	0.07	-817.9	10.7	747	0.96
	0.4	EC2B_s	-8.53	0.07	-818.8	10.7	747	1.04
(12/18/ 09)	0.1	EC1B_s	-9.54	0.08	-792.9	11.38	747	1.10
	0.1	EC2B_KNT31	-7.89	0.08	-783.8	11.99	747	1.14
	0.1	EC5T_S	-3.65	0.00	-720.5	0.69	1497	2.11
(03/23/ 10)	0.1	EC6T_s	-2.71	0.12	---	---	---	---
	0.2	EC6T_s_Cd	-4.40	0.01	-807.4	1.2	1497	1.06
	0.2	EC7T_s	-3.65	0.00	-712.1	0.3	1497	6.43
	0.3	EC6T_s_Cd	-4.38	0.01	-853.3	2.3	1497	1.03
	0.3	EC7T_s	-4.97	0.01	-840.6	0.7	1497	1.12
	0.1	EC1B_KNT31	-9.18	0.08	-873.4	11.4	747	1.05
	0.1	EC6T_Cd	-4.53	0.01	-844.1	1.7	1497	1.09
	0.1	EC7T_s	-3.80	0.00	-772.3	0.6	1497	2.79
	0.2	EC1B_KNT31	-8.03	0.08	-784.7	11.8	747	1.15

(03/26/10)	0.2	EC6T_s_Cd	-4.27	0.01	-803.0	1.9	1497	0.98
	0.2	EC7T_s	-3.38	0.00	-693.5	0.6	1497	3.57
	0.3	EC6T_s	-2.21	0.00	-576.1	0.6	1497	7.75
	0.3	EC7T_s_Cd	-5.24	0.02	-813.1	2.3	1497	1.05
	0.3	EC6T_s	-2.31	0.00	-585.7	0.6	1497	6.41
	0.3	EC7T_s_Cd	-5.33	0.02	-812.4	2.5	1497	0.97
	0.4	EC6T_s	-2.59	0.00	-646.3	0.6	1497	6.75
	0.4	EC7T_s_Cd	-5.99	0.03	-871.6	2.8	1497	1.06
	0.4	EC6T_s	-2.80	0.00	-672.5	0.6	1497	5.81
	0.4	EC7T_s_Cd	-5.98	0.03	-880.6	2.9	1497	1.03
	0.6	EC3B_KNT31	-7.65	0.04	-855.9	3.4	1497	1.05
	0.6	EC7T_s_Cd	-5.99	0.03	-877.1	2.7	1497	1.07
	0.7	EC3B_KNT31	-7.67	0.04	-817.7	3.3	1497	0.99
	0.7	EC7T_s_Cd	-5.37	0.02	-816.4	2.3	1497	1.04
(03/29/10)	0.4	MC2_KNT31	-5.63	0.06	-727.0	9.1	997	1.08
	0.4	MC3_s_MCS	-5.25	0.01	-758.5	2.5	997	0.96
	0.4	MC4_s_Cd	-5.79	0.28	---	---	---	---
	0.5	MC2_KNT31	-6.33	0.02	-792.5	3.4	997	1.04
	0.5	MC3_s_MCS	-5.51	0.02	-802.1	2.8	997	1.01
	0.5	MC4_s_Cd	-6.07	0.10	---	---	---	---
Avg.	---	CR in	-5.89	---	-777.9	---	---	---
	---	CR out	-5.41	---	-814.0	---	---	---

Table VII. Measured reactivities of YALINA configurations with 90% enriched uranium fuel in the fast zone and 1141 EK-10 fuel rods in the thermal zone, and 36% and 21% enriched uranium fuel in fast zone and 1185 EK-10 fuel rods in thermal zone

Configuration		Booster zone			Thermal zone			Moderator	Reflector	
		EC1B	EC2B	EC3B	EC5T	EC6T	EC7T	MC5	EC8R	EC9R
90% (1141)	L	-3.50	-3.29	-3.20	---	-2.73	---	---	-3.08	---
	S	-4.03	-3.80	-3.23	---	-3.44	---	---	-3.29	---
36% (1185)	L	-7.18	-6.53	-5.15	-4.34	-3.88	-3.77	-4.16	-3.80	-4.06
	S	---	---	---	-4.83	-4.15	-4.09	---	-3.91	-4.16
21% (1185) (Dec-17-2009)	L	-6.04	-5.67	-4.22	---	---	---	---	---	-2.95
	S	-9.28	-8.58	-6.95	---	---	---	---	---	-5.41

Table VIII. Measured prompt decay constants of YALINA configurations

Configuration		Booster zone			Thermal zone			Moderator	Reflector	
		EC1B	EC2B	EC3B	EC5T	EC6T	EC7T	MC5	EC8R	EC9R
90% (1141)	α_L	-604	-601	-605	---	-567	---	---	-590	---
	α_S	-614	-614	-584	---	-624	---	---	-616	---
36% (1185)	α_L	-657	-670	-673	-665	-658	-655	-675	-648	-649
	α_S	---	---	---	-667	-658	-659	---	-635	---
21% (1185) (Dec-17-2009)	α_L	-792	-797	-750	---	---	---	---	---	-602
	α_S	-795	-818	-817	---	---	---	---	---	-768

Table IX. Spatial corrections for the pulsed neutron experimental data for YALINA configuration with 90% enriched uranium fuel in fast zone and 1141 EK-10 fuel rods in thermal zone measured with He-3 detectors (β^{MCNP} = 759.4 ± 5 pcm)

Detectors	Small He-3			Long He-3	
	EC1B	EC2B	EC3B	EC6T	EC8R
ρ($)	-4.03	-3.80	-3.23	-2.73	-3.08
k_{eff}	0.9703	0.9720	0.9761	0.9797	0.9771
f	0.803	0.856	0.982	1.08	1.11
Δ_f	0.077	0.082	0.054	0.022	0.029
$\rho^{cor}$$	-3.23	-3.25	-3.17	-2.93	-3.41
k_{eff}^{cor}	0.9761	0.9760	0.9765	0.9782	0.9748
f_1^{*}	0.825	0.867	0.955	1.00	1.04
f_2^{**}	0.865	0.902	0.962	1.08	1.11

* Monte Carlo dynamic calculations with ENDF/B-VI libraries [8];

** Deterministic calculations with JEFF3.1 libraries [9]

Table X. Spatial corrections for the Pulsed Neutron Experimental data with D-D source neutrons and He-3 detectors in YALINA configuration with 36% enriched uranium fuel in fast zone and 1185 EK-10 fuel rods in thermal zone

Detectors			ρ($)	k_{eff}	f	Δ_f	ρ^{cor}($)	k_{eff}^{cor}
Long He-3 (β^{cal}=764 pcm)	Booster zone	EC1B	-7.18	0.9478	0.688	0.029	-4.94	0.9636
		EC2B	-6.53	0.9525	0.764	0.030	-4.99	0.9633
		EC3B	-5.15	0.9621	0.868	0.020	-4.47	0.9670
	Thermal zone	ECT5	-4.34	0.9679	0.919	0.013	-3.98	0.9705
		ECT6	-3.88	0.9712	1.03	0.014	-4.01	0.9703
		ECT7	-3.77	0.9720	1.07	0.015	-4.02	0.9702
	Reflector	MC5	-4.16	0.9692	1.05	0.017	-4.39	0.9675
		EC8R	-3.80	0.9718	1.08	0.015	-4.11	0.9696
		EC9R	-4.06	0.9699	1.05	0.022	-4.25	0.9685
	Average	---	-4.76	0.9649	---	---	-4.35	0.9678
Short He-3 (β^{cal}=764 pcm	Thermal zone	EC5T	-4.83	0.9644	0.912	0.020	-4.25	0.9674
		EC6T	-4.15	0.9693	1.00	0.020	-4.15	0.9692
		EC7T	-4.09	0.9697	1.00	0.021	-4.08	0.9696
	Reflector	EC8R	-3.91	0.9710	1.08	0.027	-4.22	0.9687
		EC9R	-4.16	0.9692	1.08	0.050	-4.50	0.9668
	Average	---	-4.26	0.9685	---	---	-4.33	0.9680

Table XI. Spatial corrections for the Pulsed Neutron Experimental data with D-D source neutrons and He-3 detectors in YALINA configuration with 21% enriched uranium fuel in fast zone and 1185 EK-10 fuel rods in thermal zone in Dec-03-2009 (ρ^{MCNP} = -5.175 $, β^{MCNP} = 720.8 ± 1.4 pcm)

Detectors		ρ($)	k_{eff}	f	Δ_f	ρ^{cor}($)	k_{eff}^{cor}
Booster zone	EC1B	-11.83	0.9214	0.589	0.023	-6.96	0.9522
	EC2B	-9.92	0.9336	0.719	0.024	-7.13	0.9511
	EC3B	-7.48	0.9489	0.830	0.018	-6.20	0.9572
Thermal zone	ECT5	-6.37	0.9561	0.905	0.010	-5.77	0.9601
	ECT6	-5.47	0.9621	1.051	0.010	-5.75	0.9602
	ECT7	-5.30	0.9632	1.083	0.011	-5.74	0.9603
Reflector	ECR8	-5.11	0.9645	1.125	0.012	-5.75	0.9602
	EC9R	-5.44	0.9623	1.116	0.018	-6.07	0.9581
Average	---	-7.11	0.9515	---	---	-6.17	0.9574

Table XII. Spatial correction factors for the U-235 detectors in the YALINA configuration with 36% enriched fuel in fast zone and 1185 or 802 EK-10 fuel rods in thermal zone

Confg.	Det.	Thermal zone			Moderator				Reflector	
		EC1B	EC2B	EC3B	EC5T	EC6T	EC7T	MC5	EC8R	EC9R
36%-1185 (D,D) k^{MCNP} =0.9750	*f*(U-235)	0.582	0.639	0.845	0.919	1.03	1.07	1.05	1.08	1.04
	Δ_f	0.011	0.012	0.017	0.013	0.014	0.015	0.018	0.015	0.022
	f(He-3)	0.688	0.764	0.868	0.919	1.03	1.07	1.05	1.08	1.05
	Δ_f	0.029	0.03	0.02	0.013	0.014	0.015	0.017	0.015	0.022
36%-802 (D,D) k^{MCNP} =0.8807	*f*(U-235)	0.467	0.469	0.799	0.988	1.19	1.25	---	1.28	1.21
	Δ_f	0.030	0.034	0.032	0.055	0.061	0.066	---	0.033	0.038

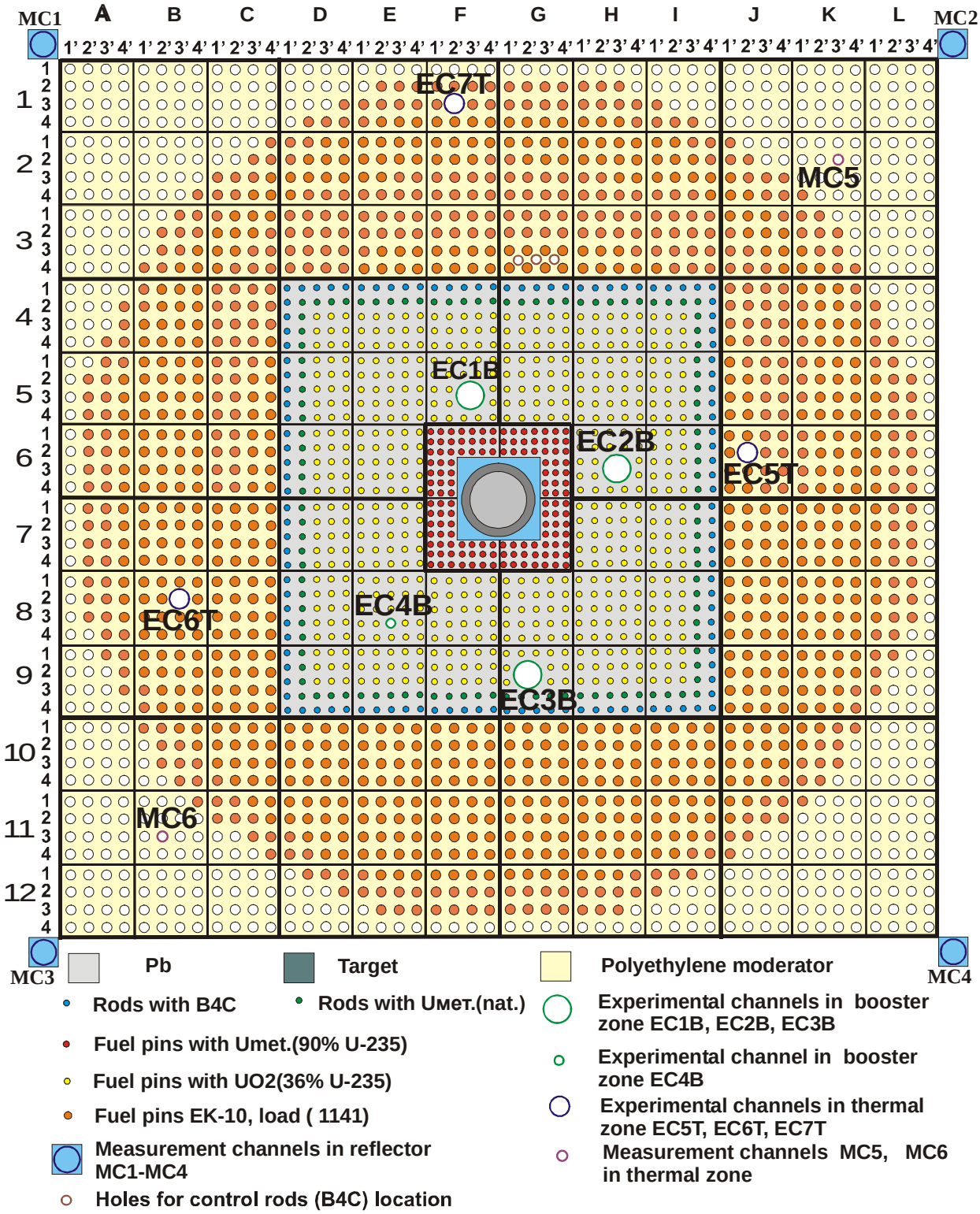

Figure 1. Fuel loading of YALINA-Booster configuration with 1141 EK-10 fuel rods in the thermal zone

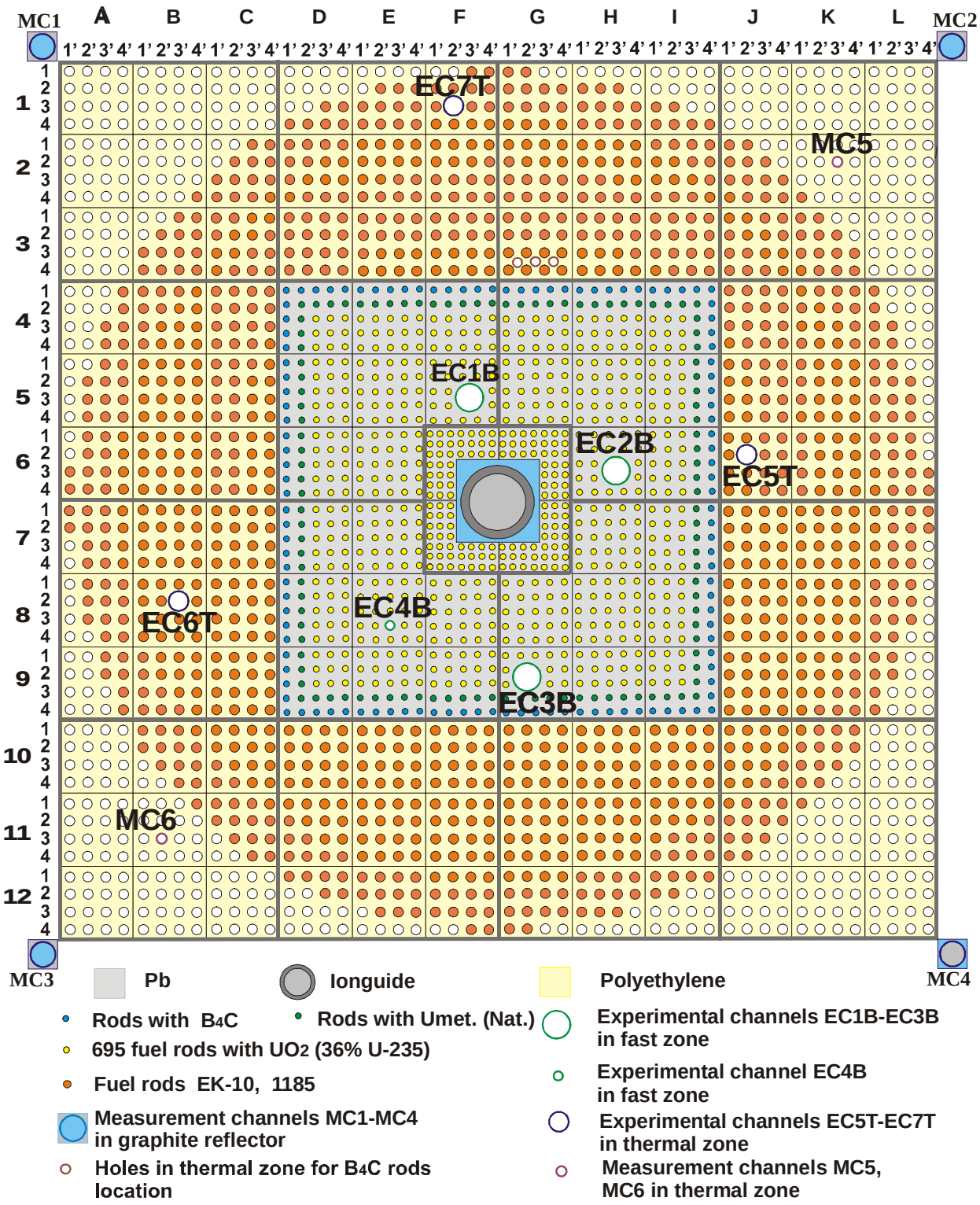

Figure 2. Fuel loading of YALINA-Booster configuration with 1185 EK-10 fuel rods in the thermal zone

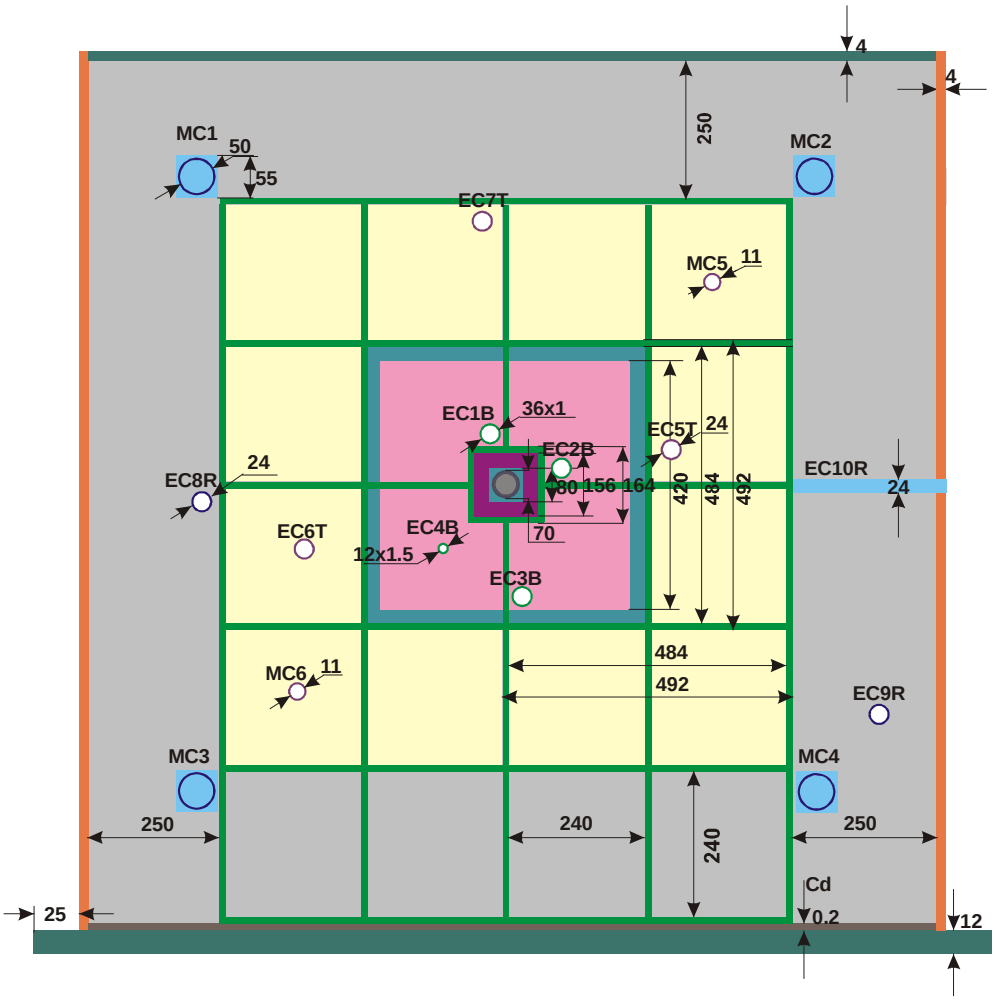

Umet. of 90% enrichment

UO2 of 36% enrichment

Thermal neutron absorber Umet.(nat)+B4C

Thermal zone

Air

Organic glass

Graphite reflector

Cd layer

Stainless steel frame

Mild (low carbon) steel

EC1B - EC4B - experimental channels in booster zone

EC5T - EC7T - experimental channels in thermal zone

EC8R - EC10R - experimental channels in reflector

MC1 - MC4 - measurement channels in reflector for neutron flux monitoring

MC5 – MC6 - experimental channels in the thermal zone for neutron flux monitoring

At the back side of the assembly, the experimental channels do not penetrate the borated polyethylene or the organic glass.

EC8R (-52, -3.2), EC9R (60, -35.6), EC11RT New (-4.2, Reflector and Poly, diameter 1 cm)

Figure 3. X-Y cross-sectional view of the YALINA-Booster assembly, dimensions in mm

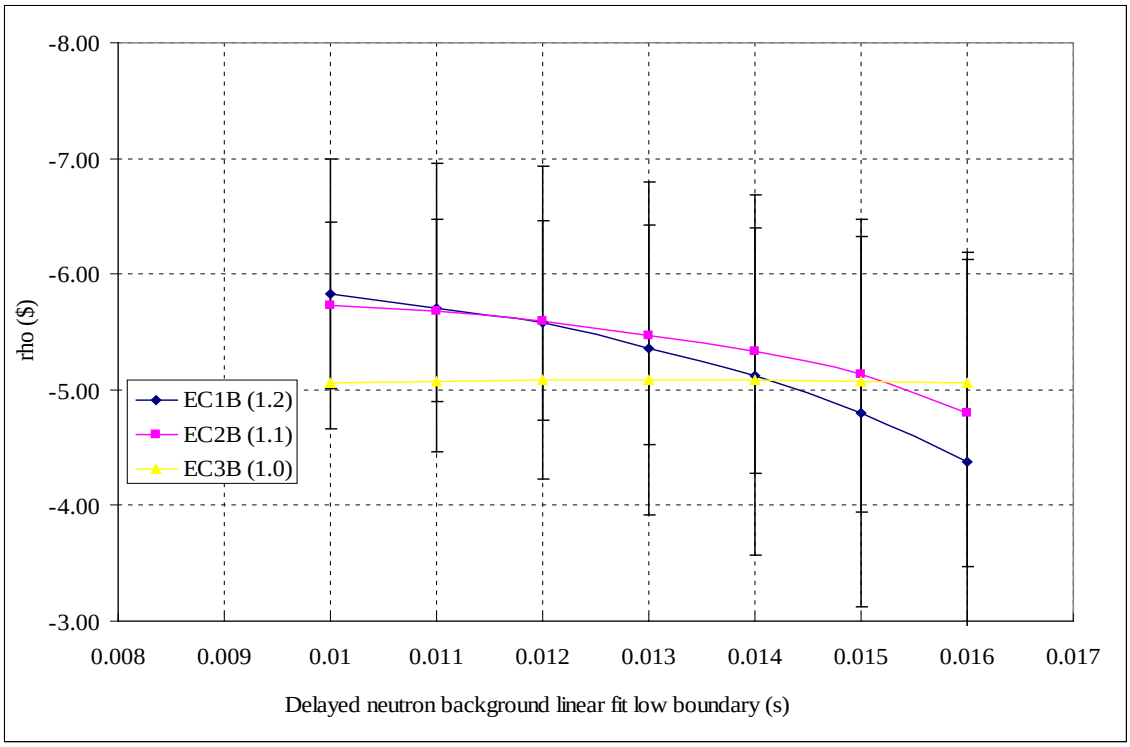

Figure 4. Obtained reactivities for YANLINA configuration with 36% enriched uranium in the fast zone and 1185 EK-10 fuel rods in the thermal zone as function of the fitting intervals for the delayed neutron background of EC1B, EC2B, and EC3B channels

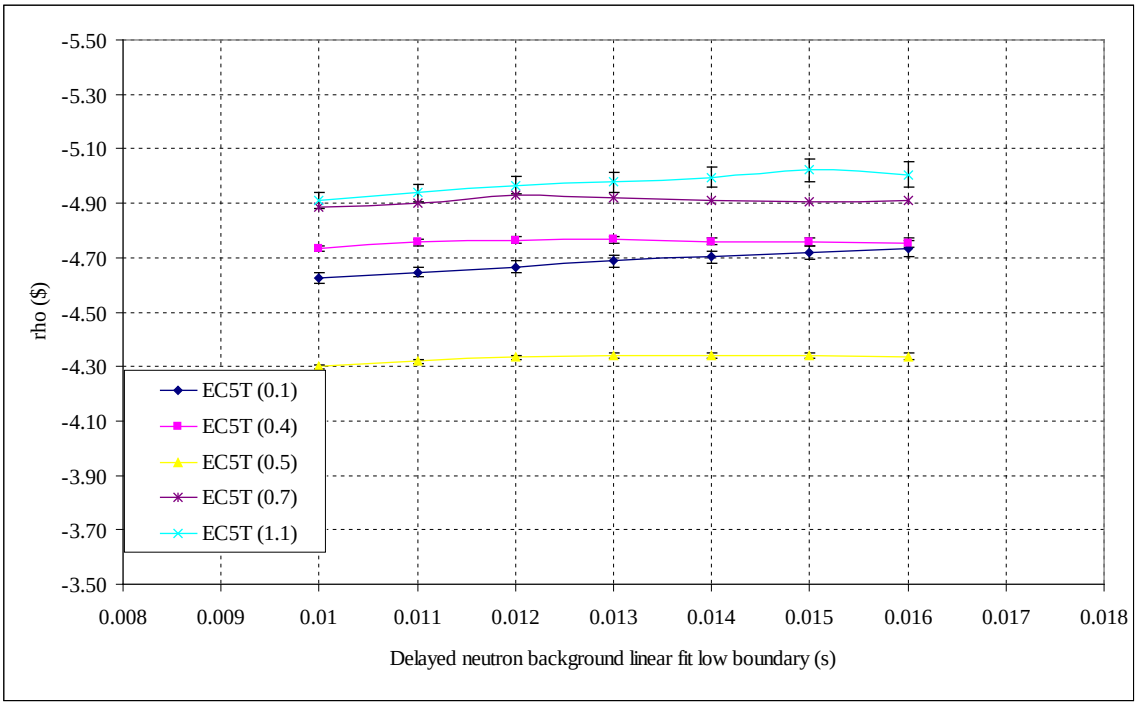

Figure 5. Obtained reactivities for YALINA configuration with 36% enriched uranium in the fast zone and 1185 EK-10 fuel rods in the thermal zone as a function of the fitting intervals for the delayed neutron background for EC5T channel

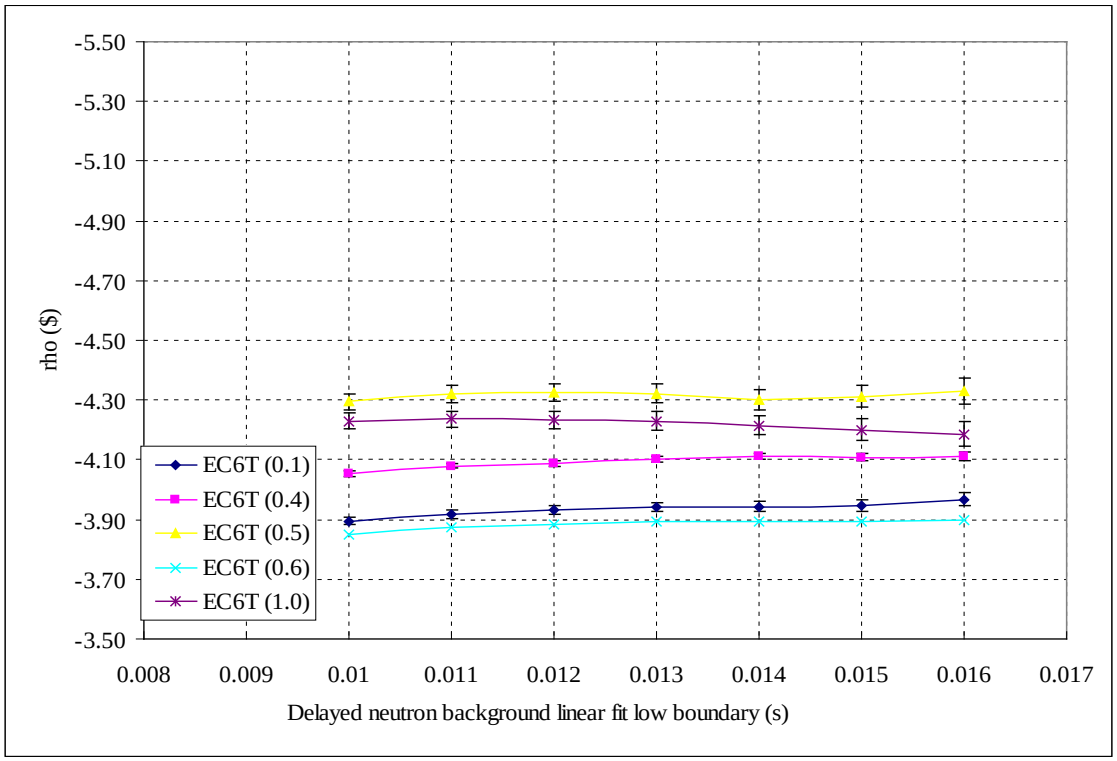

Figure 6. Obtained reactivities for YALINA configuration with 36% enriched uranium in the fast zone and 1185 EK-10 fuel rods in the thermal zone as a function of the fitting intervals for the delayed neutron background for EC6T channel

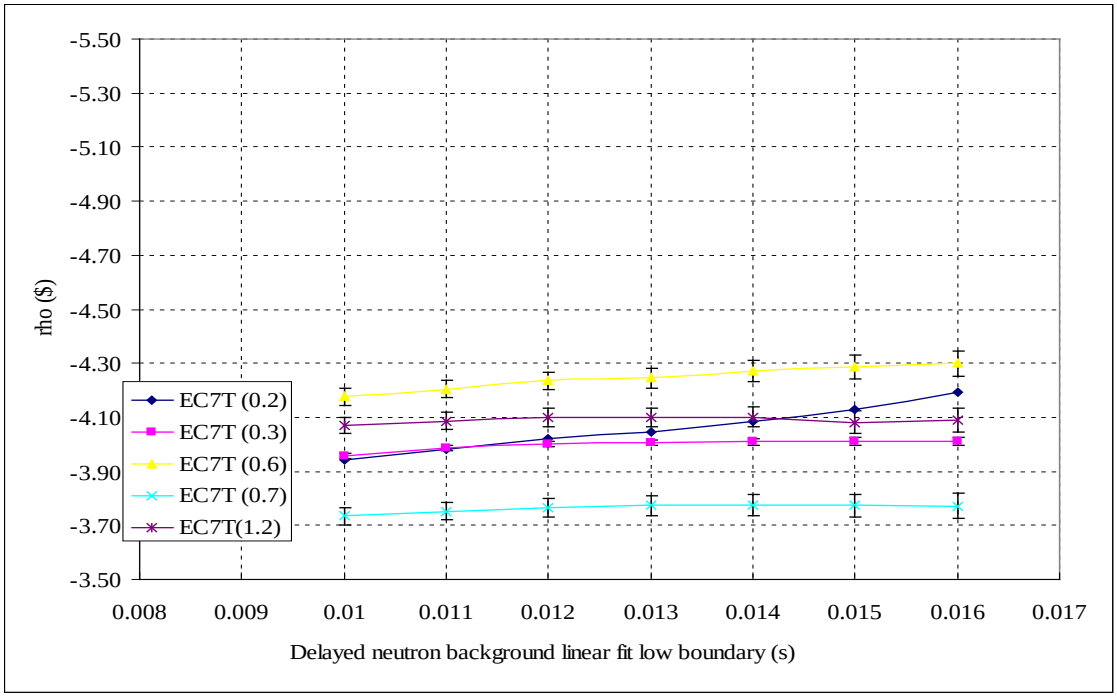

Figure 7. Obtained reactivities for YALINA configuration with 36% enriched uranium in the fast zone and 1185 EK-10 fuel rods in the thermal zone as a function of the fitting intervals for the delayed neutron background for EC7T channel

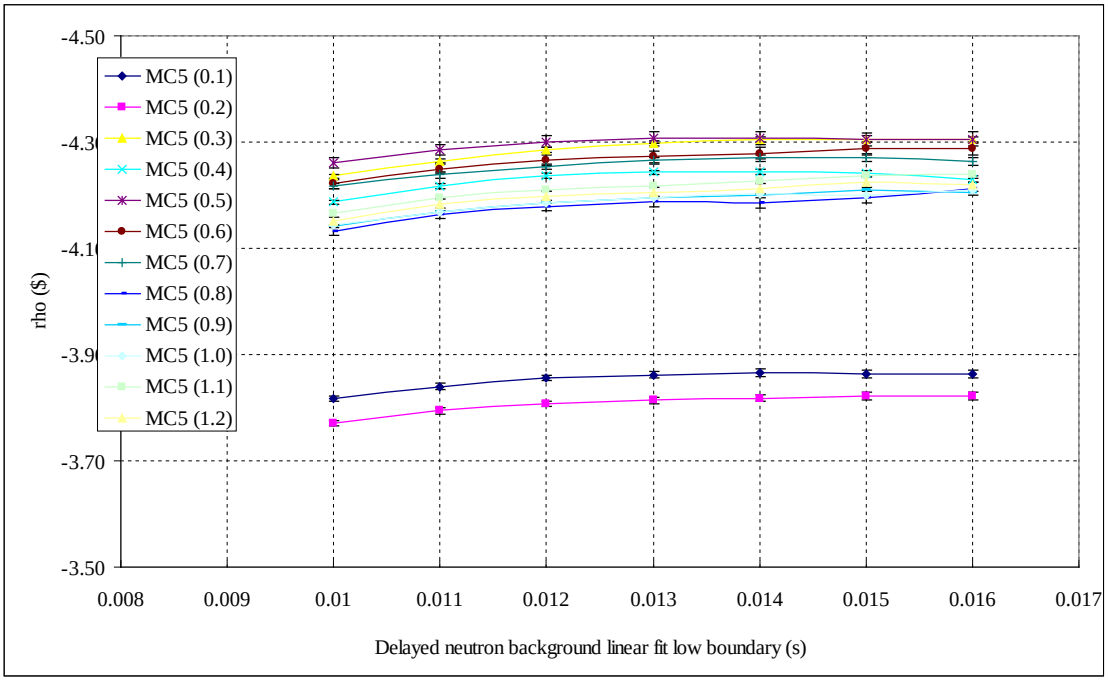

Figure 8. Obtained reactivities for YALINA configuration with 36% enriched uranium in the fast zone and 1185 EK-10 fuel rods in the thermal zone as a function of the fitting intervals for the delayed neutron background for MC5 channel

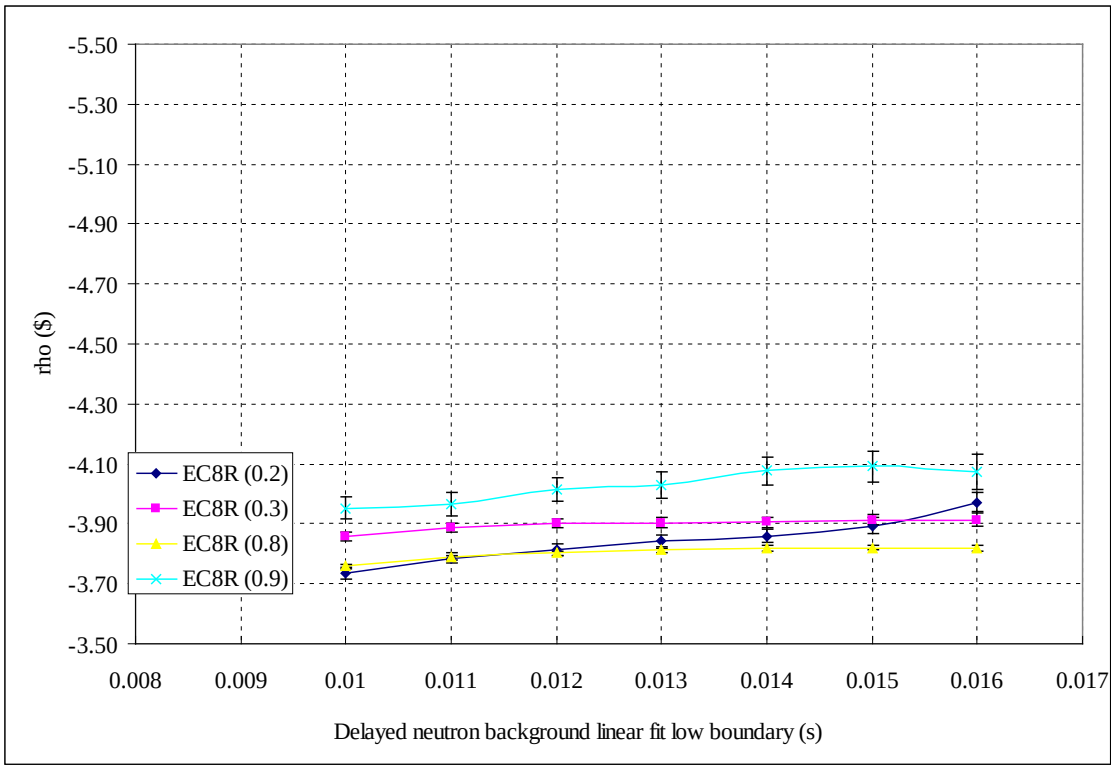

Figure 9. Obtained reactivities for YALINA configuration with 36% enriched uranium in the fast zone and 1185 EK-10 fuel rods in the thermal zone as a function of the fitting intervals for the delayed neutron background for EC8R channel

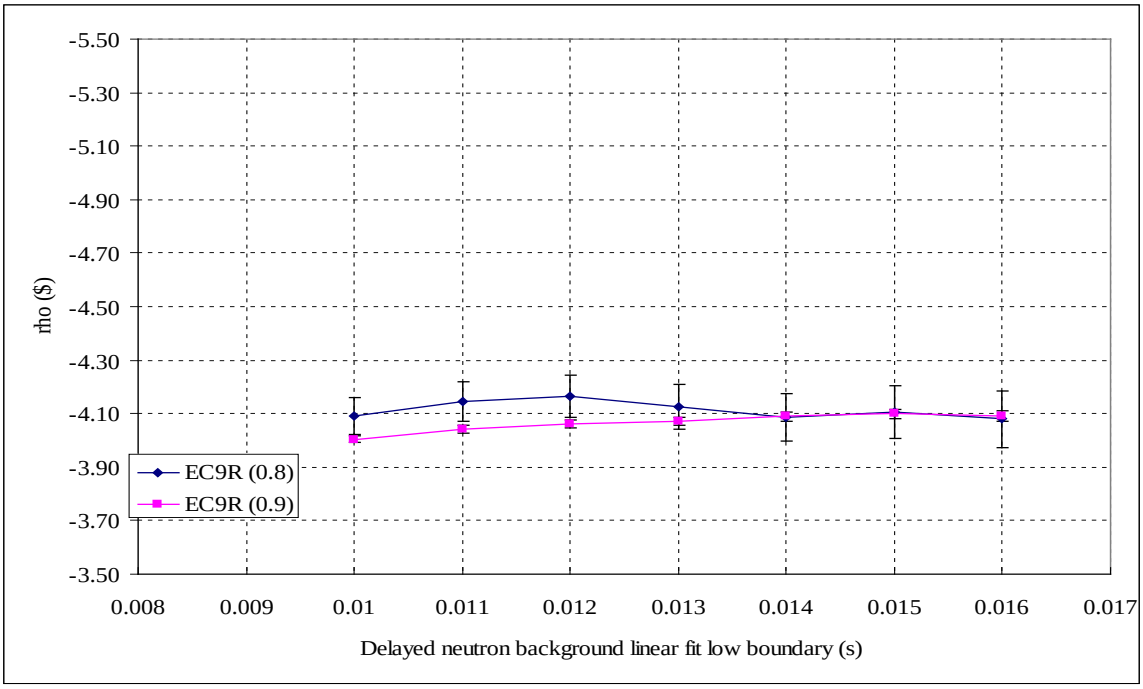

Figure 10. Obtained reactivities for YALINA configuration with 36% enriched uranium in the fast zone and 1185 EK-10 fuel rods in the thermal zone as a function of the fitting intervals for the delayed neutron background for EC9R channel

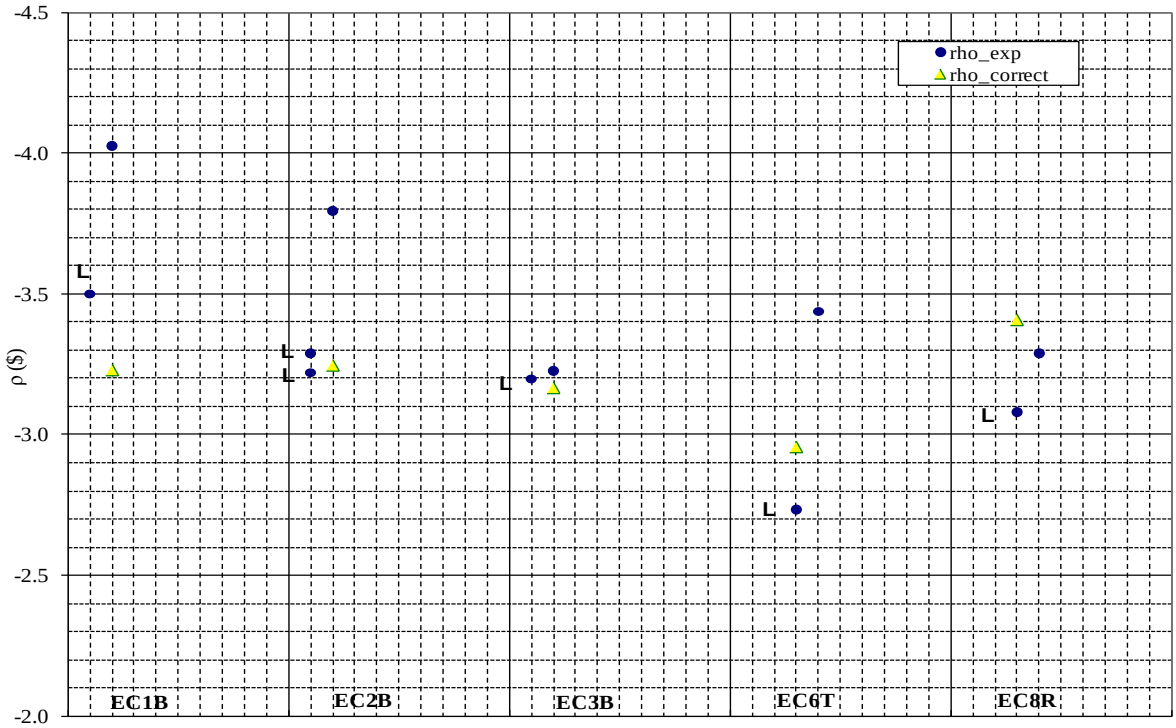

Figure 11. Uncorrected and spatially corrected reactivities from the pulsed-neutron experiments for YALINA configuration with 90% enriched fuel in the fast zone and 1141 EK-10 fuel rods in the thermal zone

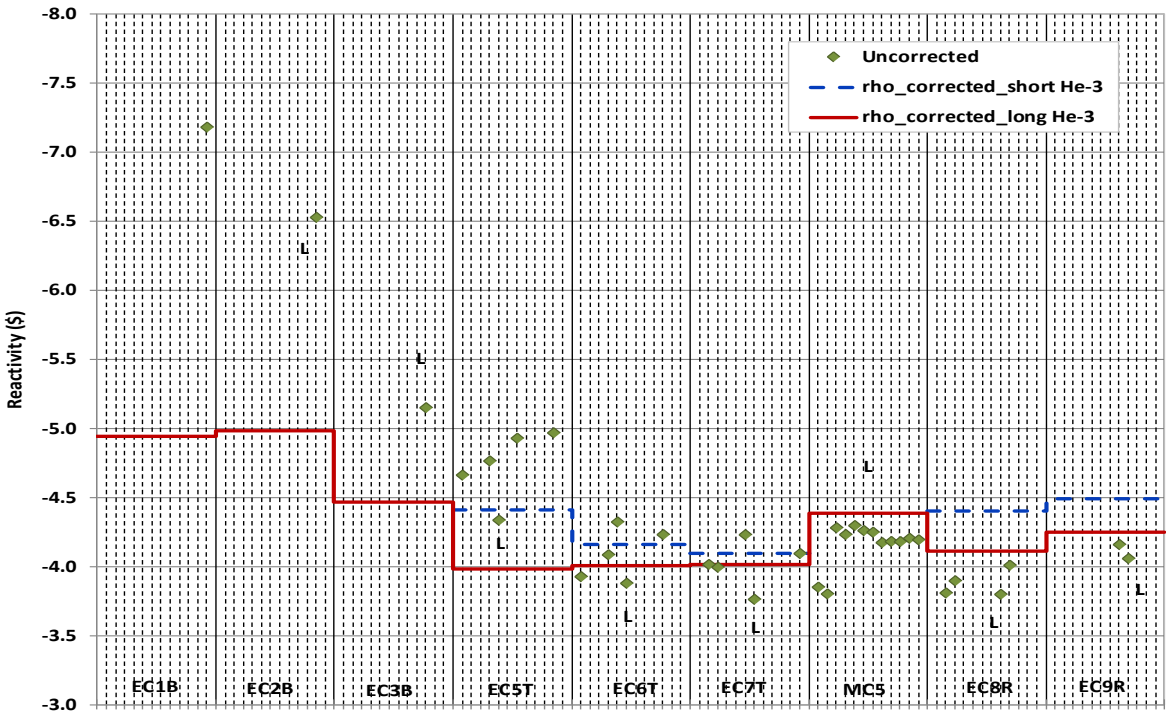

Figure 12. Uncorrected and spatially corrected reactivities from the pulsed-neutron experiments for YALINA configuration with 36% enriched fuel in the fast zone and 1185 EK-10 fuel rods in the thermal zone

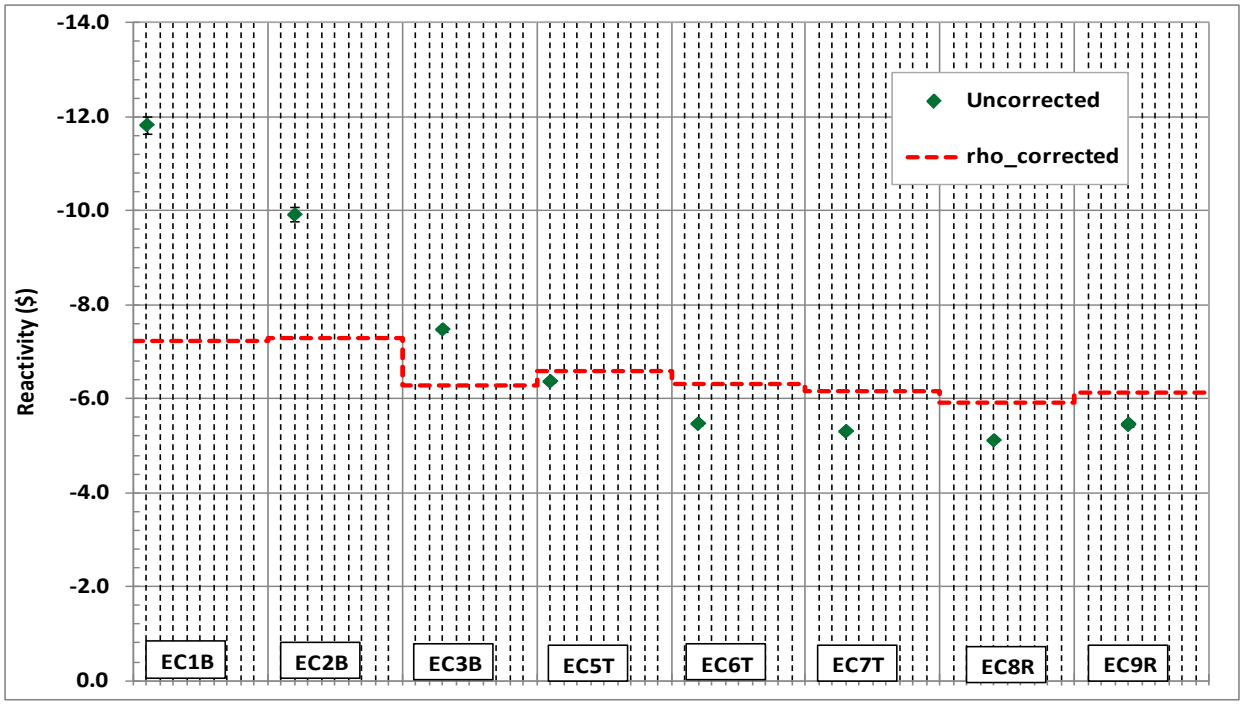

Figure 13. Uncorrected and spatially corrected reactivities from the pulsed-neutron experiments for YALINA configuration with 21% enriched fuel in the fast zone and 1185 EK-10 fuel rods in the thermal zone with CR out in Dec-03-2009

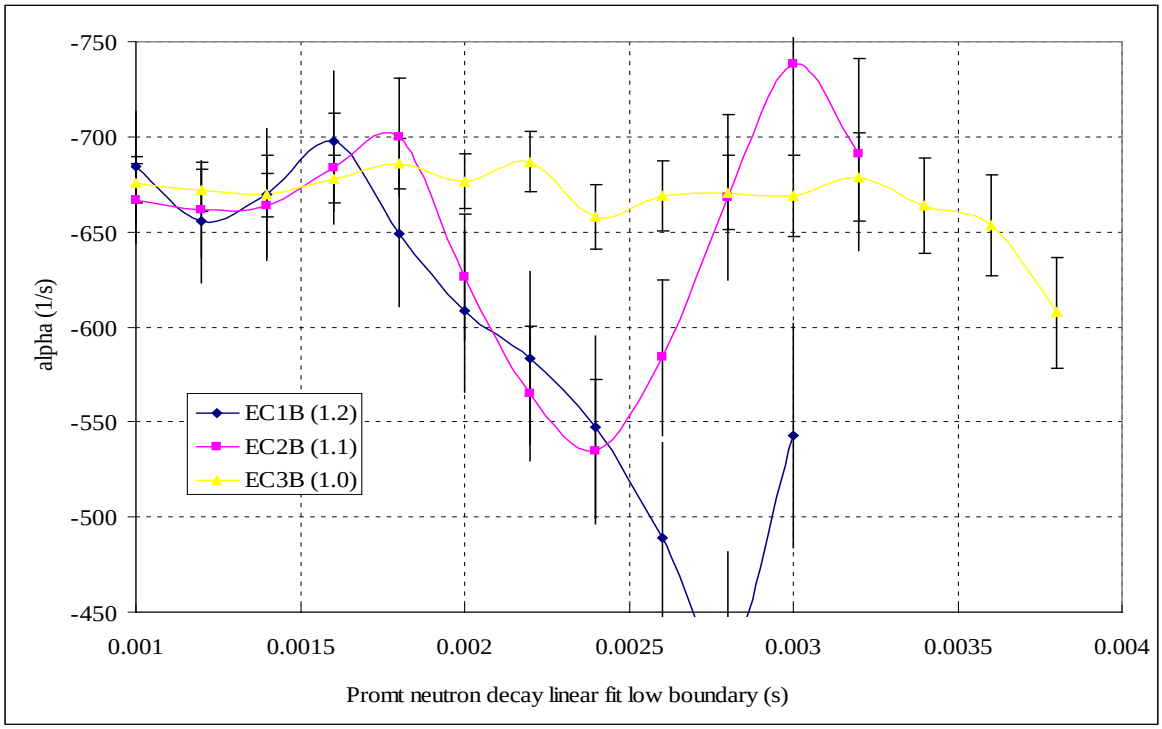

Figure 14. Prompt neutron decay constant α as a function of the fitting intervals for EC1B, EC2B, and EC3B channels for YALINA configuration with 36% enriched fuel in the fast zone and 1185 EK-10 fuel rods in the thermal zone

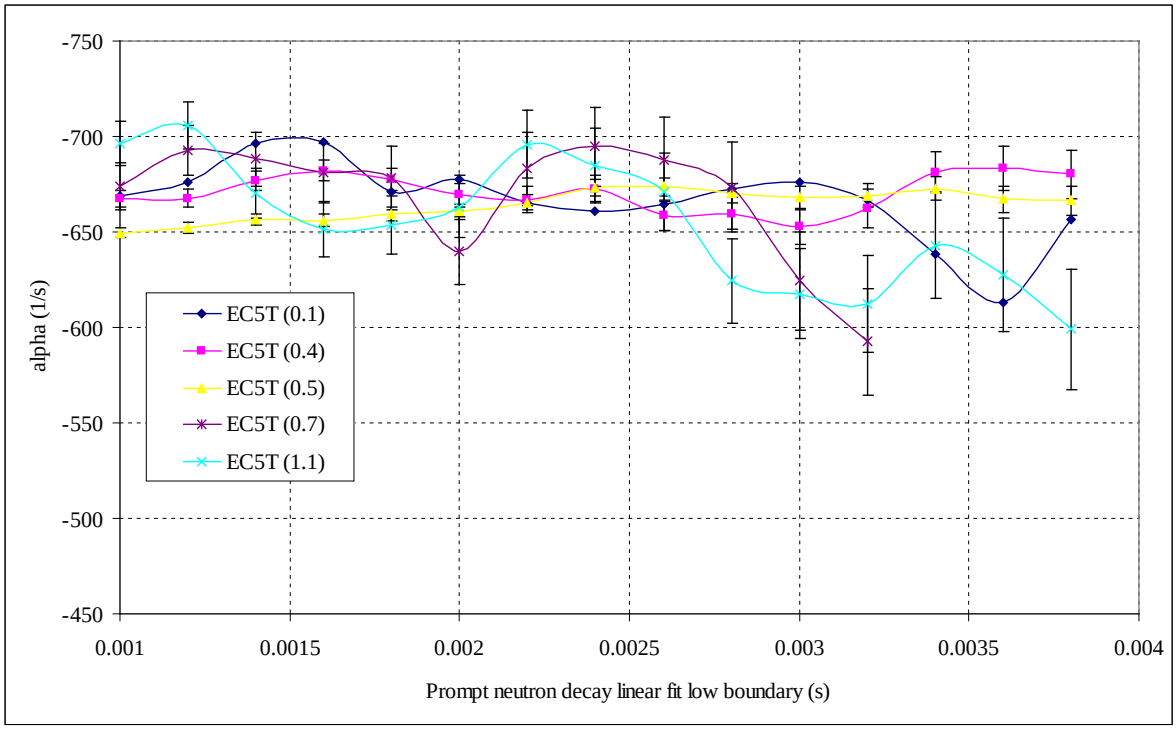

Figure 15. Prompt neutron decay constant α as a function of the fitting intervals for EC5T channel for YALINA configuration with 36% enriched fuel in the fast zone and 1185 EK-10 fuel rods in the thermal zone

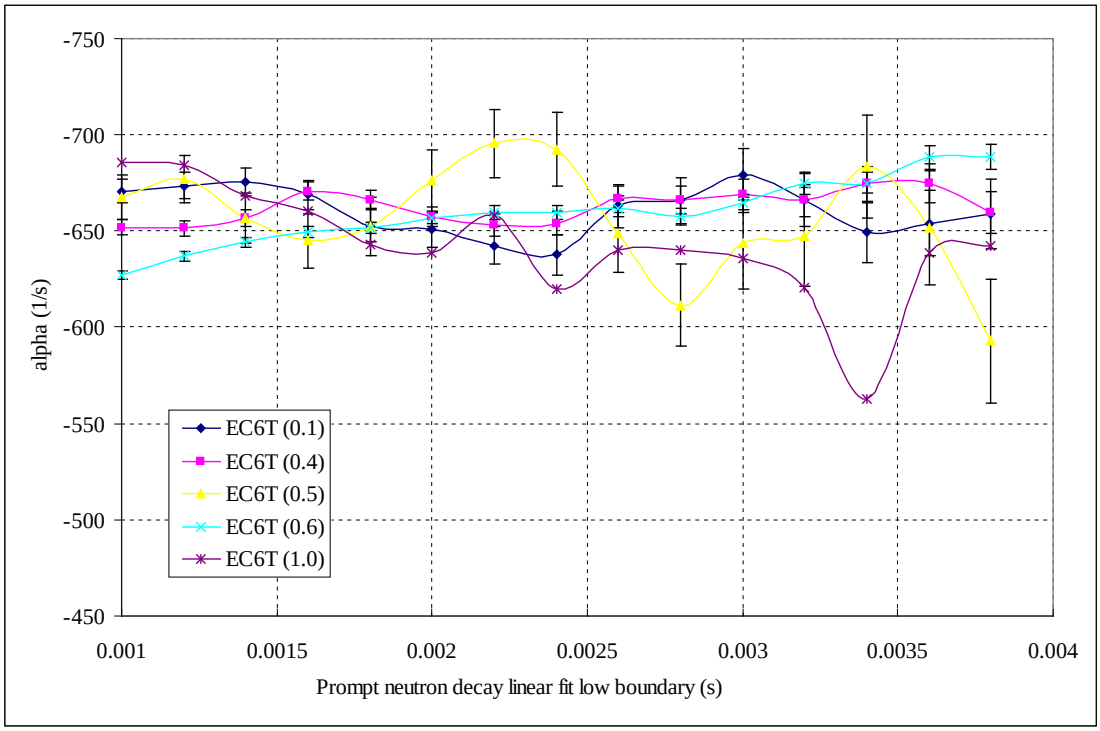

Figure 16. Prompt neutron decay constant α as a function of the fitting intervals for EC6T channel for YALINA configuration with 36% enriched fuel in the fast zone and 1185 EK-10 fuel rods in the thermal zone

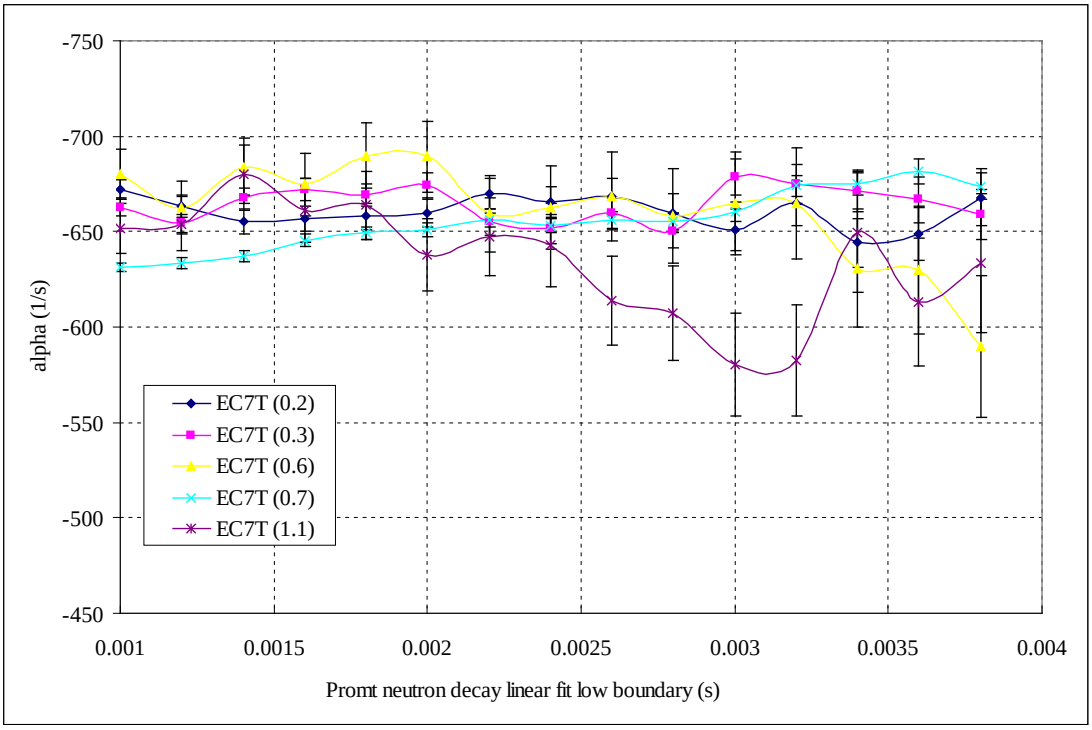

Figure 17. Prompt neutron decay constant α as a function of the fitting intervals for EC7T channel for YALINA configuration with 36% enriched fuel in the fast zone and 1185 EK-10 fuel rods in the thermal zone

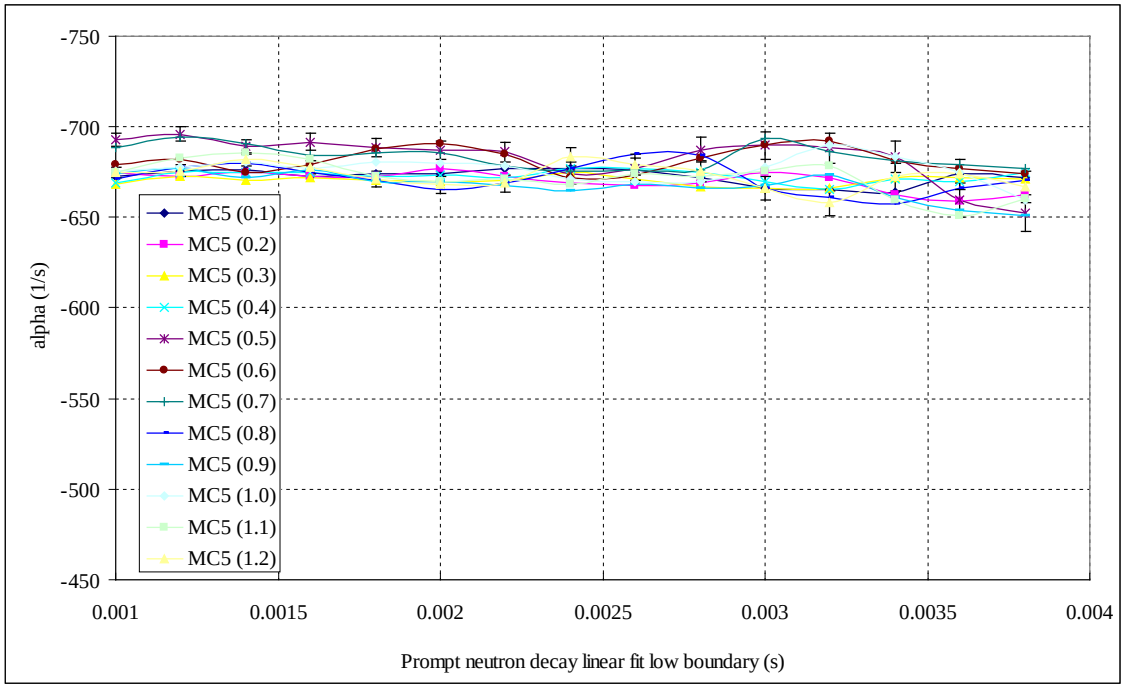

Figure 18. Prompt neutron decay constant α as a function of the fitting intervals for MC5 channel for YALINA configuration with 36% enriched fuel in the fast zone and 1185 EK-10 fuel rods in the thermal zone

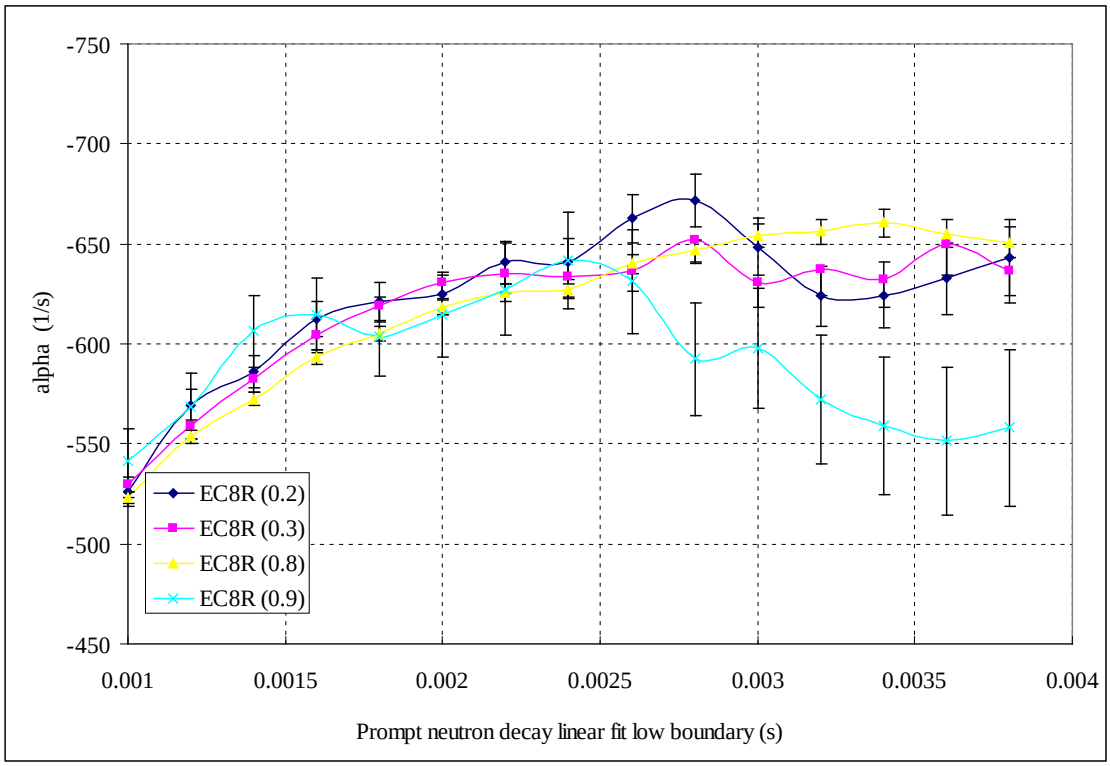

Figure 19. Prompt neutron decay constant α as a function of the fitting intervals for EC8R channel for YALINA configuration with 36% enriched fuel in the fast zone and 1185 EK-10 fuel rods in the thermal zone

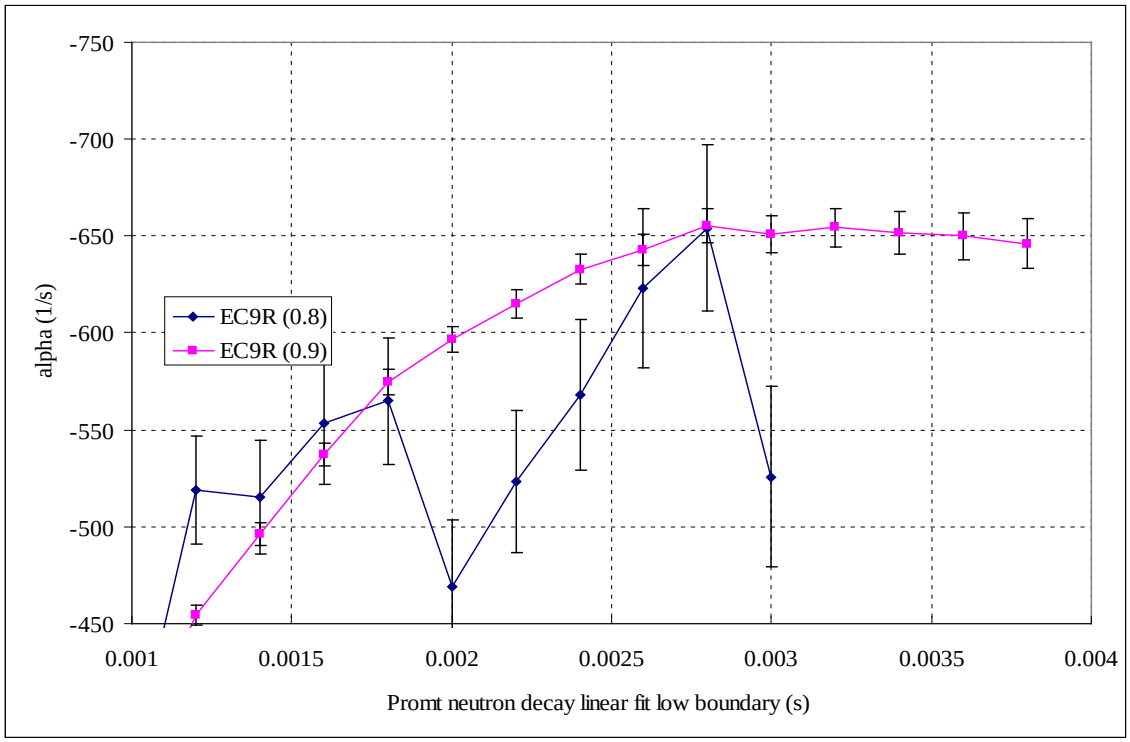

Figure 20. Prompt neutron decay constant α as a function of the fitting intervals for EC9R channel for YALINA configuration with 36% enriched fuel in the fast zone and 1185 EK-10 fuel rods in the thermal zone

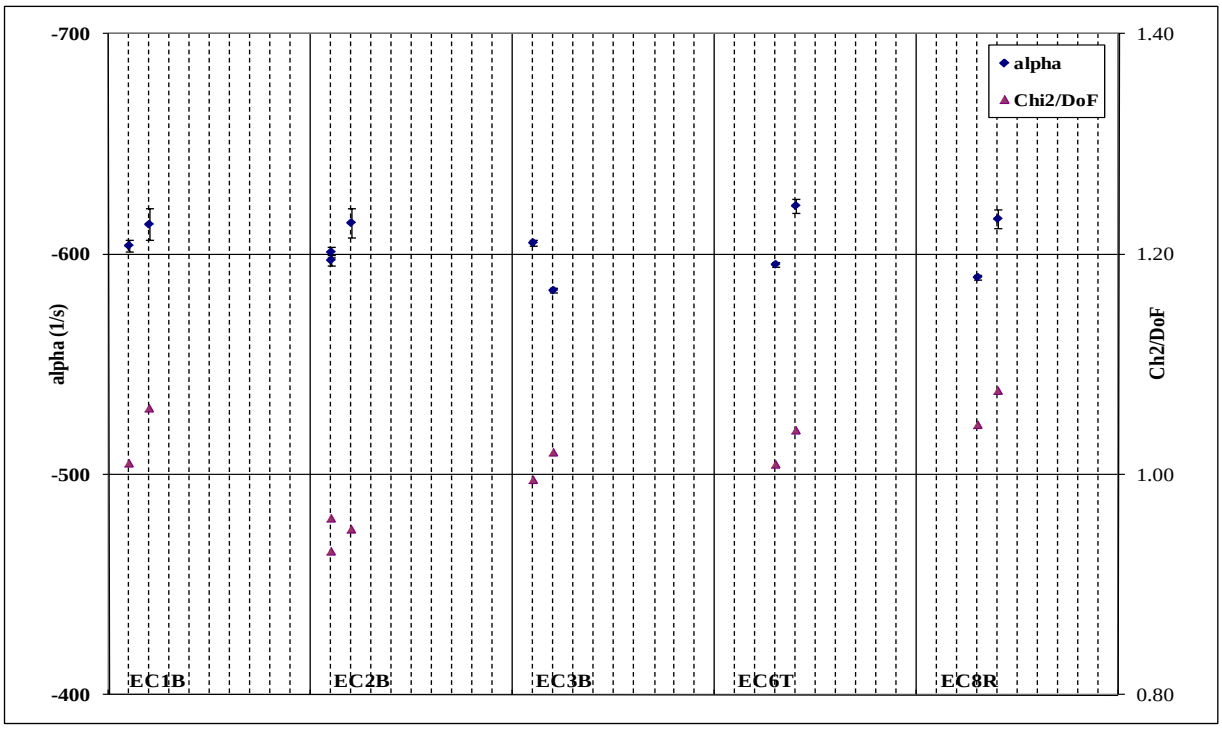

Figure 21. Prompt decay constant α obtained from the pulsed-neutron experiment of YALINA configuration with 90% enriched uranium fuel in the fast zone and 1141 EK-10 fuel rods in the thermal zone

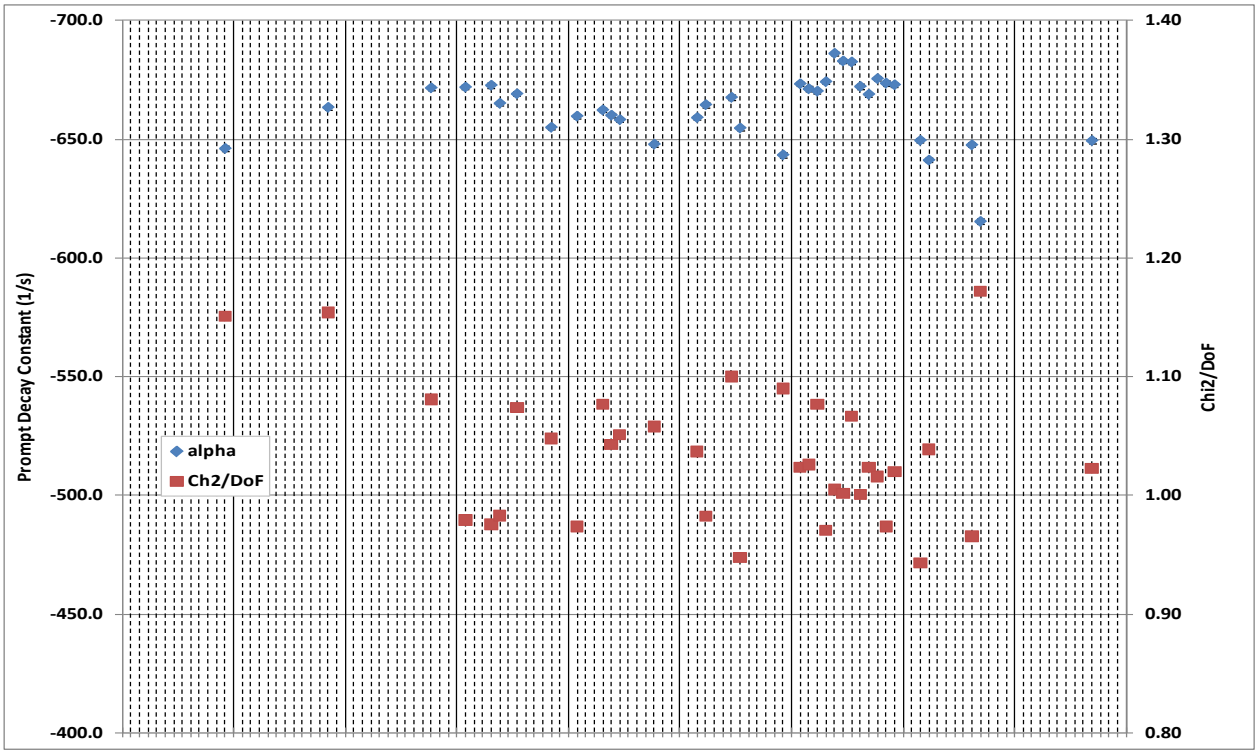

Figure 22. Prompt decay constant α obtained from the pulsed-neutron experiment of YALINA configuration with 36% enriched uranium fuel in the fast zone and 1185 EK-10 fuel rods in the thermal zone

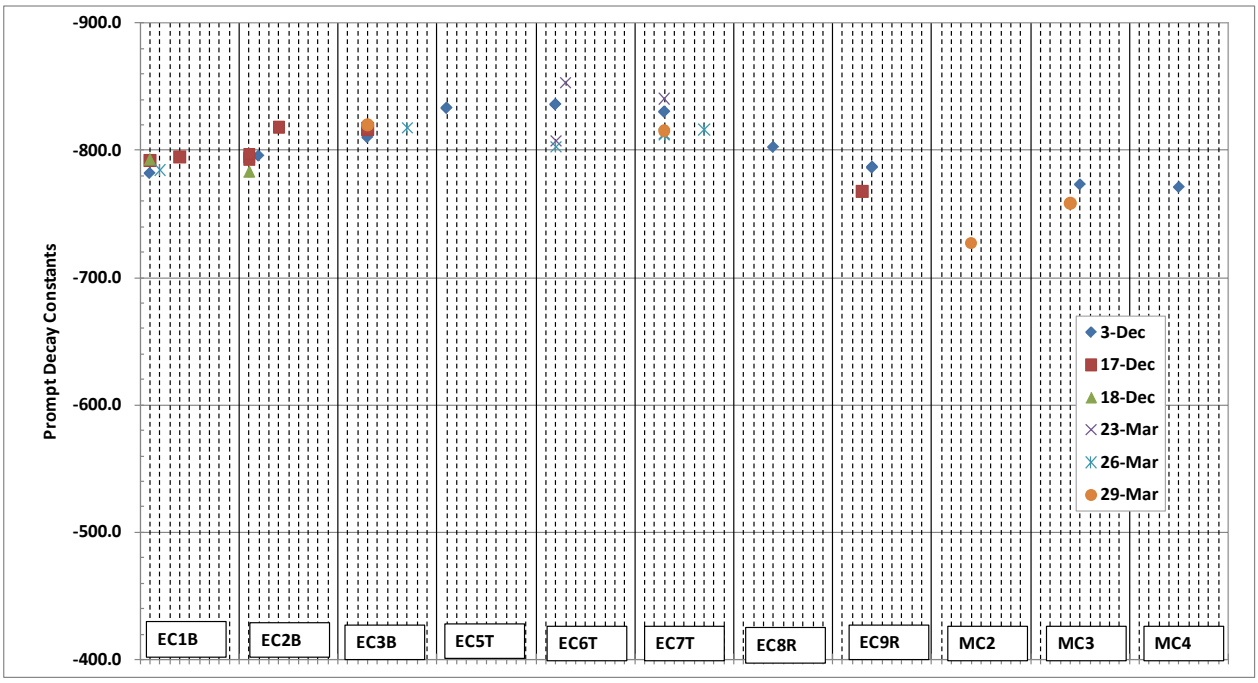

Figure 23. Prompt decay constant α obtained from the pulsed-neutron experiment of YALINA configuration with 21% enriched uranium fuel in the fast zone and 1185 EK-10 fuel rods in the thermal zone with CR out

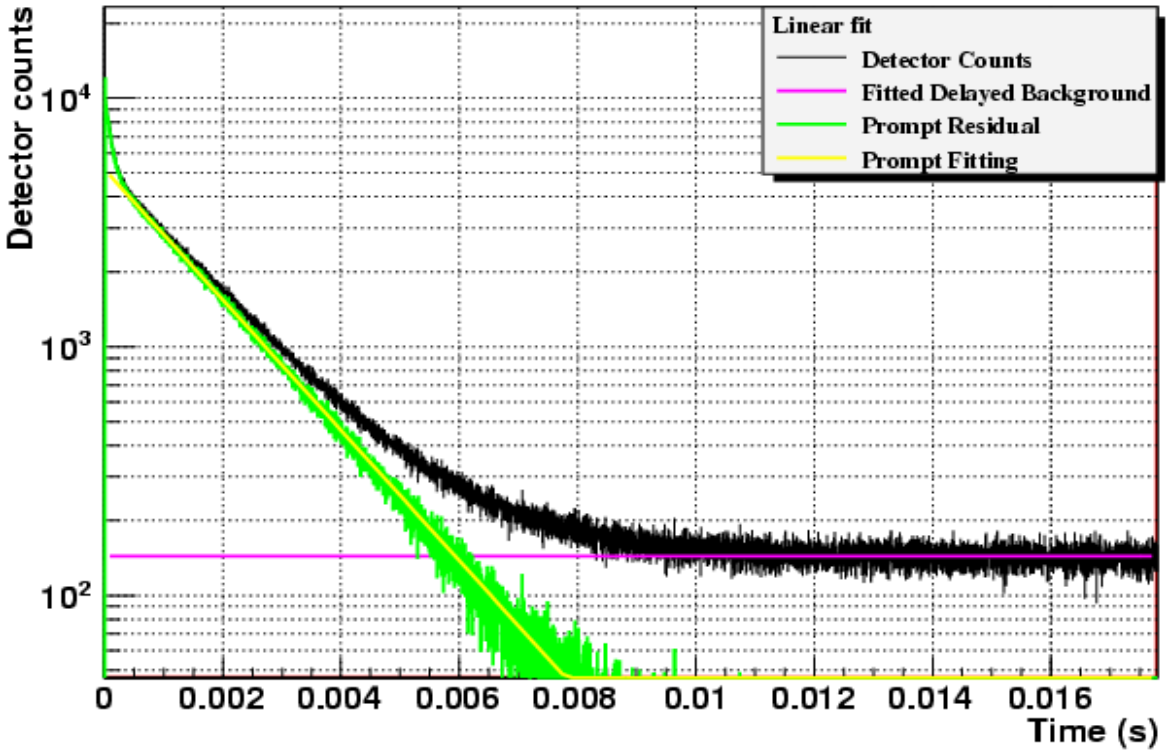

Figure 24. Linear fit of the pulsed neutron experiment recorded by long He-3 detector in EC1B channel of YALINA configuration with 90% enriched fuel in the fast zone and 1141 EK-10 fuel rods in the thermal zone in batch 0.1

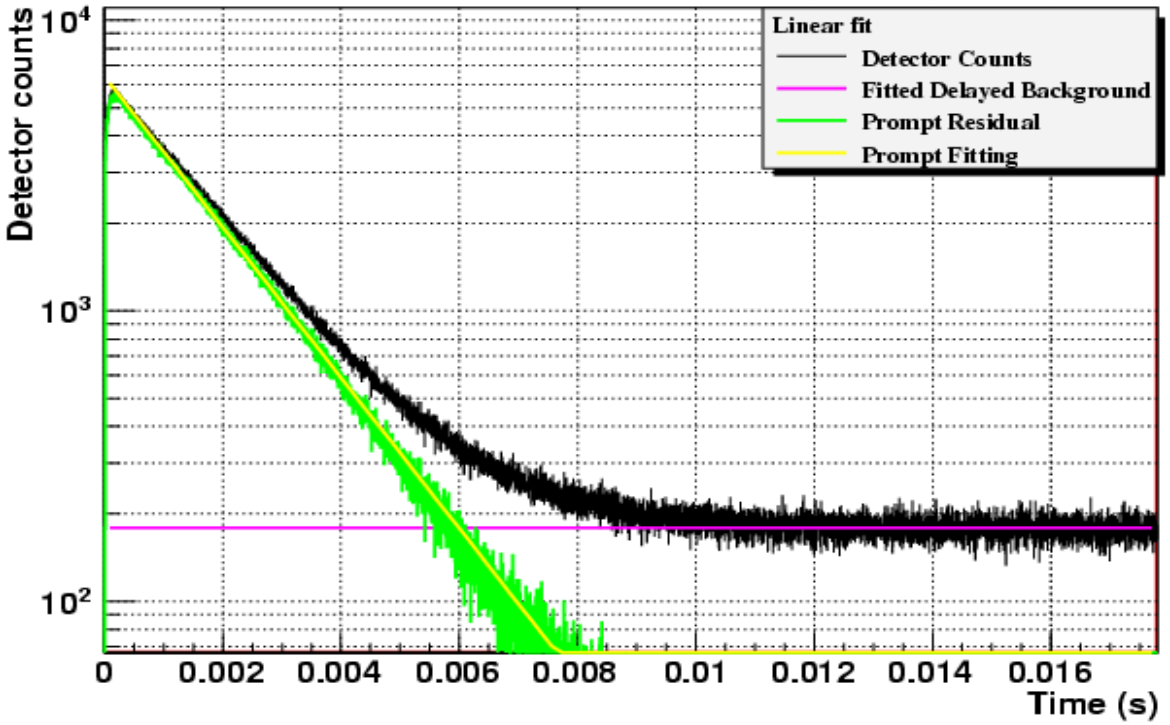

Figure 25. Linear fit of the pulsed neutron experiment recorded by long He-3 detector in EC2B channel of YALINA configuration with 90% enriched fuel in the fast zone and 1141 EK-10 fuel rods in the thermal zone in batch 0.1

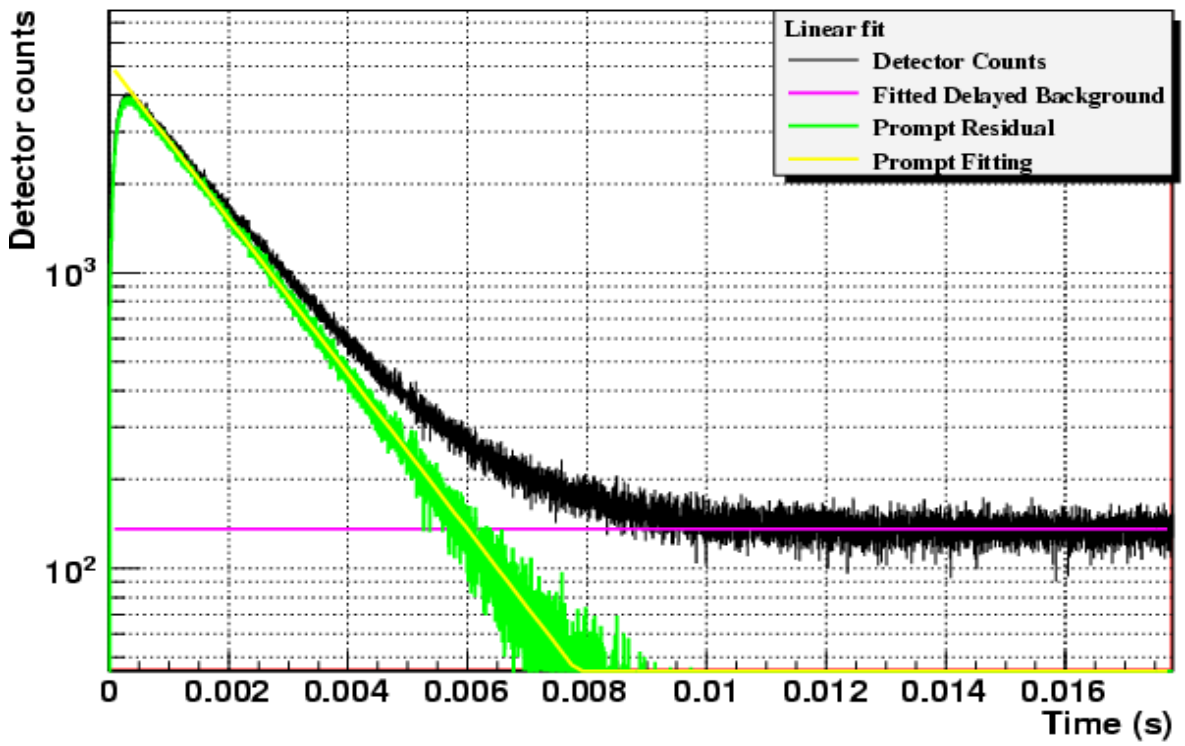

Figure 26. Linear fit of the pulsed neutron experiment recorded by long He-3 detector in EC3B channel of YALINA configuration with 90% enriched fuel in the fast zone and 1141 EK-10 fuel rods in the thermal zone in batch 0.1

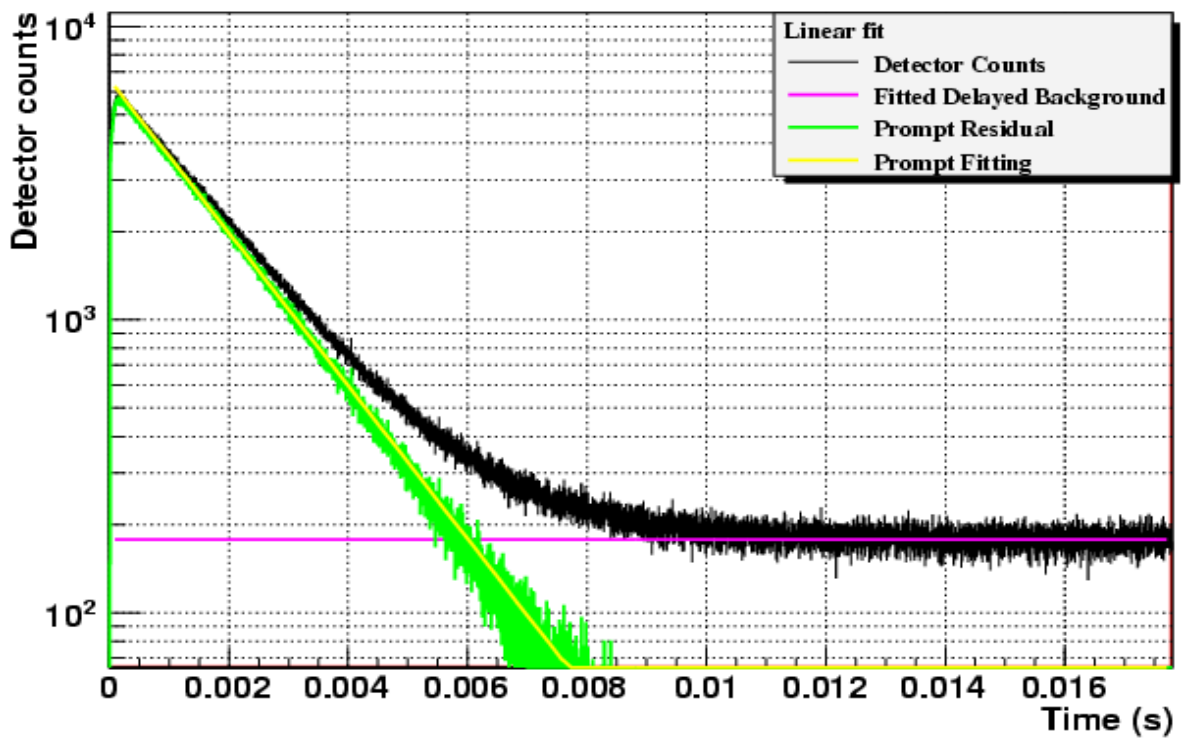

Figure 27. Linear fit of the pulsed neutron experiment recorded by long He-3 detector in EC2B channel of YALINA configuration with 90% enriched fuel in the fast zone and 1141 EK-10 fuel rods in the thermal zone in batch 0.1

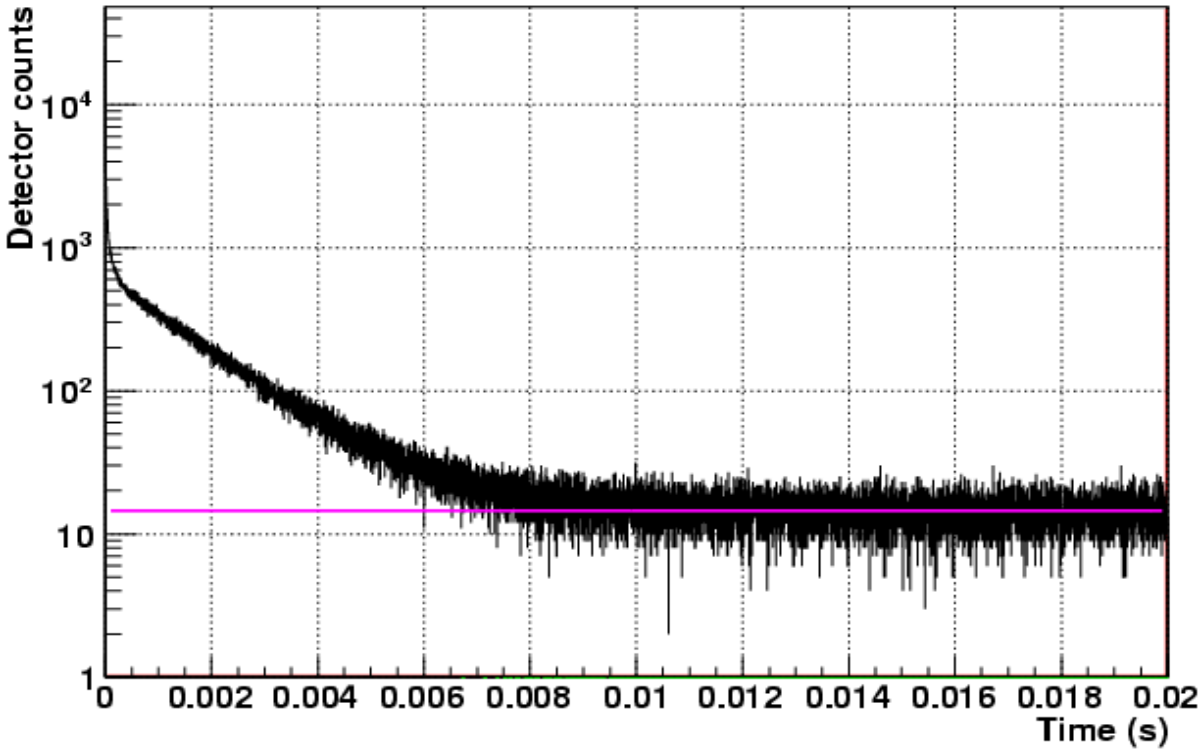

Figure 28. Linear fit of the pulsed neutron experiment recorded by small He-3 detector in EC1B channel of YALINA configuration with 90% enriched fuel in the fast zone and 1141 EK-10 fuel rods in the thermal zone in batch 0.2

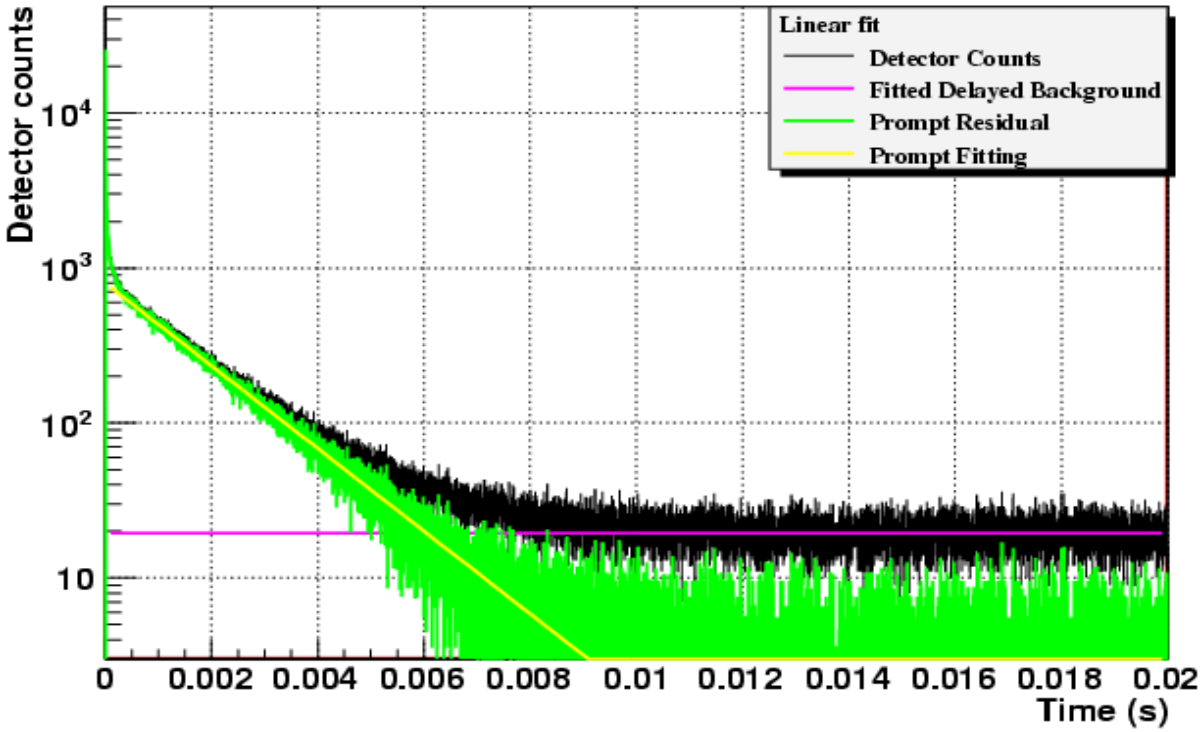

Figure 29. Linear fit of the pulsed neutron experiment recorded by small He-3 detector in EC2B channel of YALINA configuration with 90% enriched fuel in the fast zone and 1141 EK-10 fuel rods in the thermal zone in batch 0.2

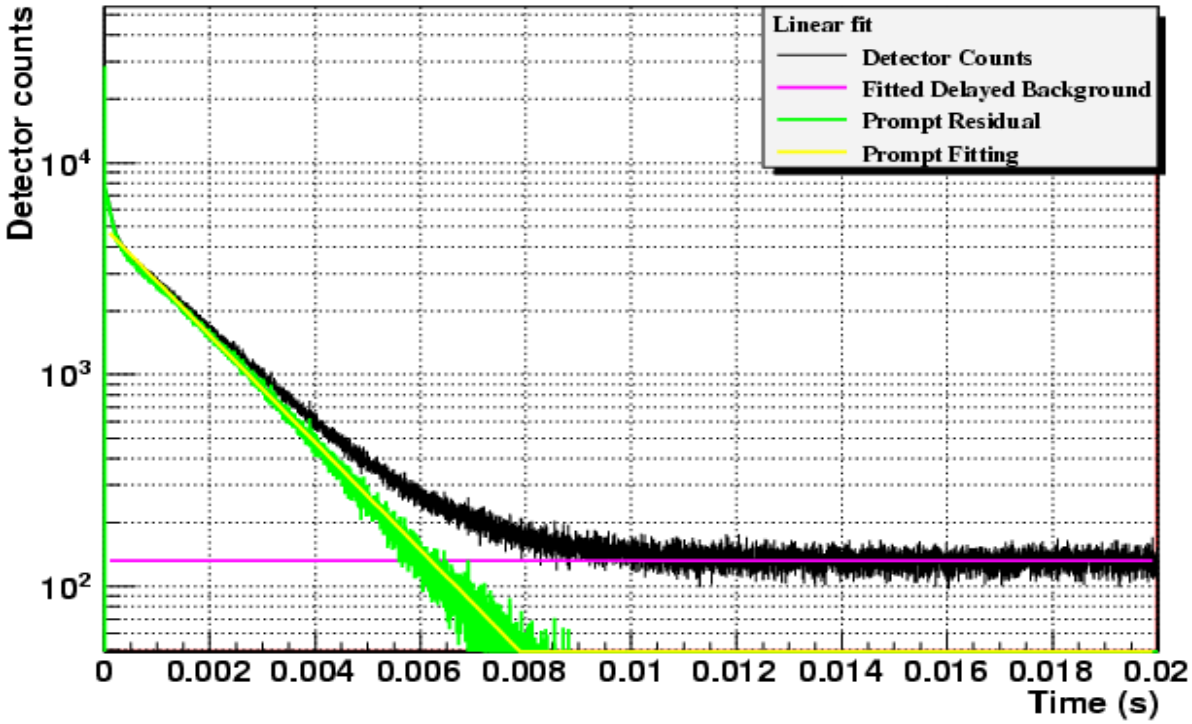

Figure 30. Linear fit of the pulsed neutron experiment recorded by small He-3 detector in EC3B channel of YALINA configuration with 90% enriched fuel in the fast zone and 1141 EK-10 fuel rods in the thermal zone in batch 0.2

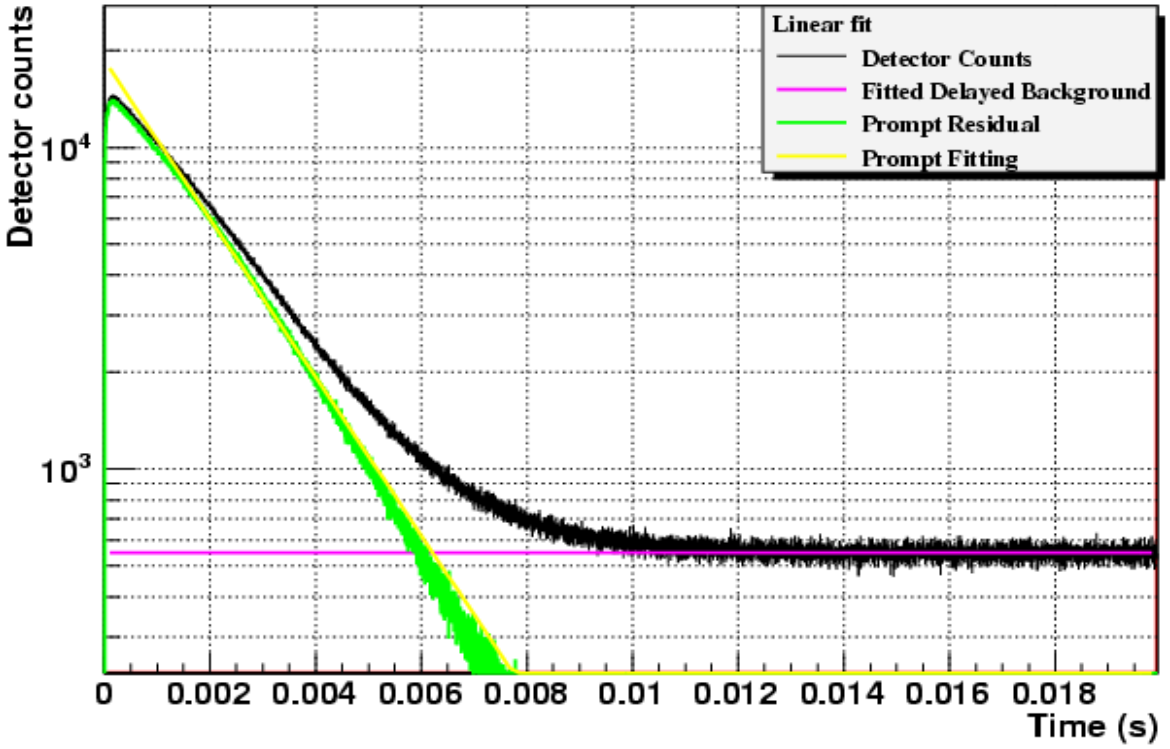

Figure 31. Linear fit of the pulsed neutron experiment recorded by long He-3 detector in EC6T channel of YALINA configuration with 90% enriched fuel in the fast zone and 1141 EK-10 fuel rods in the thermal zone in batch 0.3

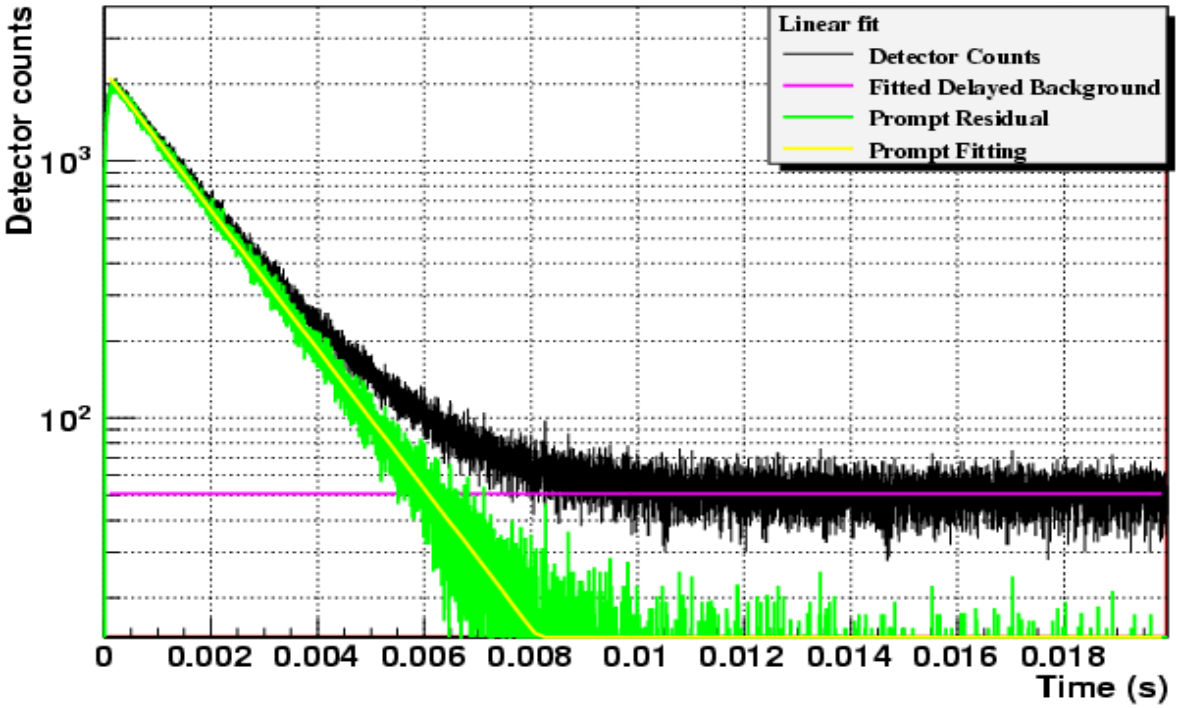

Figure 32. Linear fit of the pulsed neutron experiment recorded by small He-3 detector in EC6T channel of YALINA configuration with 90% enriched fuel in the fast zone and 1141 EK-10 fuel rods in the thermal zone in batch 0.4

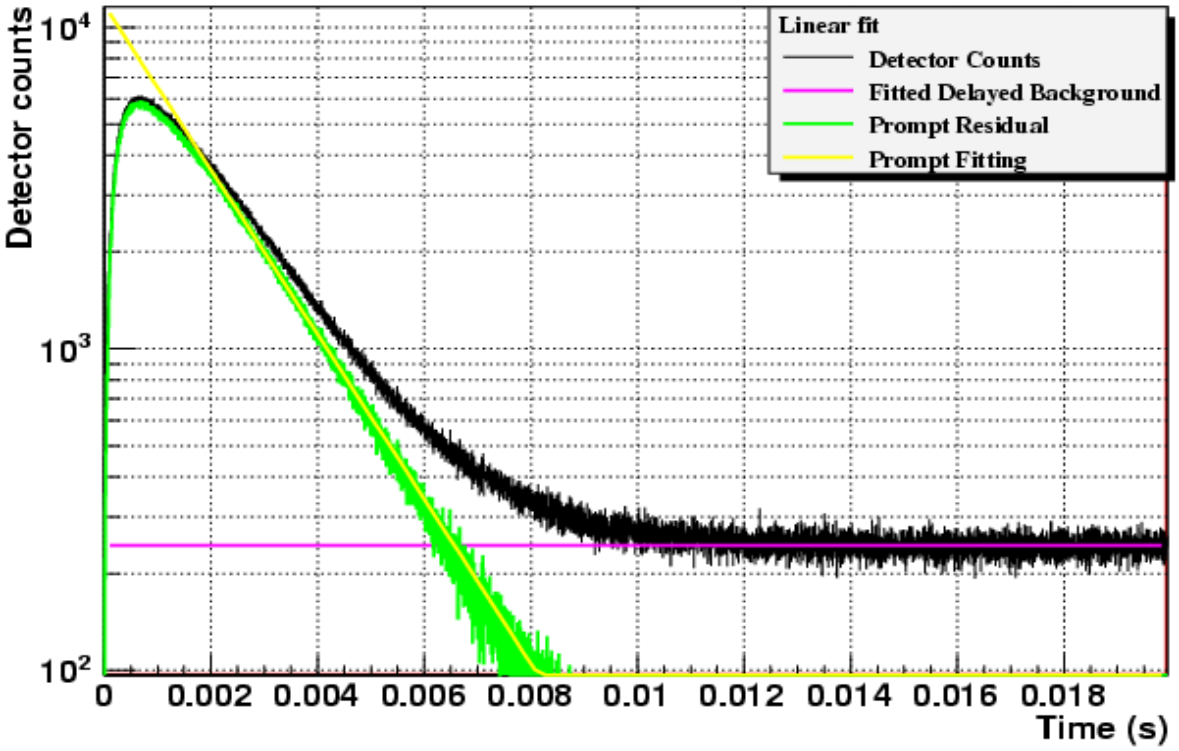

Figure 33. Linear fit of the pulsed neutron experiment recorded by long He-3 detector in EC8R channel of YALINA configuration with 90% enriched fuel in the fast zone and 1141 EK-10 fuel rods in the thermal zone in batch 0.3

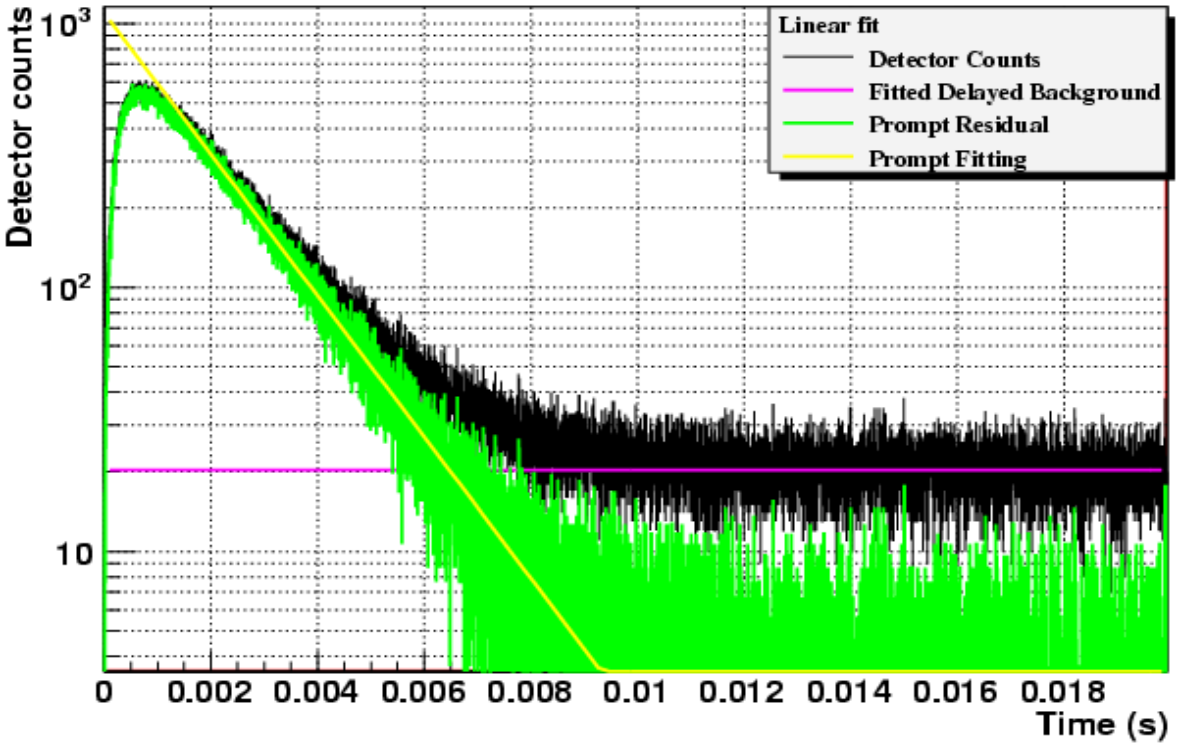

Figure 34. Linear fit of the pulsed neutron experiment recorded by small He-3 detector in EC8R channel of YALINA configuration with 90% enriched fuel in the fast zone and 1141 EK-10 fuel rods in the thermal zone in batch 0.4

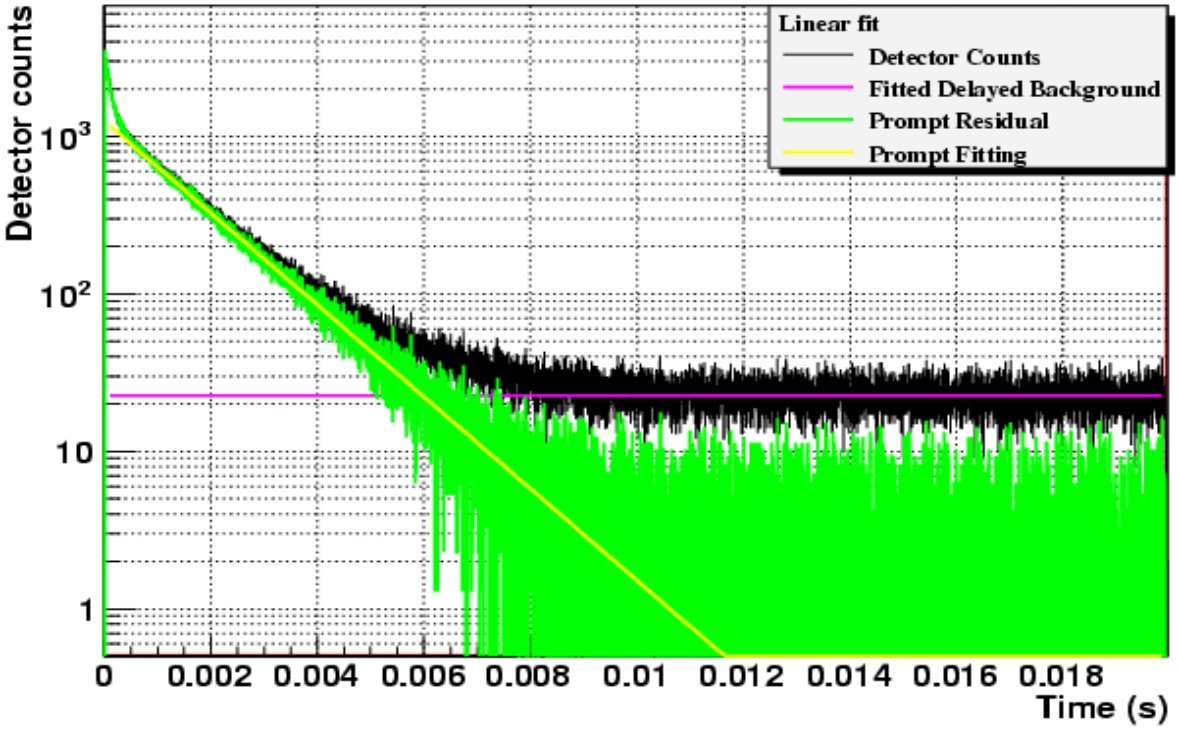

Figure 35. Linear fit of the pulsed neutron experiment recorded by small He-3 detector in EC5T channel of YALINA configuration with 36% enriched fuel in the fast zone and 1185 EK-10 fuel rods in the thermal zone in batch 0.1

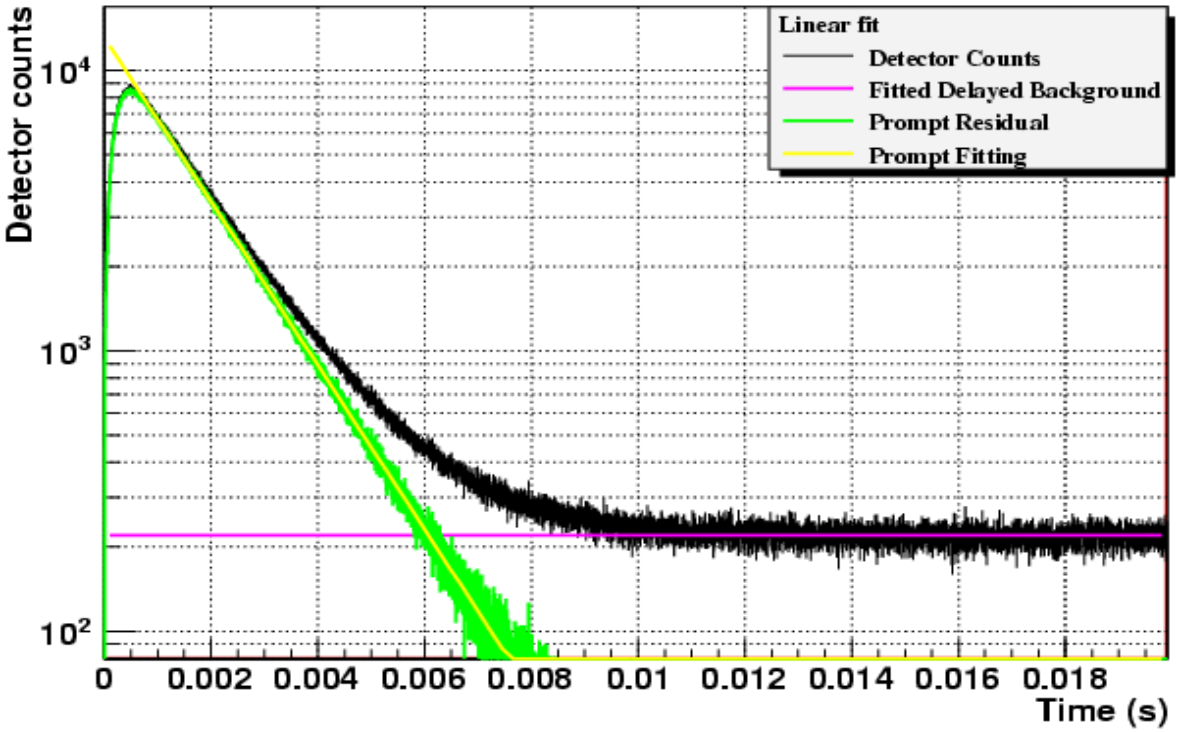

Figure 36. Linear fit of the pulsed neutron experiment recorded by long He-3 detector in MC5 channel of YALINA configuration with 36% enriched fuel in the fast zone and 1185 EK-10 fuel rods in the thermal zone in batch 0.1

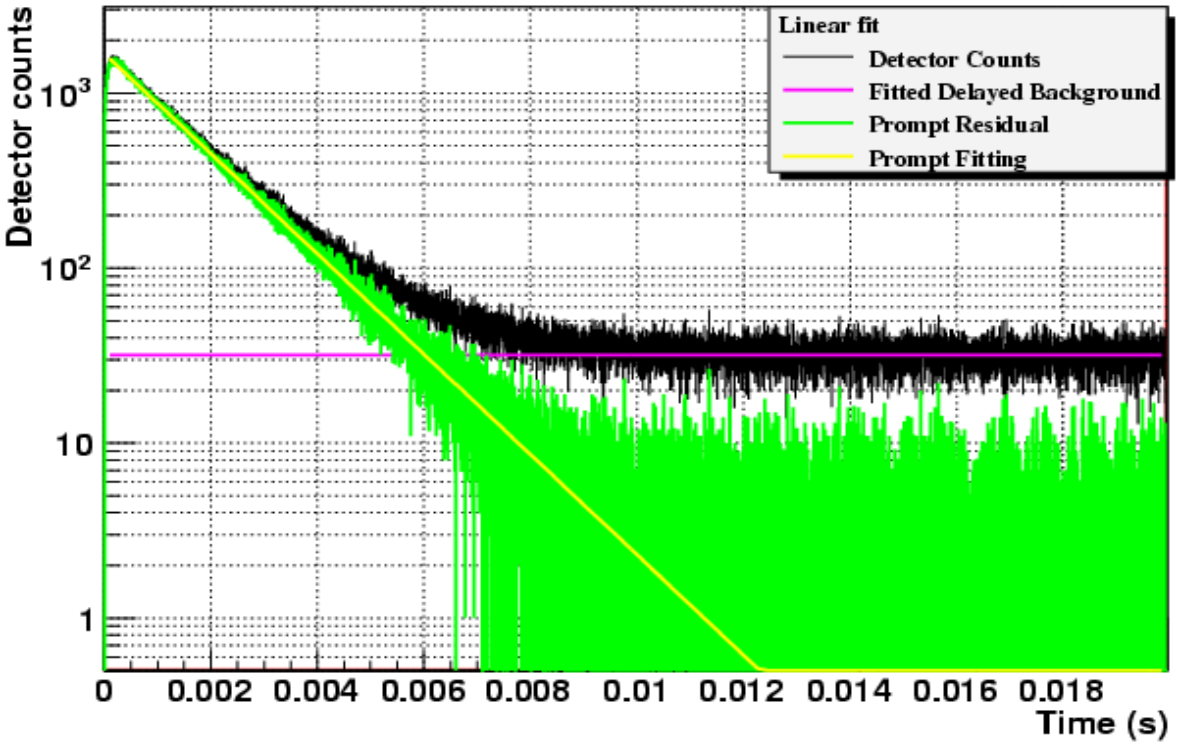

Figure 37. Linear fit of the pulsed neutron experiment recorded by small He-3 detector in EC6T channel of YALINA configuration with 36% enriched fuel in the fast zone and 1185 EK-10 fuel rods in the thermal zone in batch 0.1

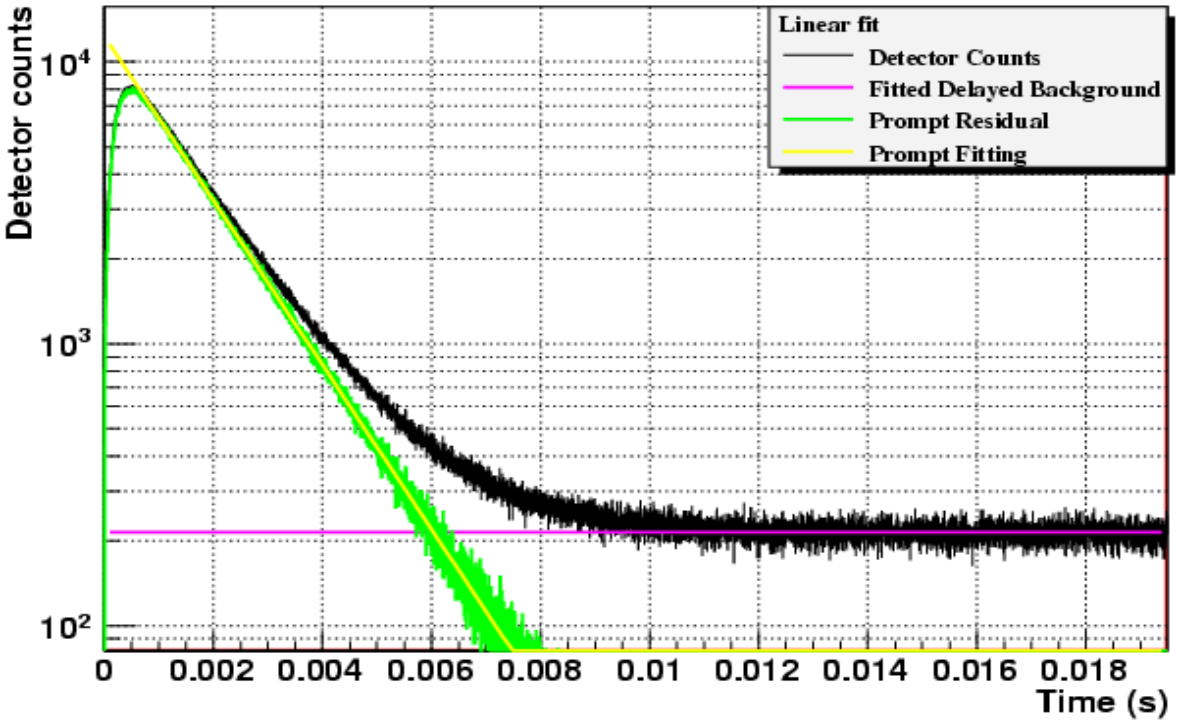

Figure 38. Linear fit of the pulsed neutron experiment recorded by long He-3 detector in MC5 channel of YALINA configuration with 36% enriched fuel in the fast zone and 1185 EK-10 fuel rods in the thermal zone in batch 0.2

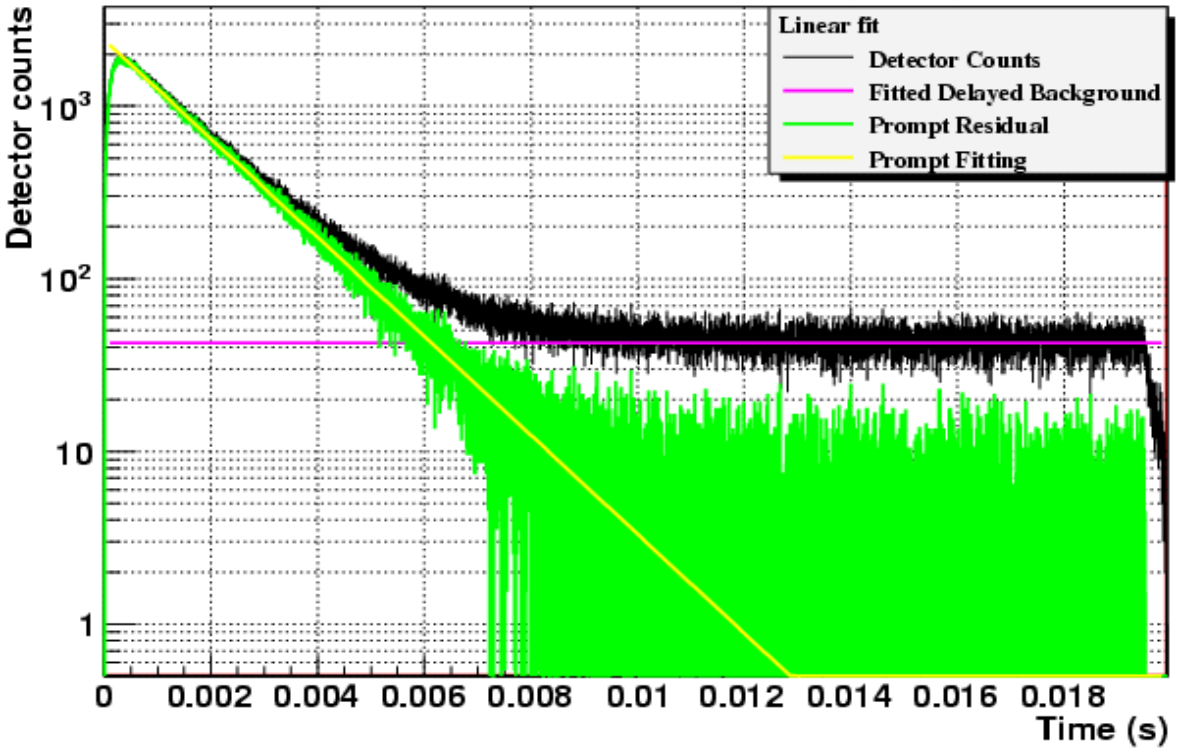

Figure 39. Linear fit of the pulsed neutron experiment recorded by small He-3 detector in EC7T channel of YALINA configuration with 36% enriched fuel in the fast zone and 1185 EK-10 fuel rods in the thermal zone in batch 0.2

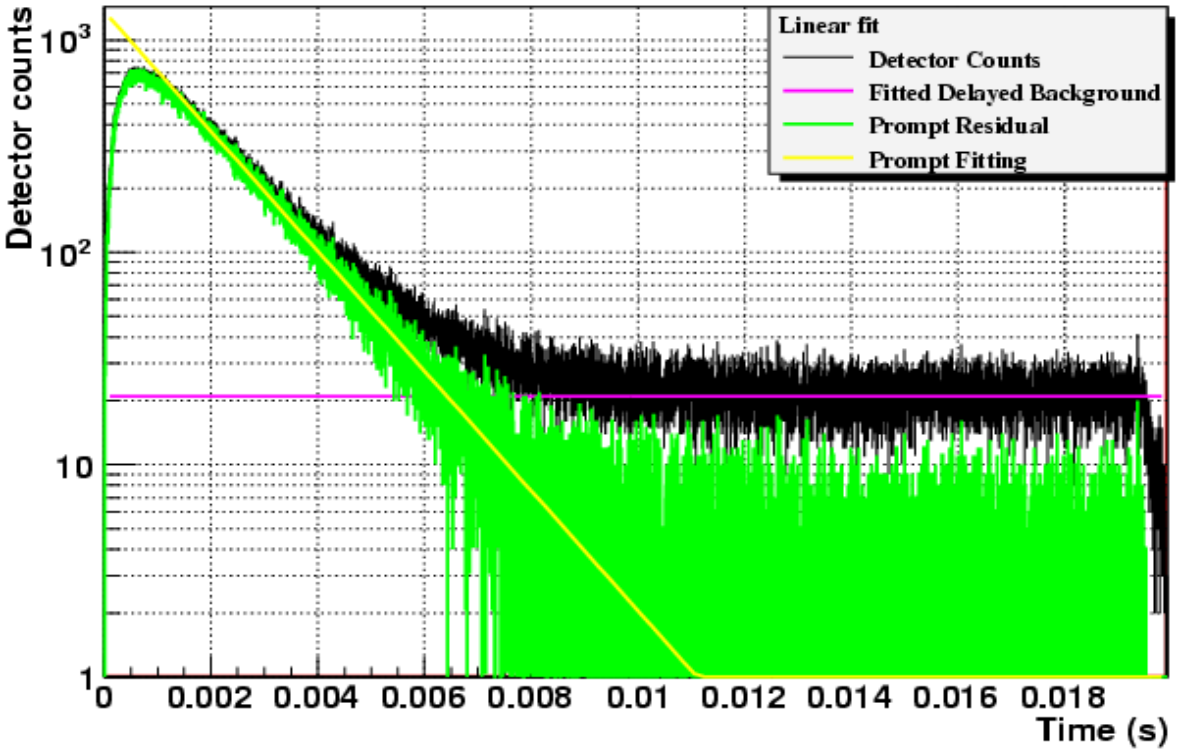

Figure 40. Linear fit of the pulsed neutron experiment recorded by small He-3 detector in EC8R channel of YALINA configuration with 36% enriched fuel in the fast zone and 1185 EK-10 fuel rods in the thermal zone in batch 0.2

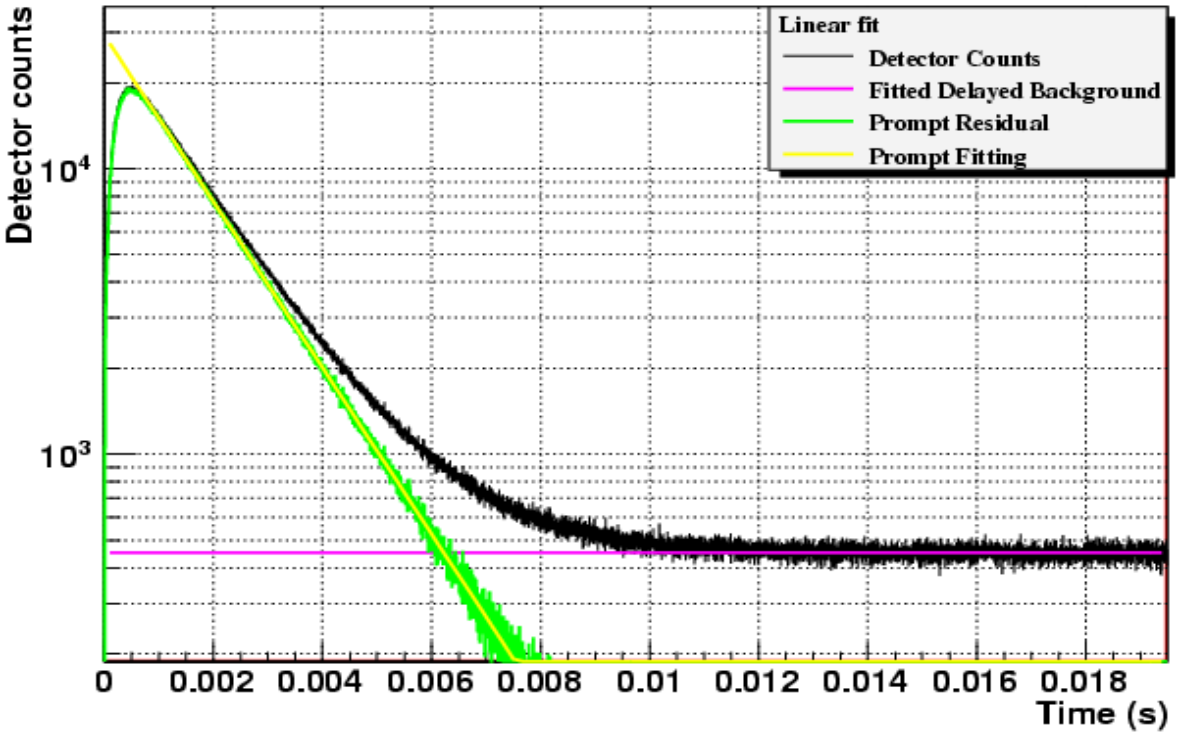

Figure 41. Linear fit of the pulsed neutron experiment recorded by long He-3 detector in MC5 channel of YALINA configuration with 36% enriched fuel in the fast zone and 1185 EK-10 fuel rods in the thermal zone in batch 0.3

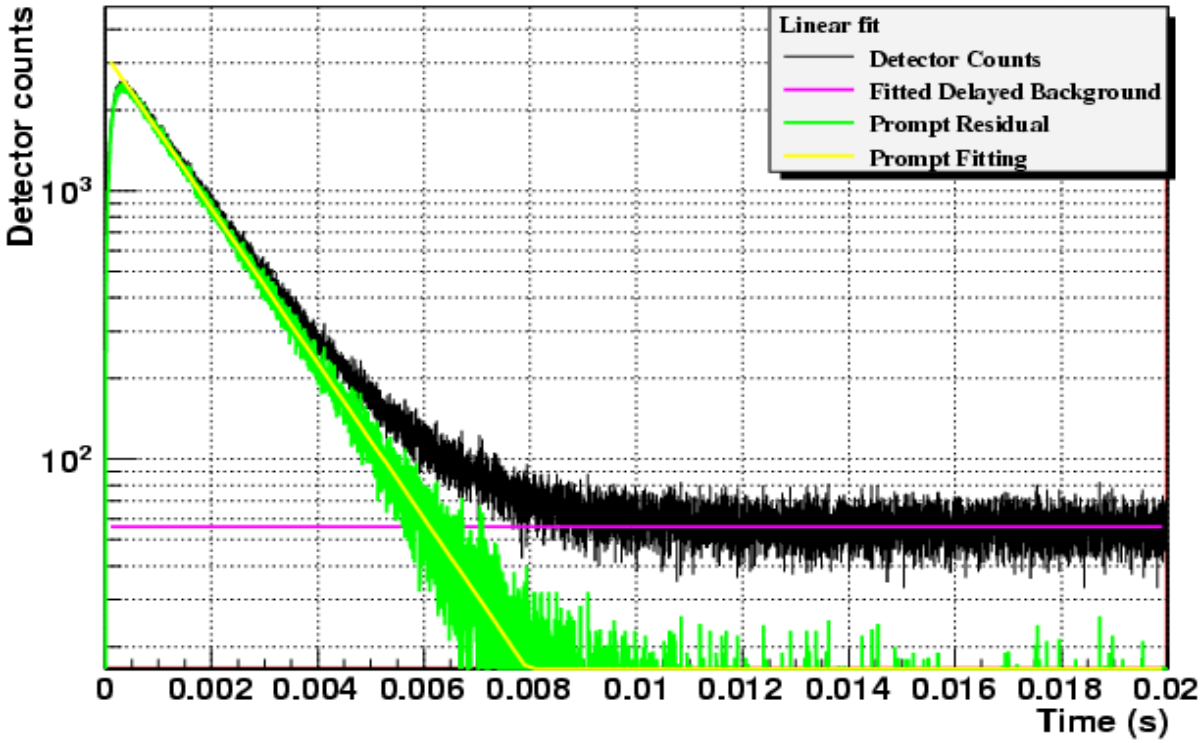

Figure 42. Linear fit of the pulsed neutron experiment recorded by small He-3 detector in EC7T channel of YALINA configuration with 36% enriched fuel in the fast zone and 1185 EK-10 fuel rods in the thermal zone in batch 0.3

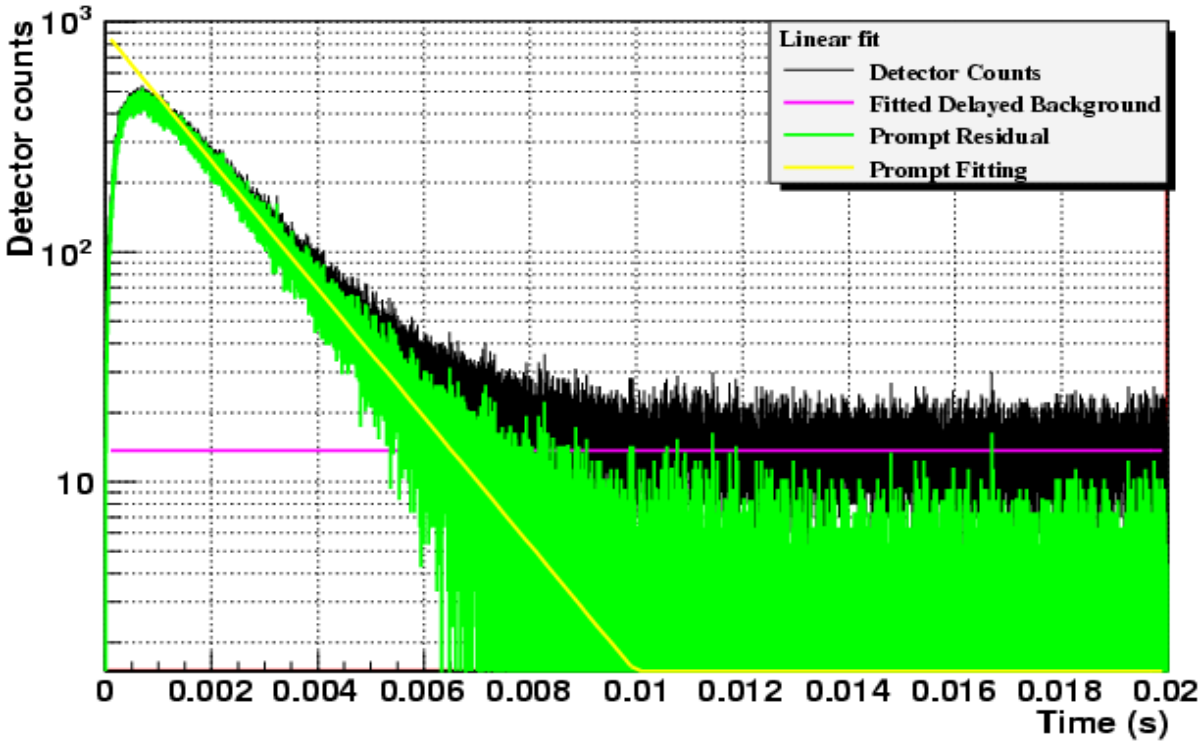

Figure 43. Linear fit of the pulsed neutron experiment recorded by small He-3 detector in EC8R channel of YALINA configuration with 36% enriched fuel in the fast zone and 1185 EK-10 fuel rods in the thermal zone in batch 0.3

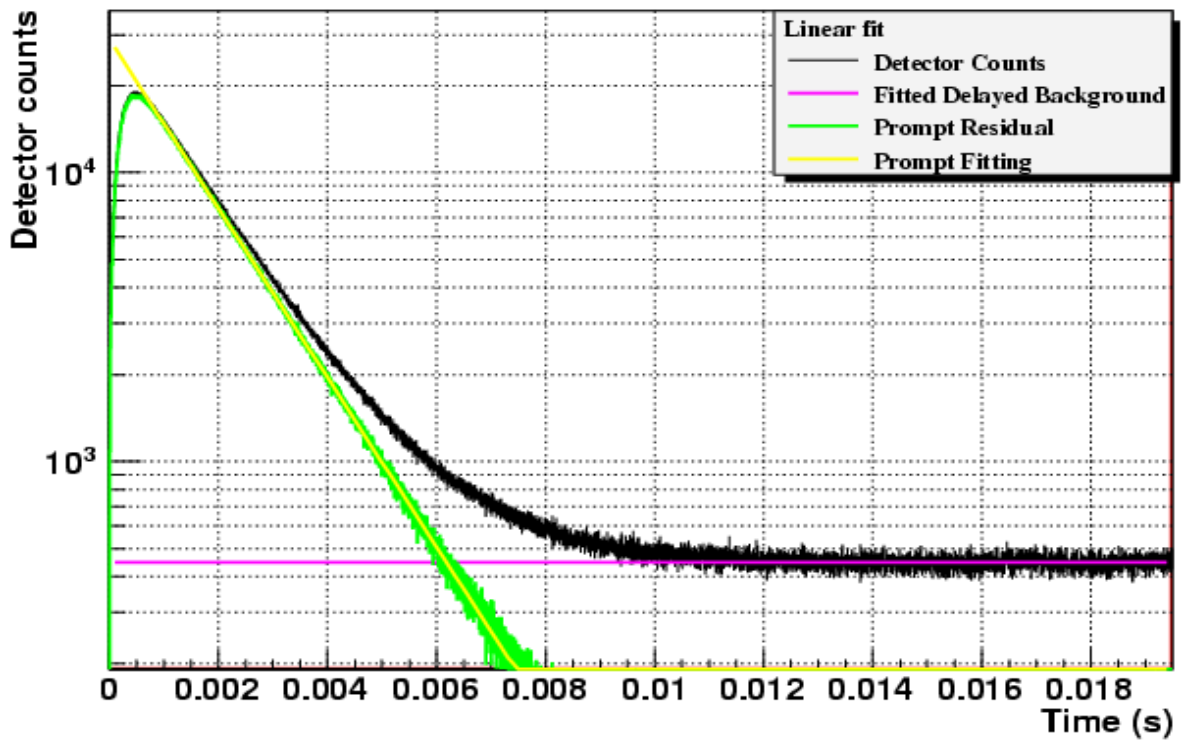

Figure 44. Linear fit of the pulsed neutron experiment recorded by long He-3 detector in MC5 channel of YALINA configuration with 36% enriched fuel in the fast zone and 1185 EK-10 fuel rods in the thermal zone in batch 0.4

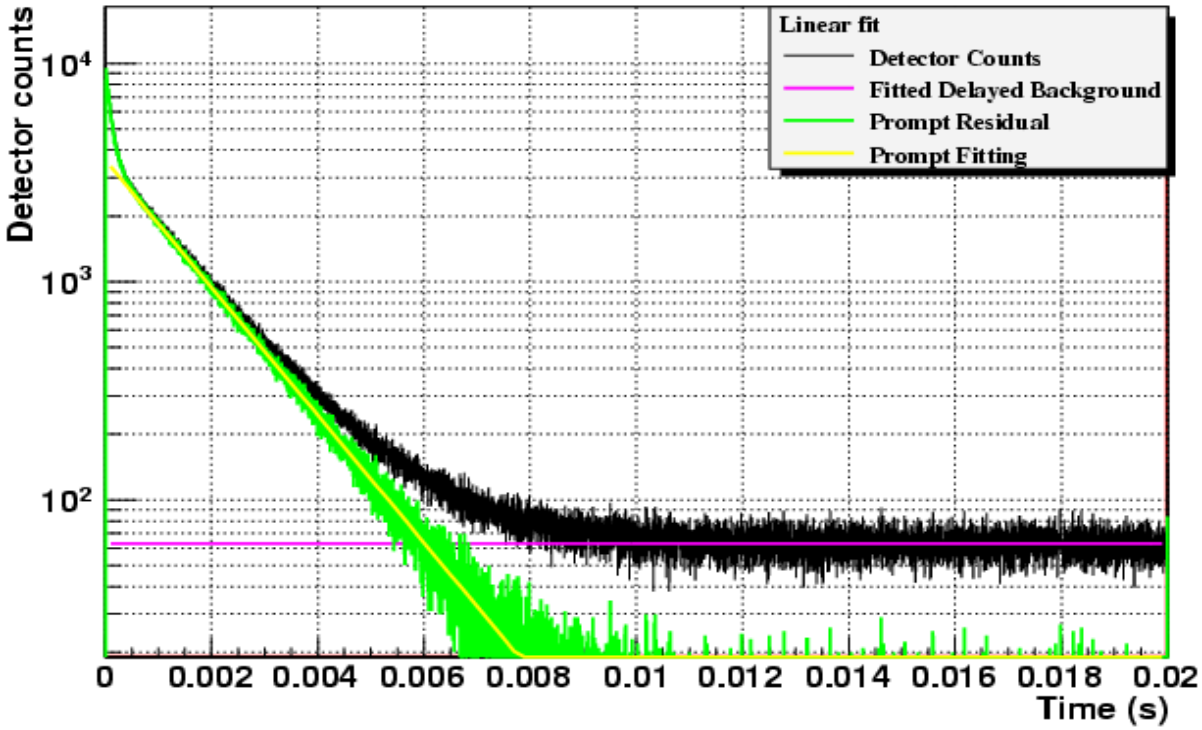

Figure 45. Linear fit of the pulsed neutron experiment recorded by small He-3 detector in EC5T channel of YALINA configuration with 36% enriched fuel in the fast zone and 1185 EK-10 fuel rods in the thermal zone in batch 0.4

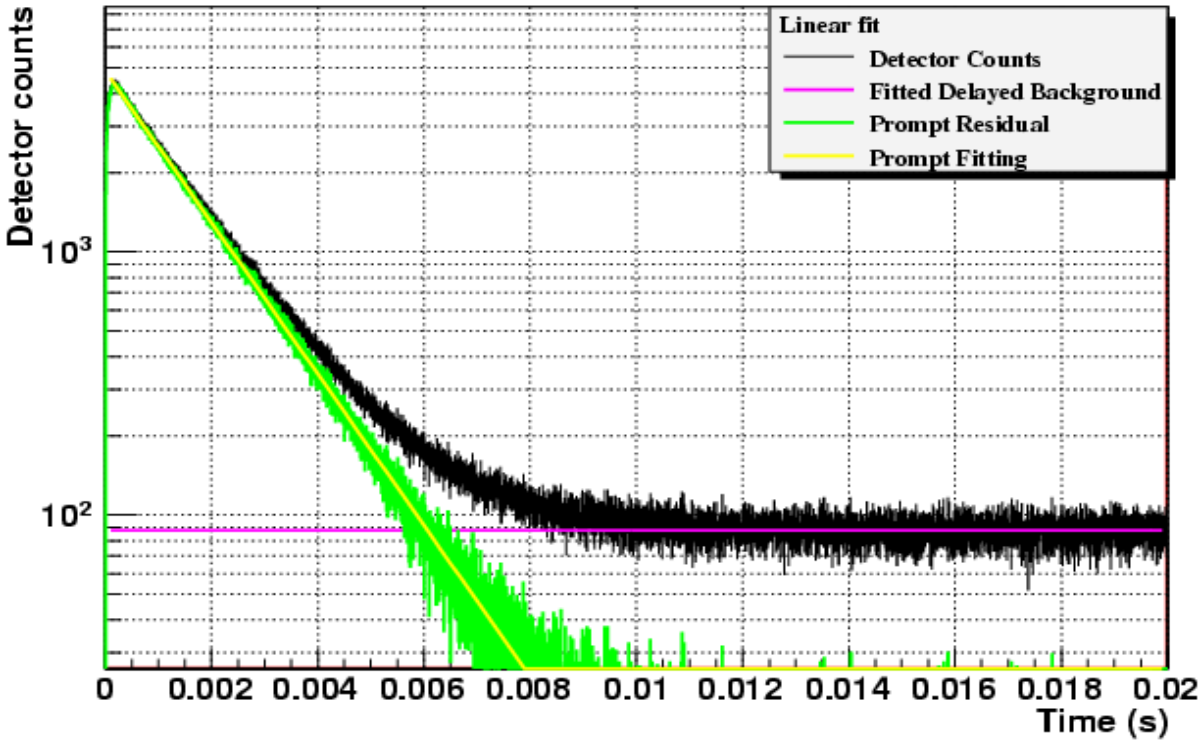

Figure 46. Linear fit of the pulsed neutron experiment recorded by small He-3 detector in EC6T channel of YALINA configuration with 36% enriched fuel in the fast zone and 1185 EK-10 fuel rods in the thermal zone in batch 0.4

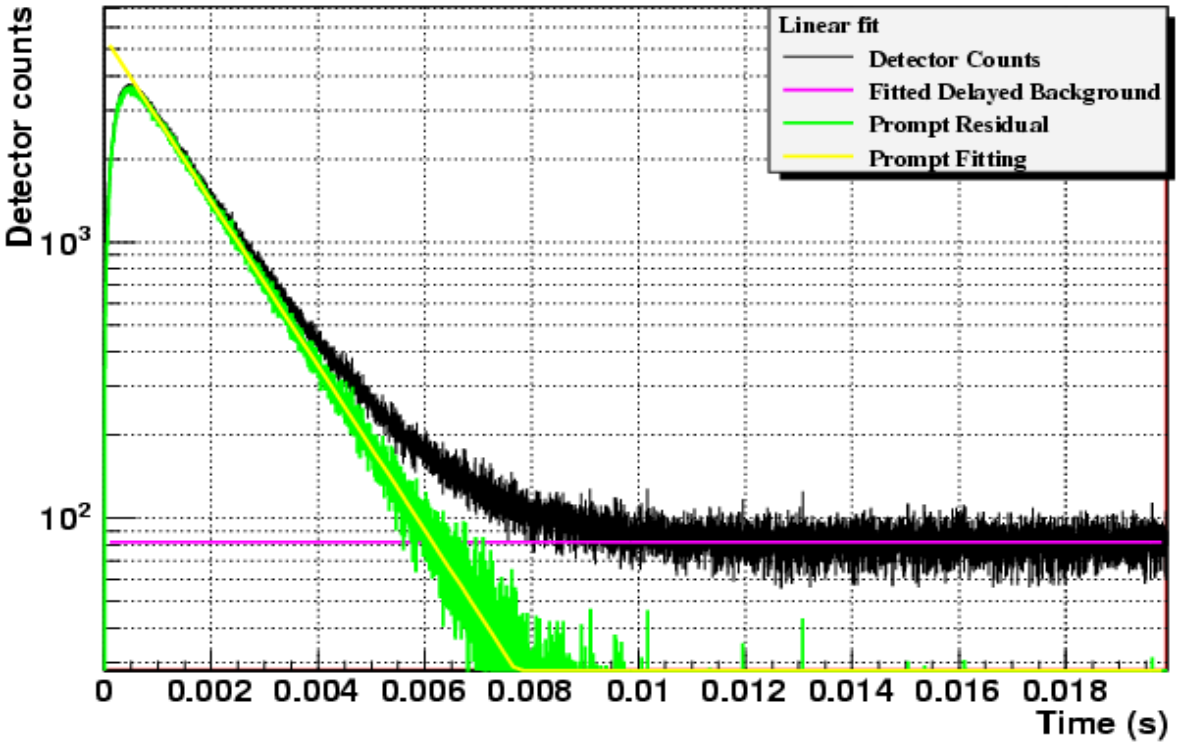

Figure 47. Linear fit of the pulsed neutron experiment recorded by long He-3 detector in MC5 channel of YALINA configuration with 36% enriched fuel in the fast zone and 1185 EK-10 fuel rods in the thermal zone in batch 0.5

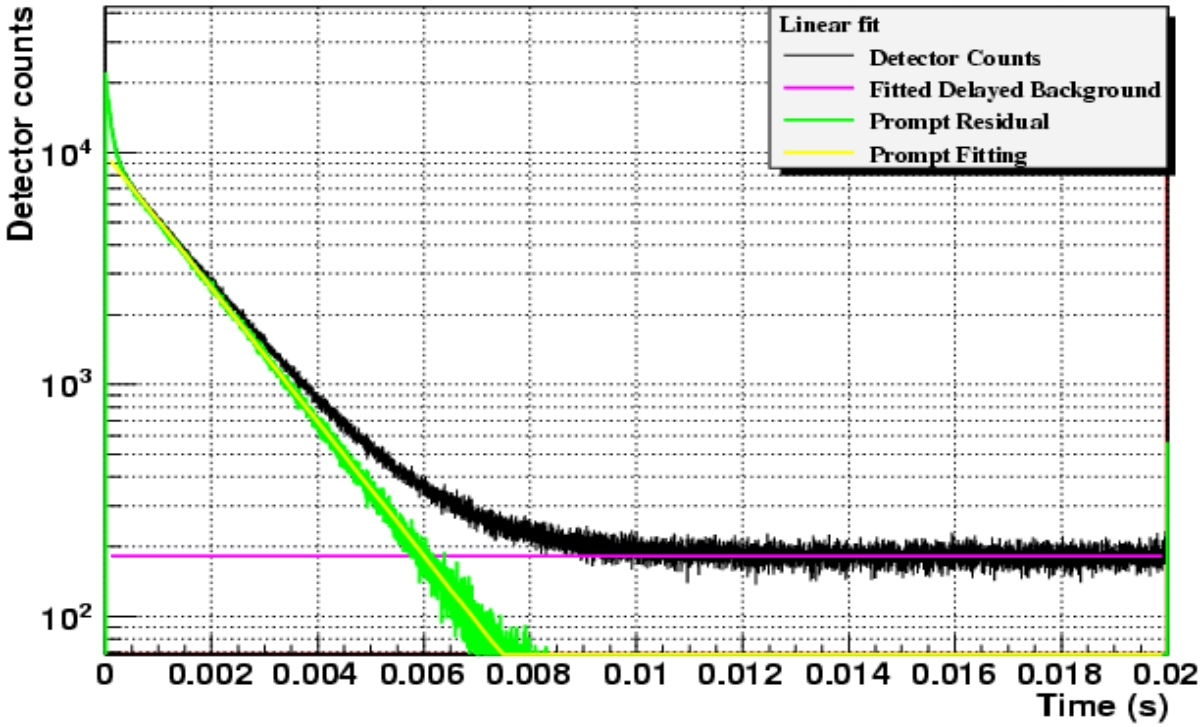

Figure 48. Linear fit of the pulsed neutron experiment recorded by long He-3 detector in EC5T channel of YALINA configuration with 36% enriched fuel in the fast zone and 1185 EK-10 fuel rods in the thermal zone in batch 0.5

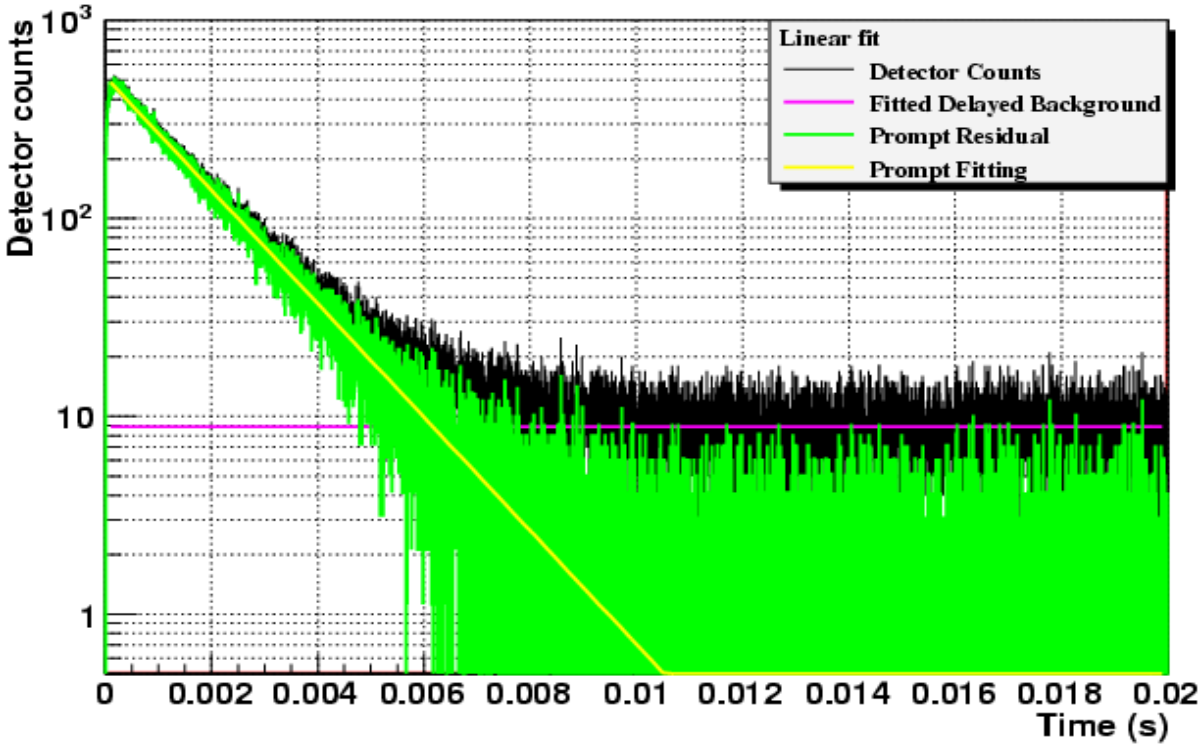

Figure 49. Linear fit of the pulsed neutron experiment recorded by small He-3 detector in EC6T channel of YALINA configuration with 36% enriched fuel in the fast zone and 1185 EK-10 fuel rods in the thermal zone in batch 0.5

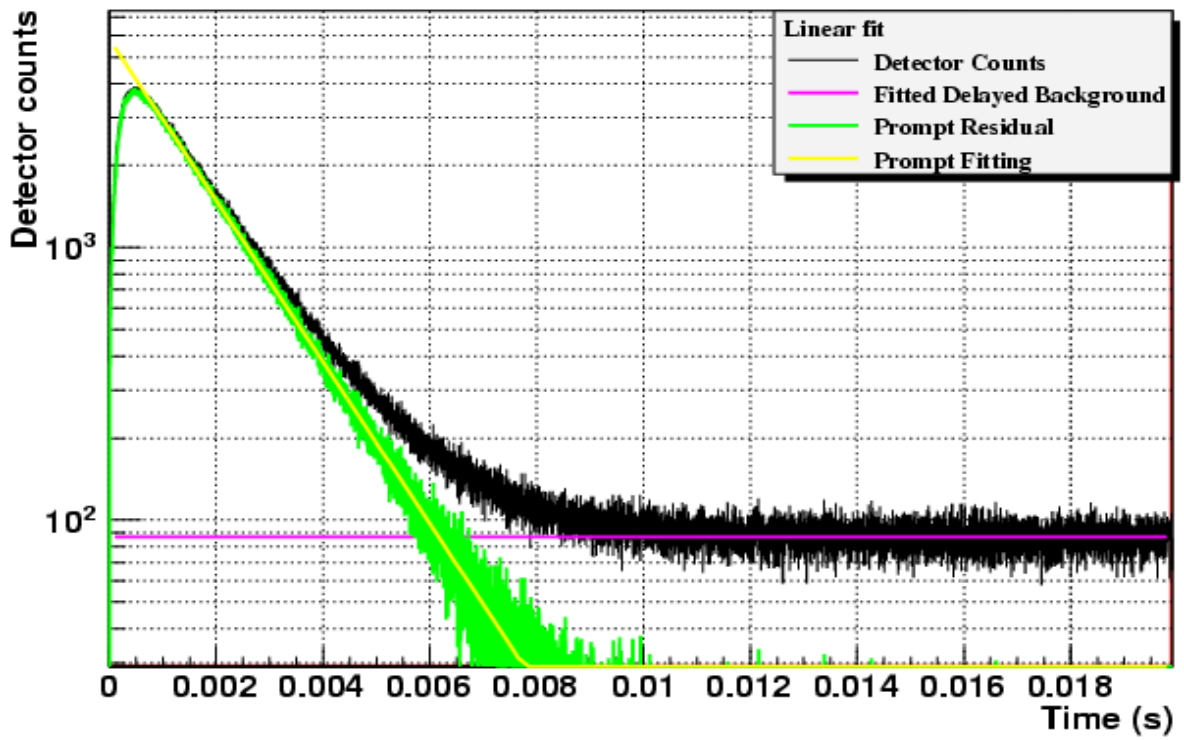

Figure 50. Linear fit of the pulsed neutron experiment recorded by long He-3 detector in MC5 channel of YALINA configuration with 36% enriched fuel in the fast zone and 1185 EK-10 fuel rods in the thermal zone in batch 0.6

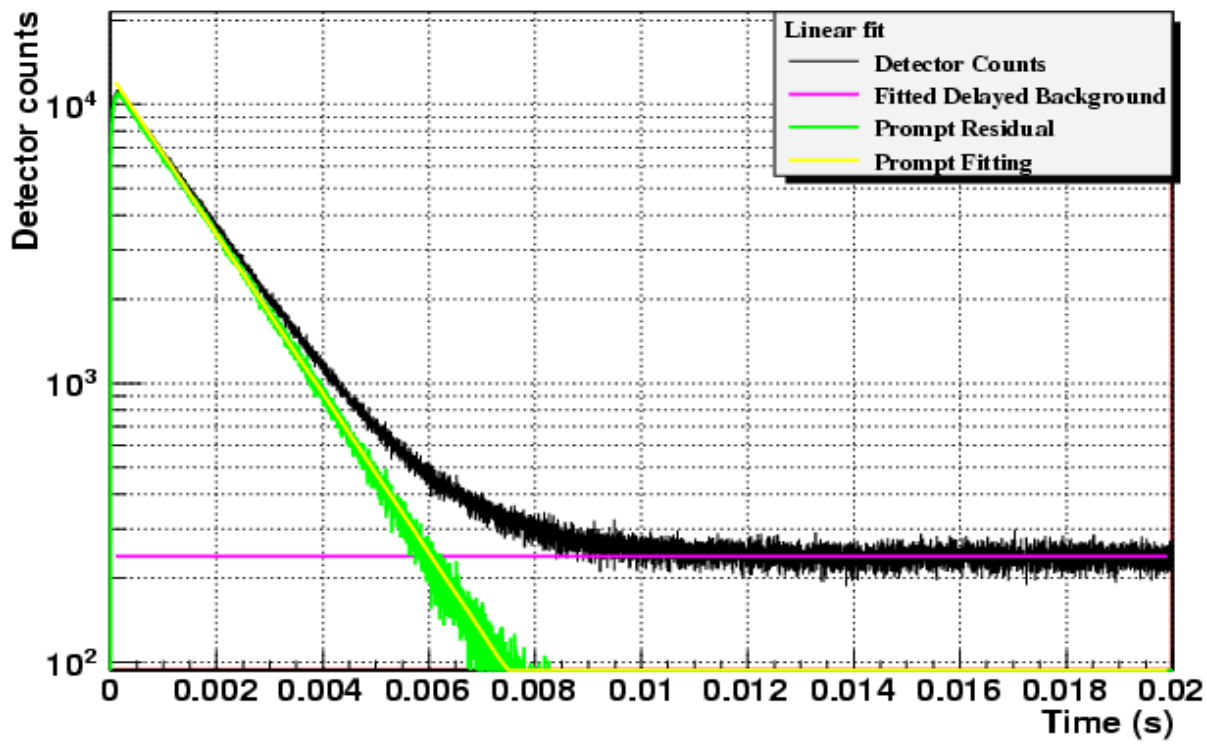

Figure 51. Linear fit of the pulsed neutron experiment recorded by long He-3 detector in EC6T channel of YALINA configuration with 36% enriched fuel in the fast zone and 1185 EK-10 fuel rods in the thermal zone in batch 0.6

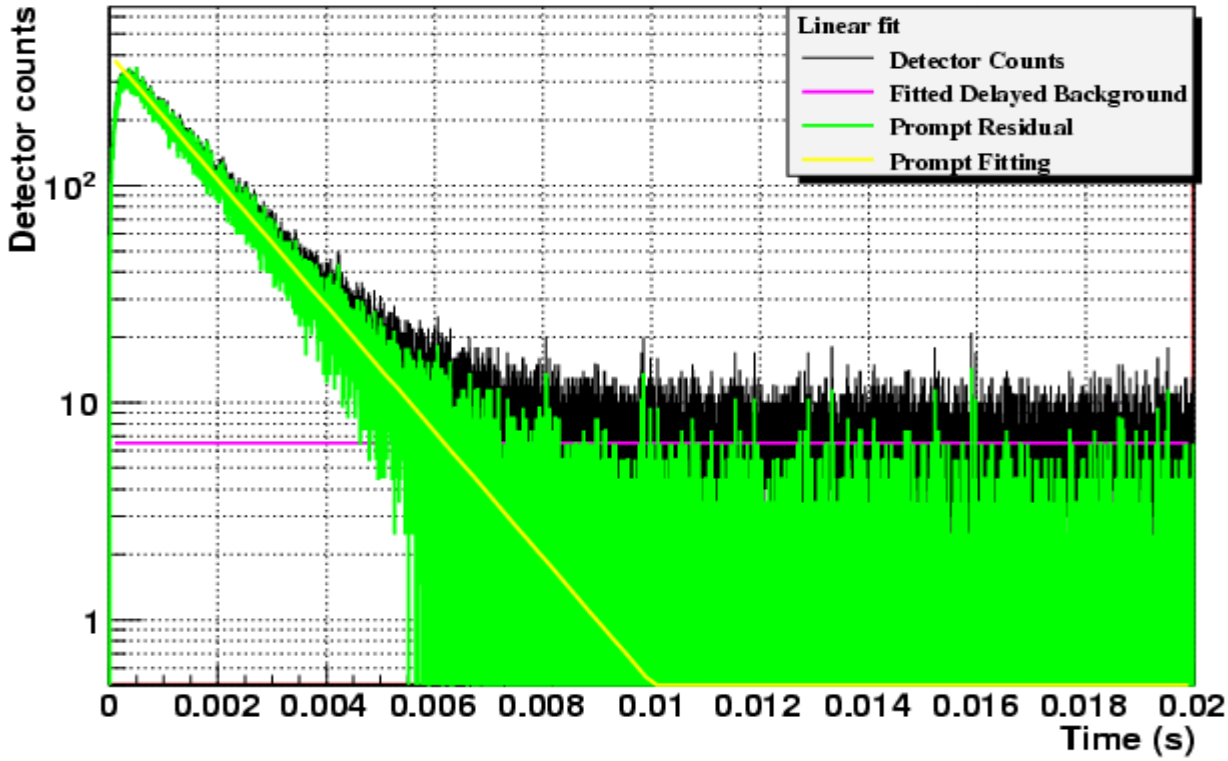

Figure 52. Linear fit of the pulsed neutron experiment recorded by small He-3 detector in EC7T channel of YALINA configuration with 36% enriched fuel in the fast zone and 1185 EK-10 fuel rods in the thermal zone in batch 0.6

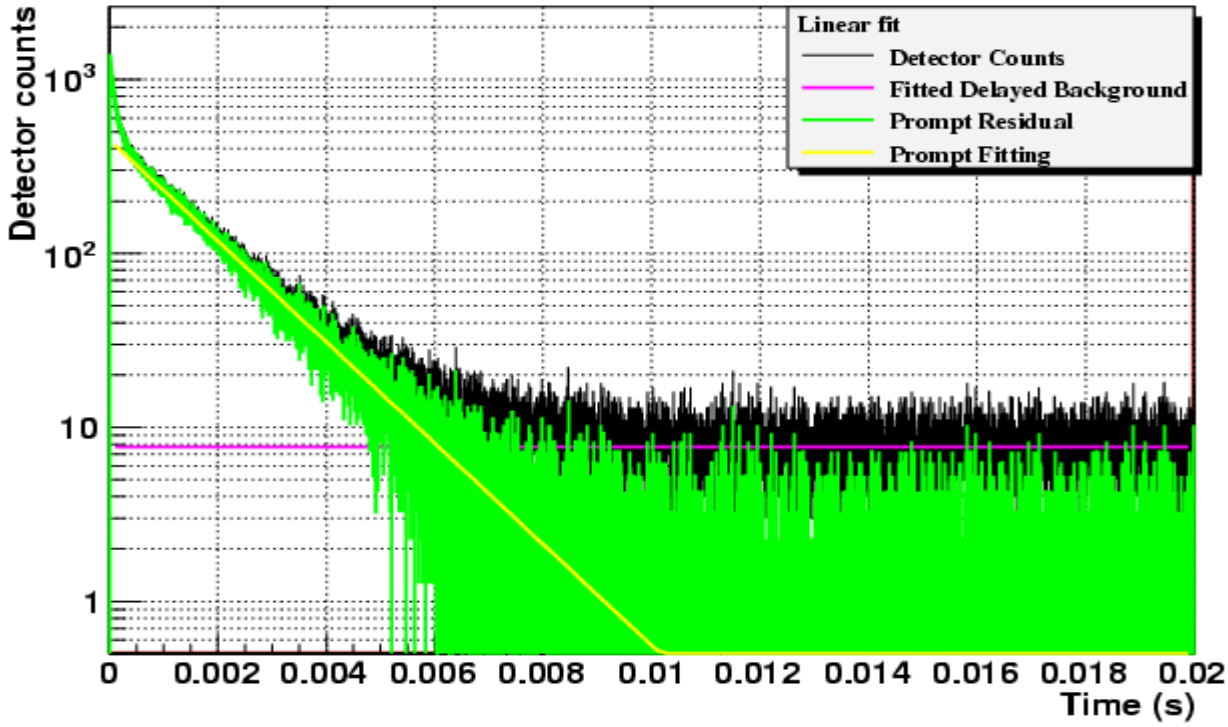

Figure 53. Linear fit of the pulsed neutron experiment recorded by small He-3 detector in EC5T channel of YALINA configuration with 36% enriched fuel in the fast zone and 1185 EK-10 fuel rods in the thermal zone in batch 0.7

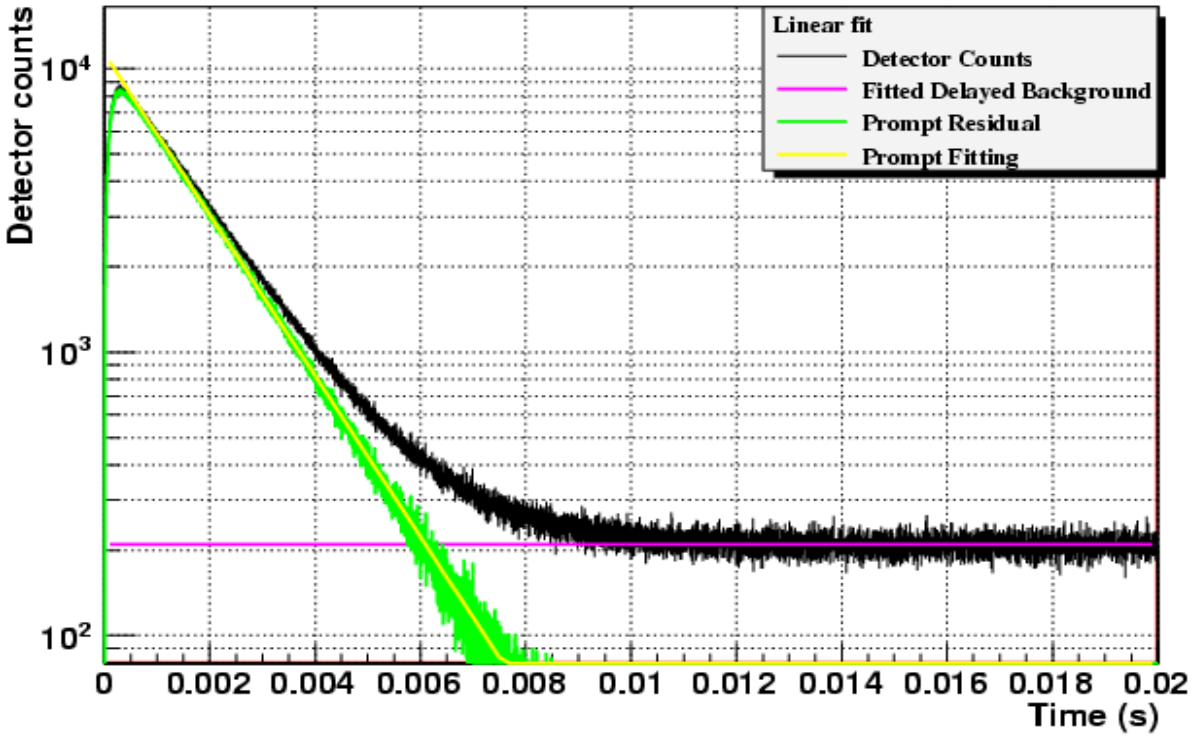

Figure 54. Linear fit of the pulsed neutron experiment recorded by long He-3 detector in EC7T channel of YALINA configuration with 36% enriched fuel in the fast zone and 1185 EK-10 fuel rods in the thermal zone in batch 0.7

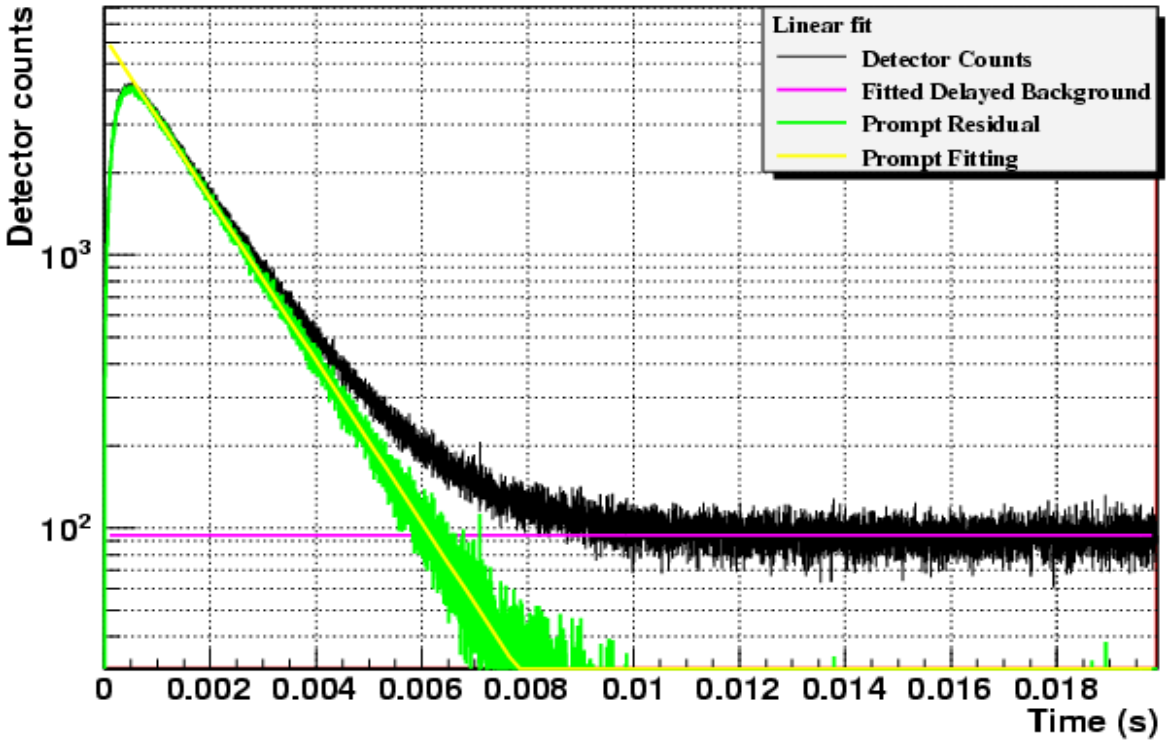

Figure 55. Linear fit of the pulsed neutron experiment recorded by long He-3 detector in MC5 channel of YALINA configuration with 36% enriched fuel in the fast zone and 1185 EK-10 fuel rods in the thermal zone in batch 0.7

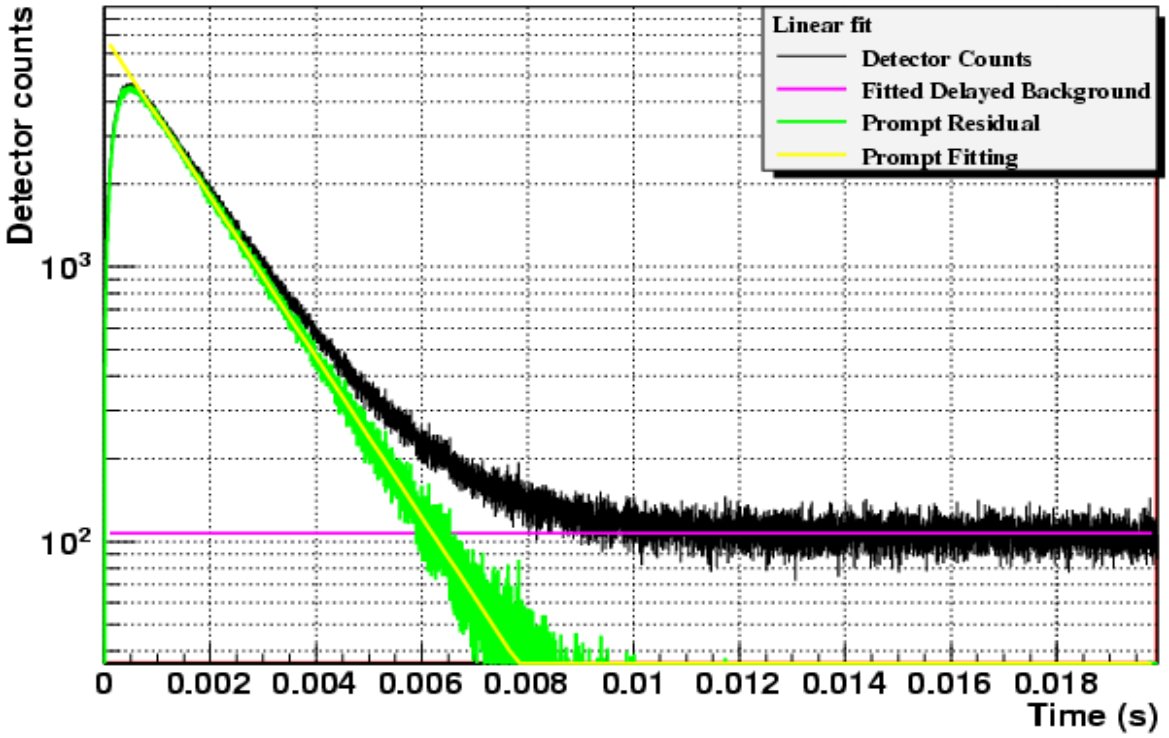

Figure 56. Linear fit of the pulsed neutron experiment recorded by long He-3 detector in MC5 channel of YALINA configuration with 36% enriched fuel in the fast zone and 1185 EK-10 fuel rods in the thermal zone in batch 0.8

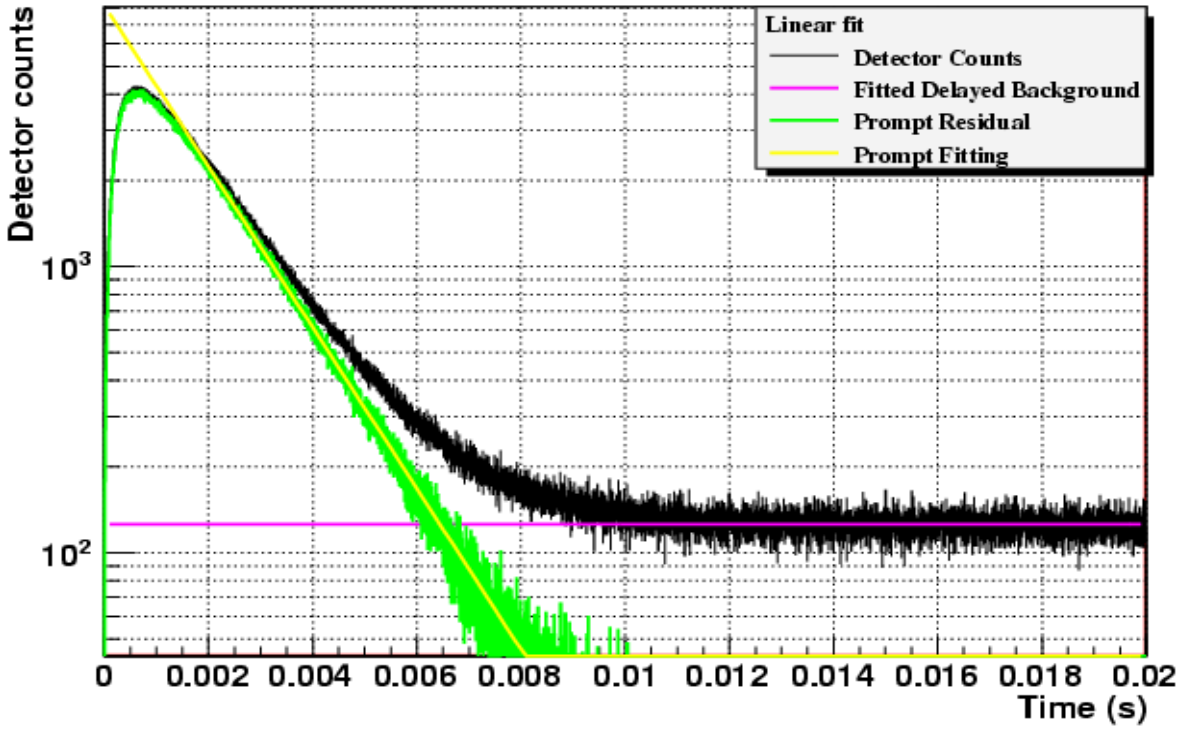

Figure 57. Linear fit of the pulsed neutron experiment recorded by long He-3 detector in EC8R channel of YALINA configuration with 36% enriched fuel in the fast zone and 1185 EK-10 fuel rods in the thermal zone in batch 0.8

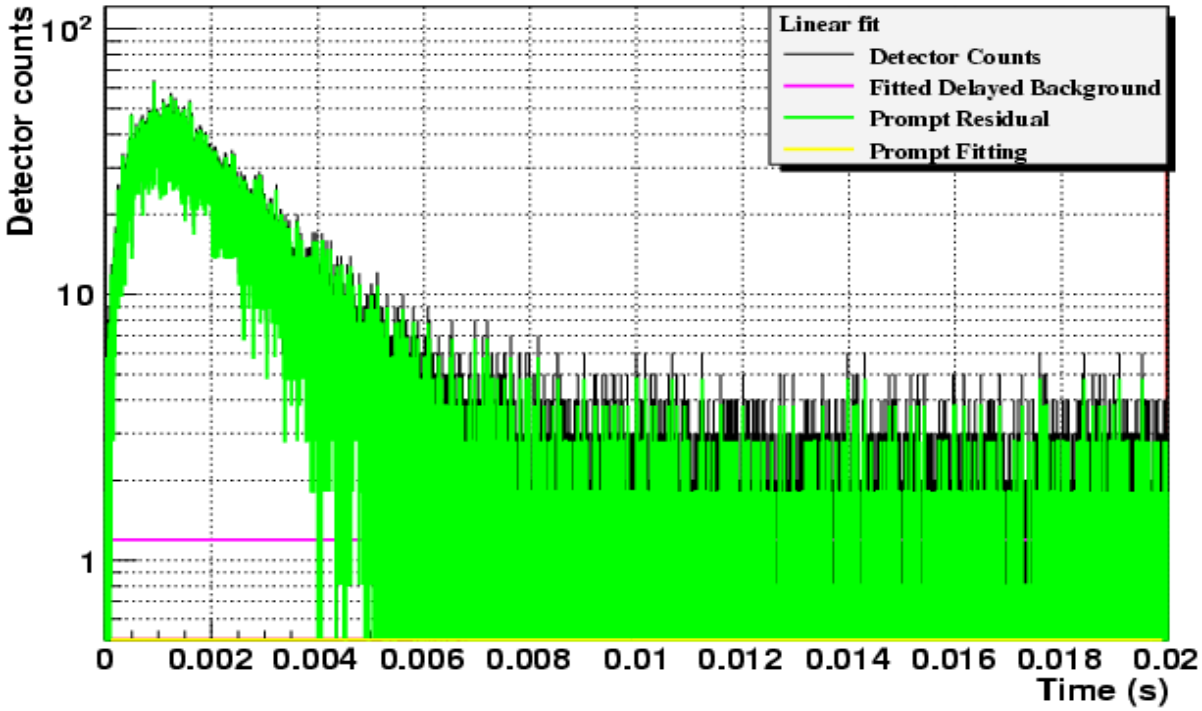

Figure 58. Linear fit of the pulsed neutron experiment recorded by small He-3 detector in EC9R channel of YALINA configuration with 36% enriched fuel in the fast zone and 1185 EK-10 fuel rods in the thermal zone in batch 0.8

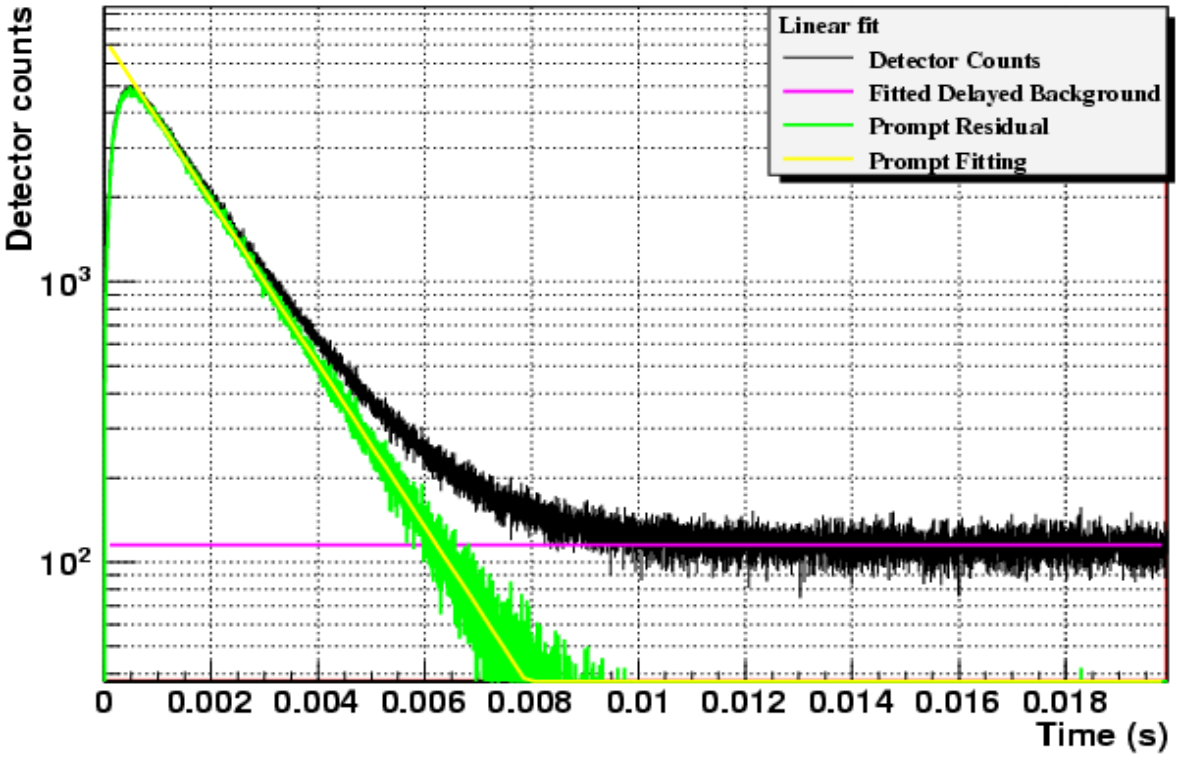

Figure 59. Linear fit of the pulsed neutron experiment recorded by long He-3 detector in MC5 channel of YALINA configuration with 36% enriched fuel in the fast zone and 1185 EK-10 fuel rods in the thermal zone in batch 0.9

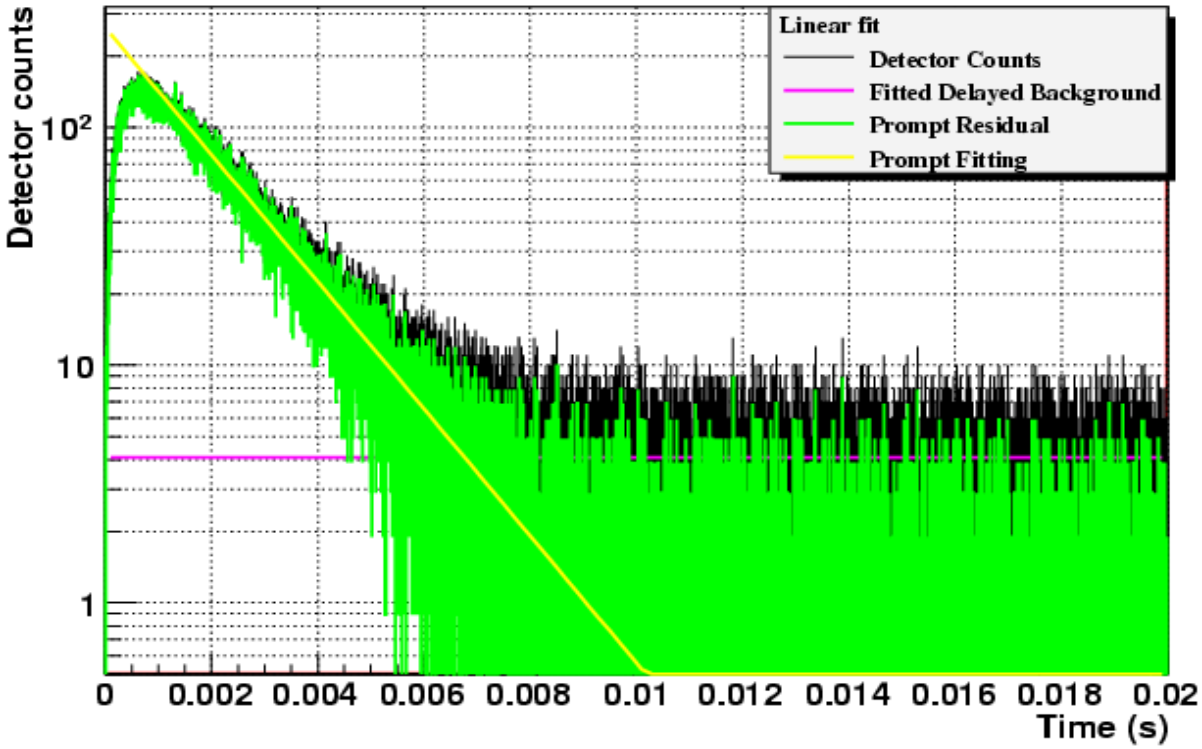

Figure 60. Linear fit of the pulsed neutron experiment recorded by small He-3 detector in EC8R channel of YALINA configuration with 36% enriched fuel in the fast zone and 1185 EK-10 fuel rods in the thermal zone in batch 0.9

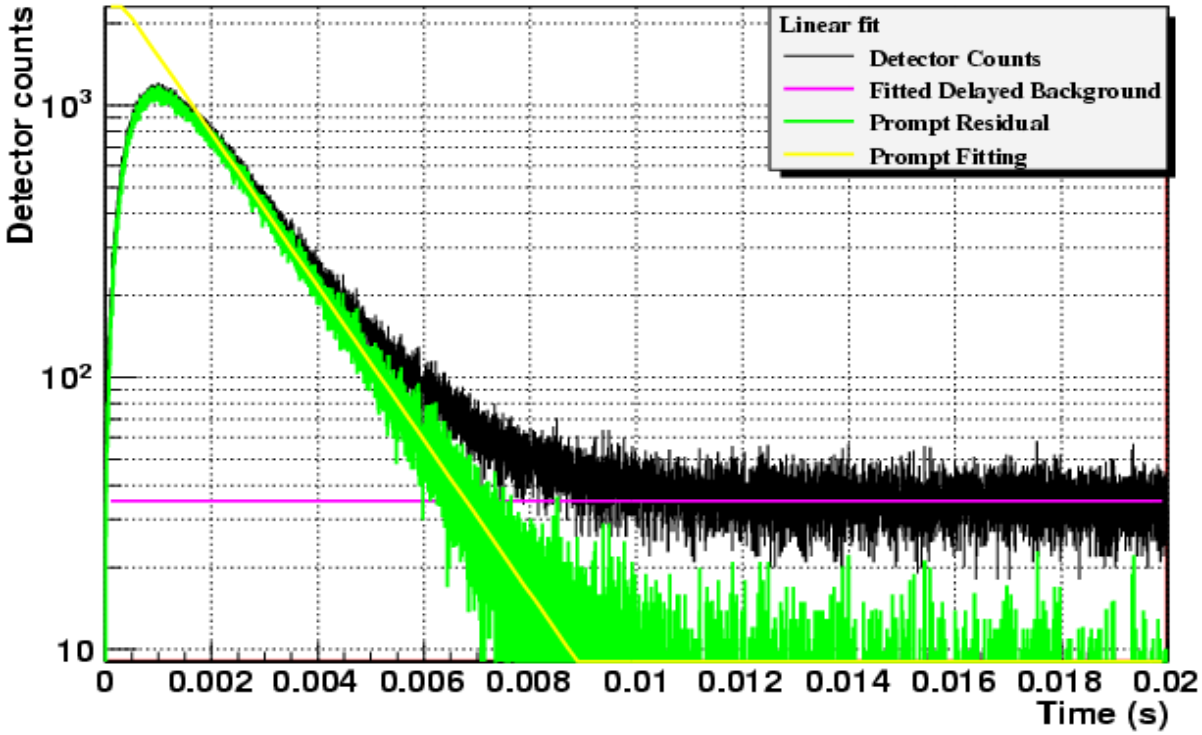

Figure 61. Linear fit of the pulsed neutron experiment recorded by long He-3 detector in EC9R channel of YALINA configuration with 36% enriched fuel in the fast zone and 1185 EK-10 fuel rods in the thermal zone in batch 0.9

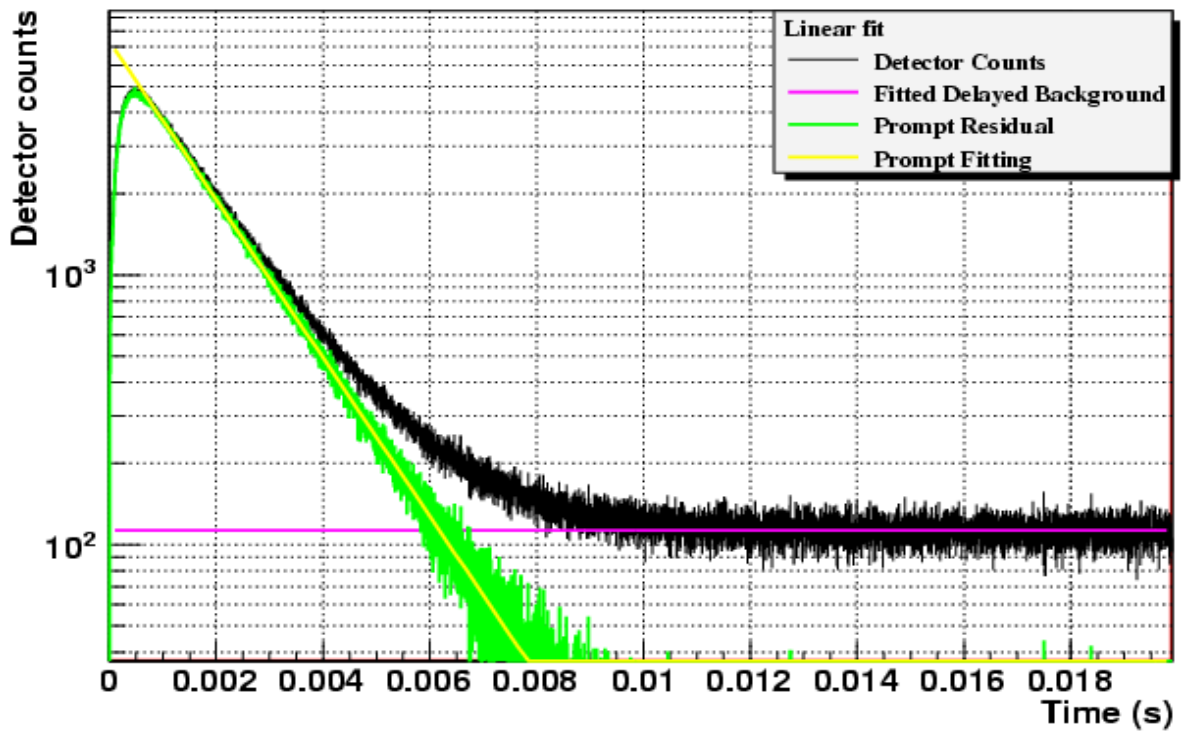

Figure 62. Linear fit of the pulsed neutron experiment recorded by long He-3 detector in MC5 channel of YALINA configuration with 36% enriched fuel in the fast zone and 1185 EK-10 fuel rods in the thermal zone in batch 1.0

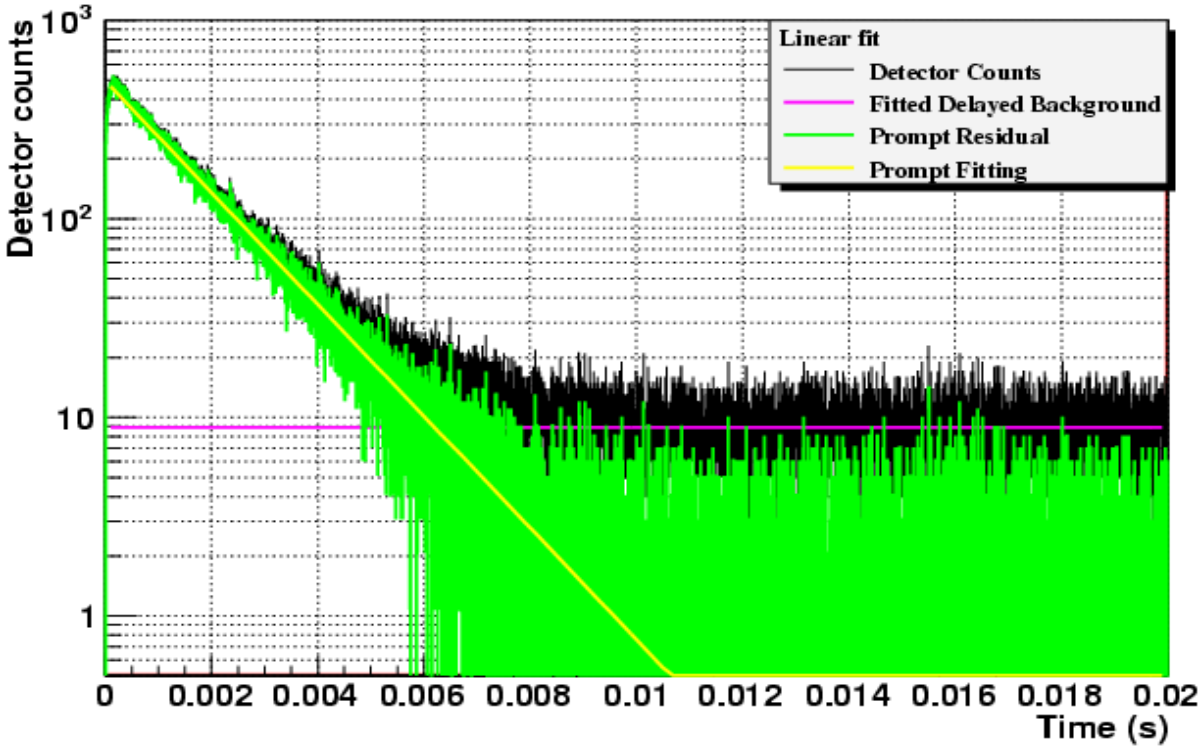

Figure 63. Linear fit of the pulsed neutron experiment recorded by small He-3 detector in EC6T channel of YALINA configuration with 36% enriched fuel in the fast zone and 1185 EK-10 fuel rods in the thermal zone in batch 1.0

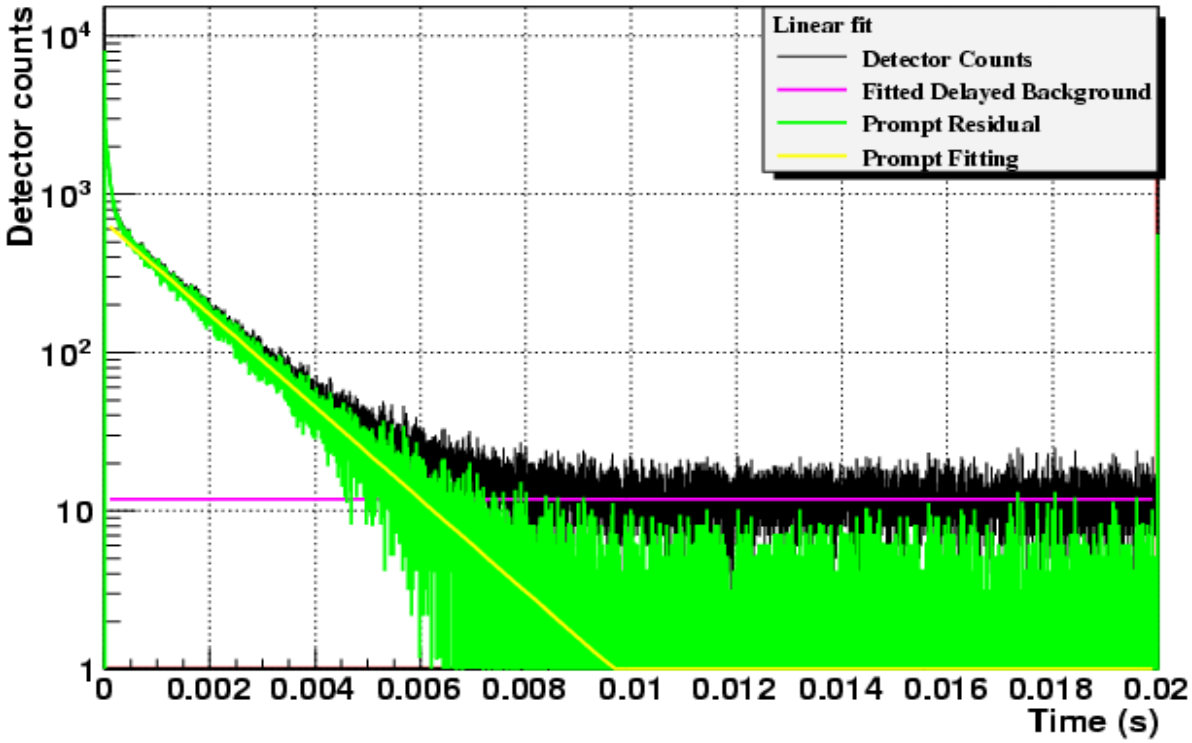

Figure 64. Linear fit of the pulsed neutron experiment recorded by long He-3 detector in EC3B channel of YALINA configuration with 36% enriched fuel in the fast zone and 1185 EK-10 fuel rods in the thermal zone in batch 1.0

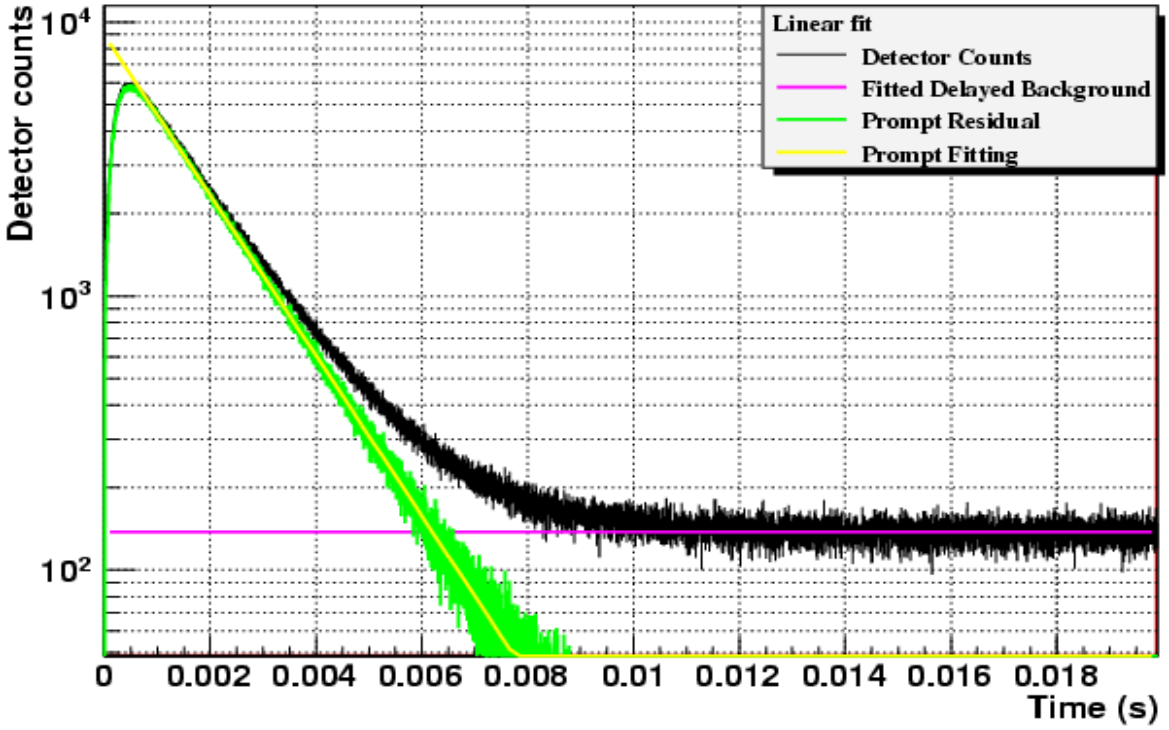

Figure 65. Linear fit of the pulsed neutron experiment recorded by long He-3 detector in MC5 channel of YALINA configuration with 36% enriched fuel in the fast zone and 1185 EK-10 fuel rods in the thermal zone in batch 1.1

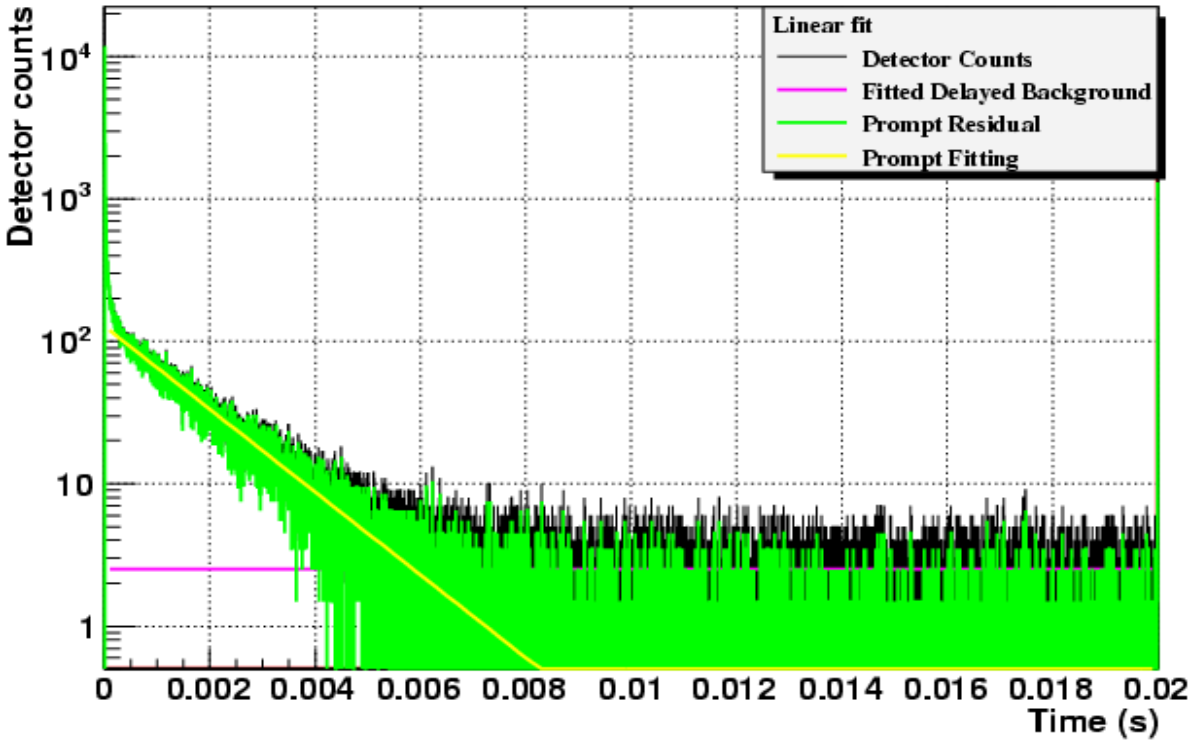

Figure 66. Linear fit of the pulsed neutron experiment recorded by long He-3 detector in EC2B channel of YALINA configuration with 36% enriched fuel in the fast zone and 1185 EK-10 fuel rods in the thermal zone in batch 1.1

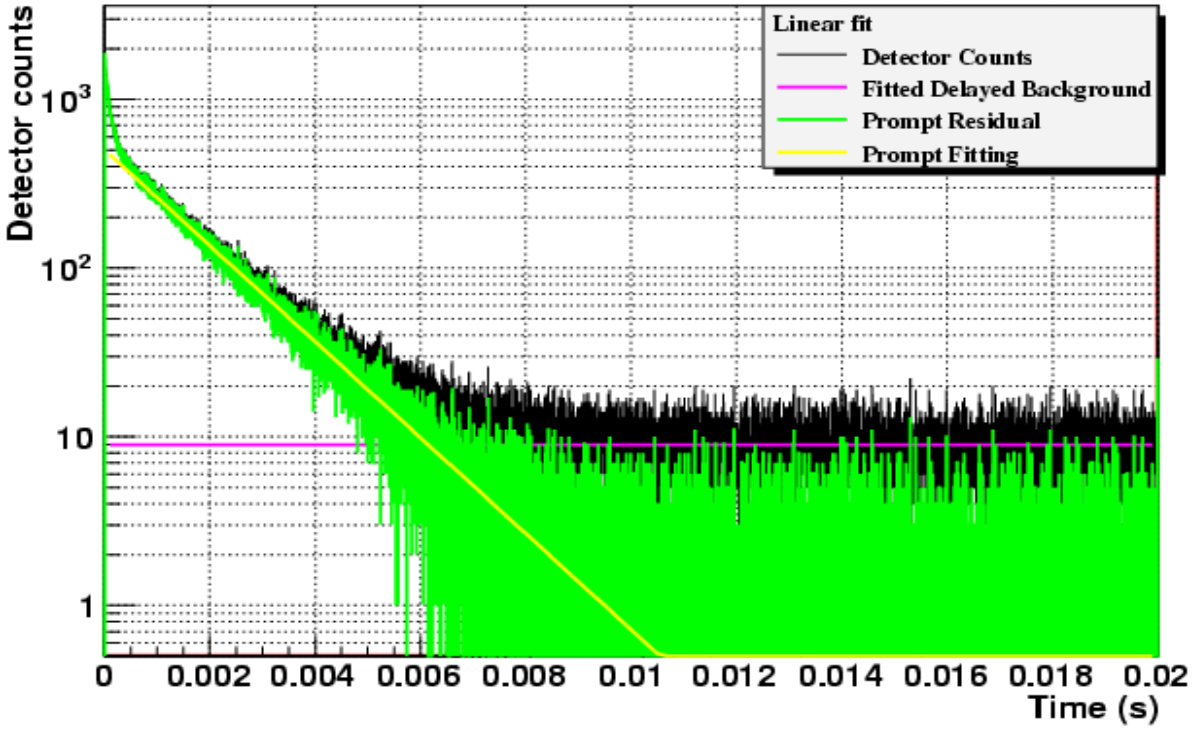

Figure 67. Linear fit of the pulsed neutron experiment recorded by small He-3 detector in EC5T channel of YALINA configuration with 36% enriched fuel in the fast zone and 1185 EK-10 fuel rods in the thermal zone in batch 1.1

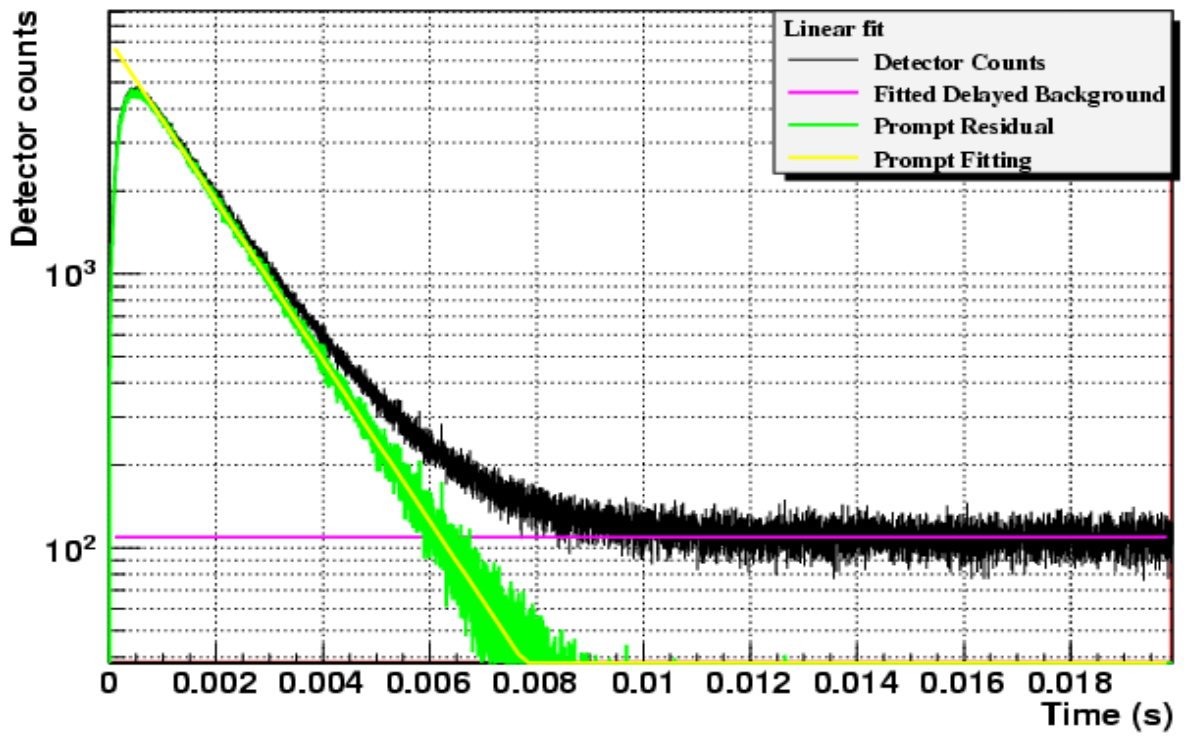

Figure 68. Linear fit of the pulsed neutron experiment recorded by long He-3 detector in MC5 channel of YALINA configuration with 36% enriched fuel in the fast zone and 1185 EK-10 fuel rods in the thermal zone in batch 1.2

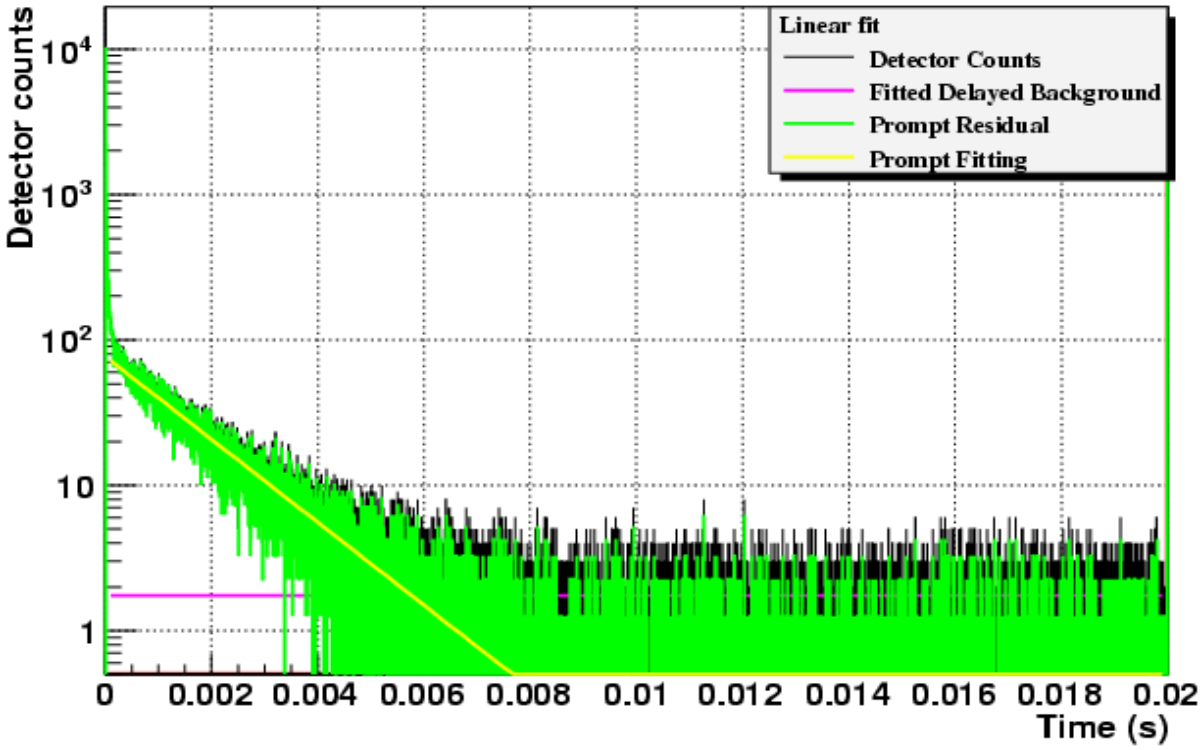

Figure 69. Linear fit of the pulsed neutron experiment recorded by long He-3 detector in EC1B channel of YALINA configuration with 36% enriched fuel in the fast zone and 1185 EK-10 fuel rods in the thermal zone in batch 1.2

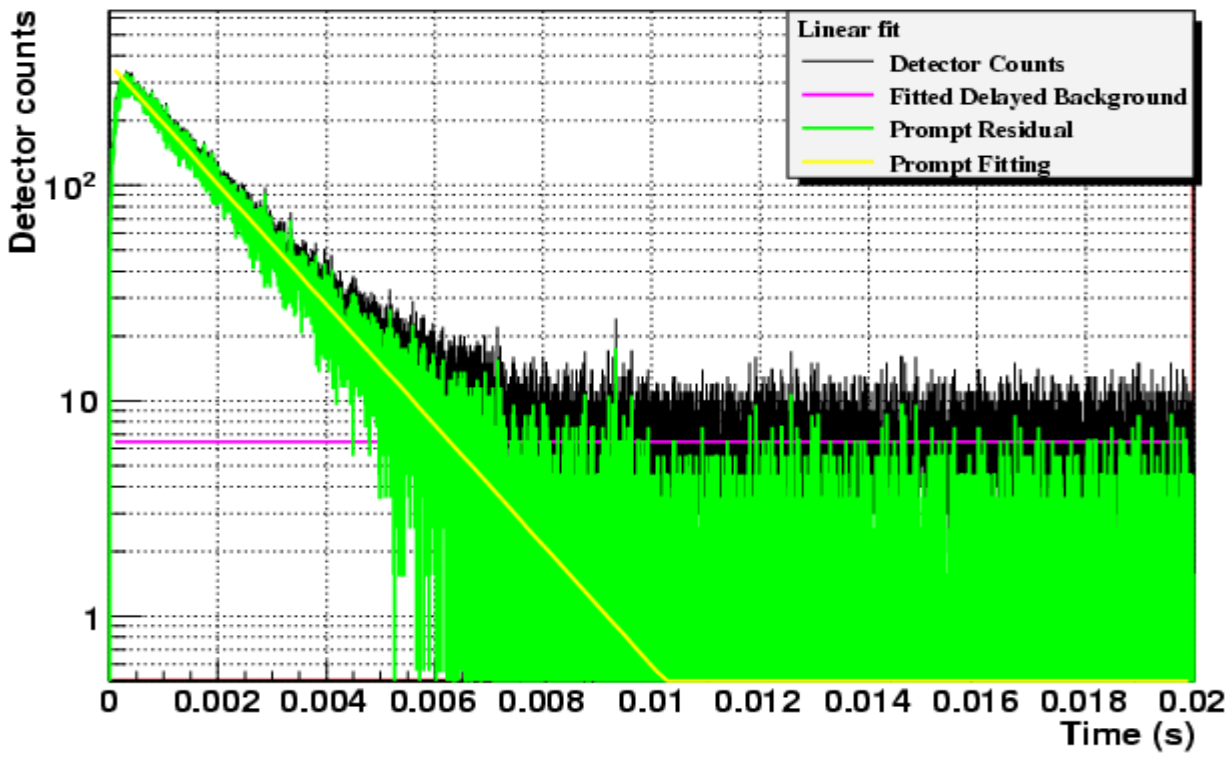

Figure 70. Linear fit of the pulsed neutron experiment recorded by small He-3 detector in EC7T channel of YALINA configuration with 36% enriched fuel in the fast zone and 1185 EK-10 fuel rods in the thermal zone in batch 1.2

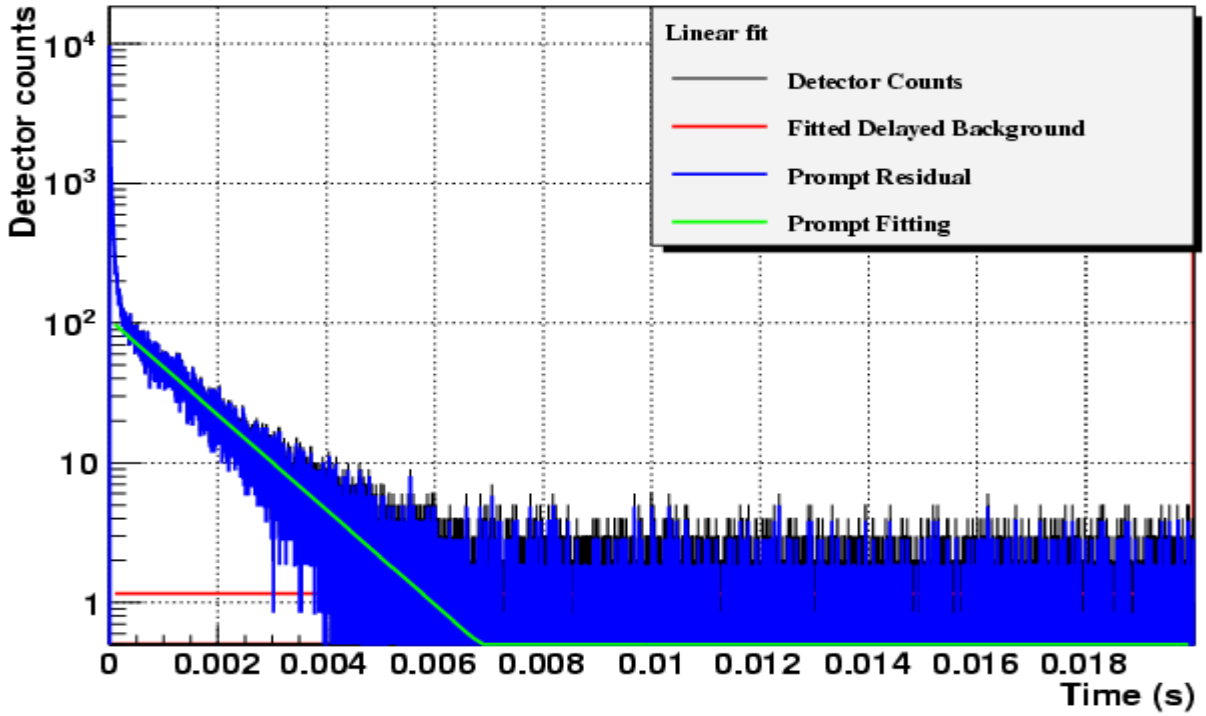

Figure 71. Linear fit of the pulsed neutron experiment recorded by DAQ system with long He-3 detector in EC1B channel of YALINA configuration with 21% enriched fuel in the fast zone and 1185 EK-10 fuel rods in the thermal zone in batch 0.1 in Dec-03-2009

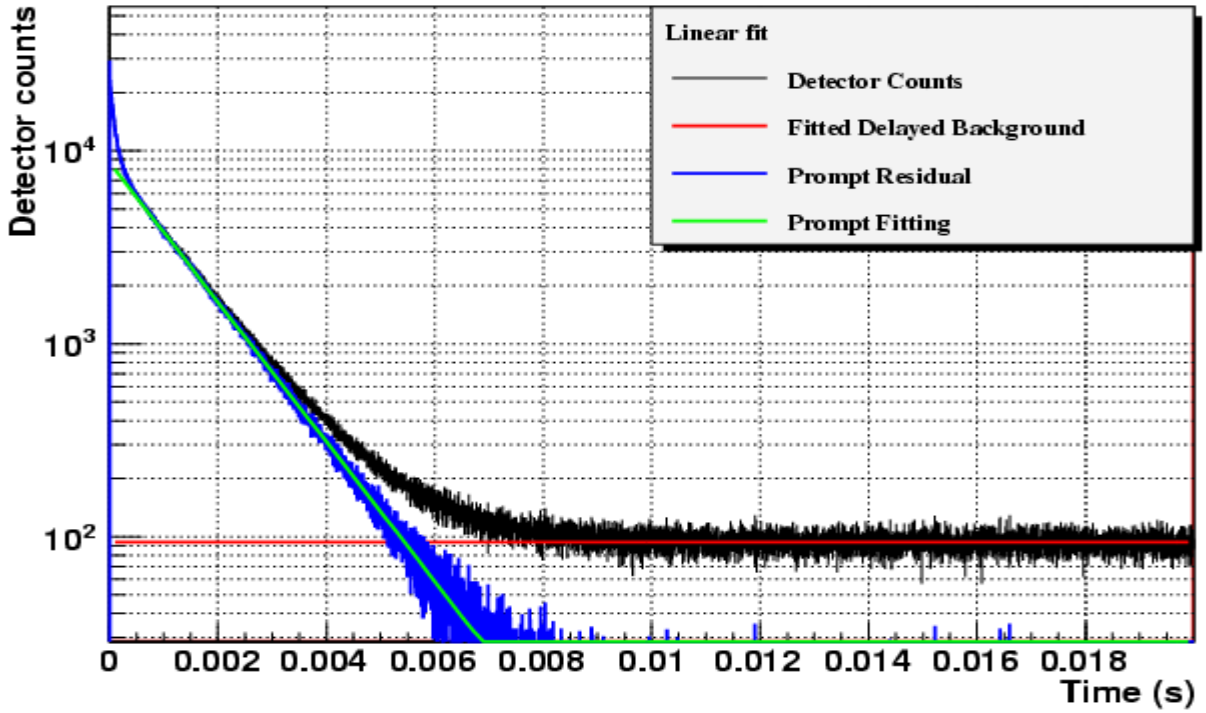

Figure 72. Linear fit of the pulsed neutron experiment recorded by DAQ system with long He-3 detector in EC5T channel of YALINA configuration with 21% enriched fuel in the fast zone and 1185 EK-10 fuel rods in the thermal zone in batch 0.1 in Dec-03-2009

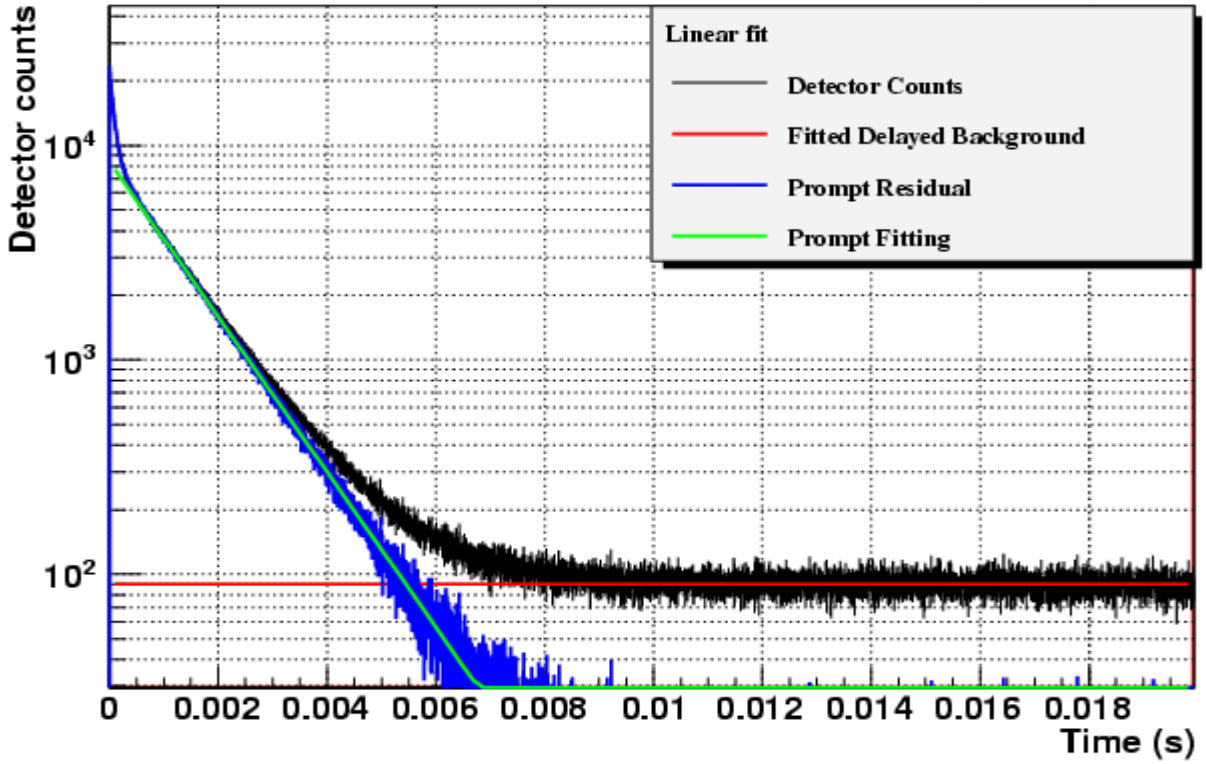

Figure 73. Linear fit of the pulsed neutron experiment recorded by MCS with long He-3 detector in EC5T channel of YALINA configuration with 21% enriched fuel in the fast zone and 1185 EK-10 fuel rods in the thermal zone in batch 0.1 in Dec-03-2009

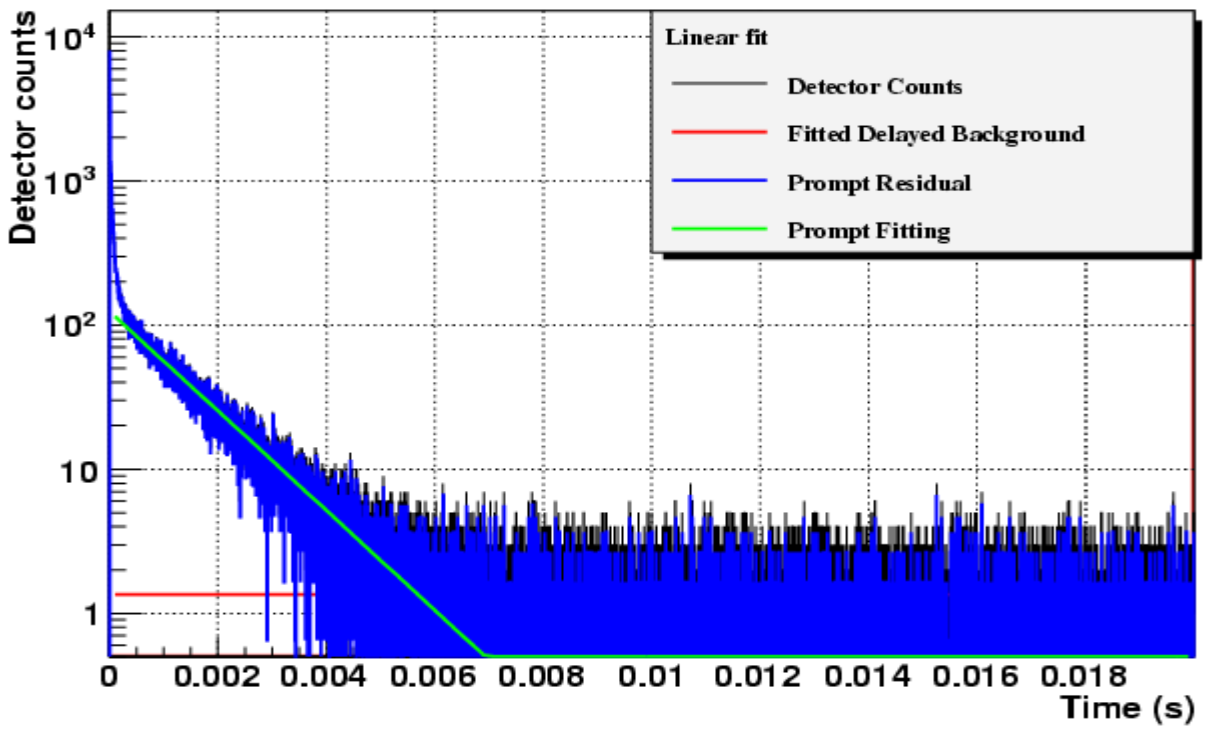

Figure 74. Linear fit of the pulsed neutron experiment recorded by DAQ system with long He-3 detector in EC2B channel of YALINA configuration with 21% enriched fuel in the fast zone and 1185 EK-10 fuel rods in the thermal zone in batch 0.2 in Dec-03-2009

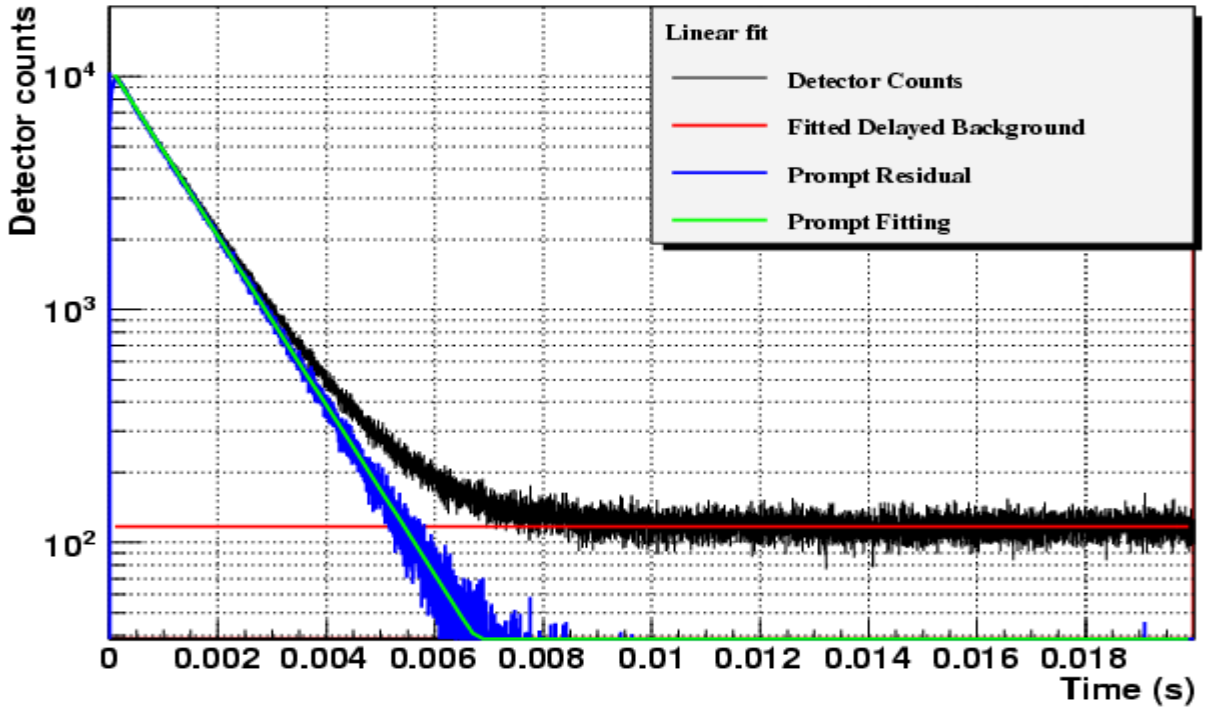

Figure 75. Linear fit of the pulsed neutron experiment recorded by DAQ system with long He-3 detector in EC6T channel of YALINA configuration with 21% enriched fuel in the fast zone and 1185 EK-10 fuel rods in the thermal zone in batch 0.2 in Dec-03-2009

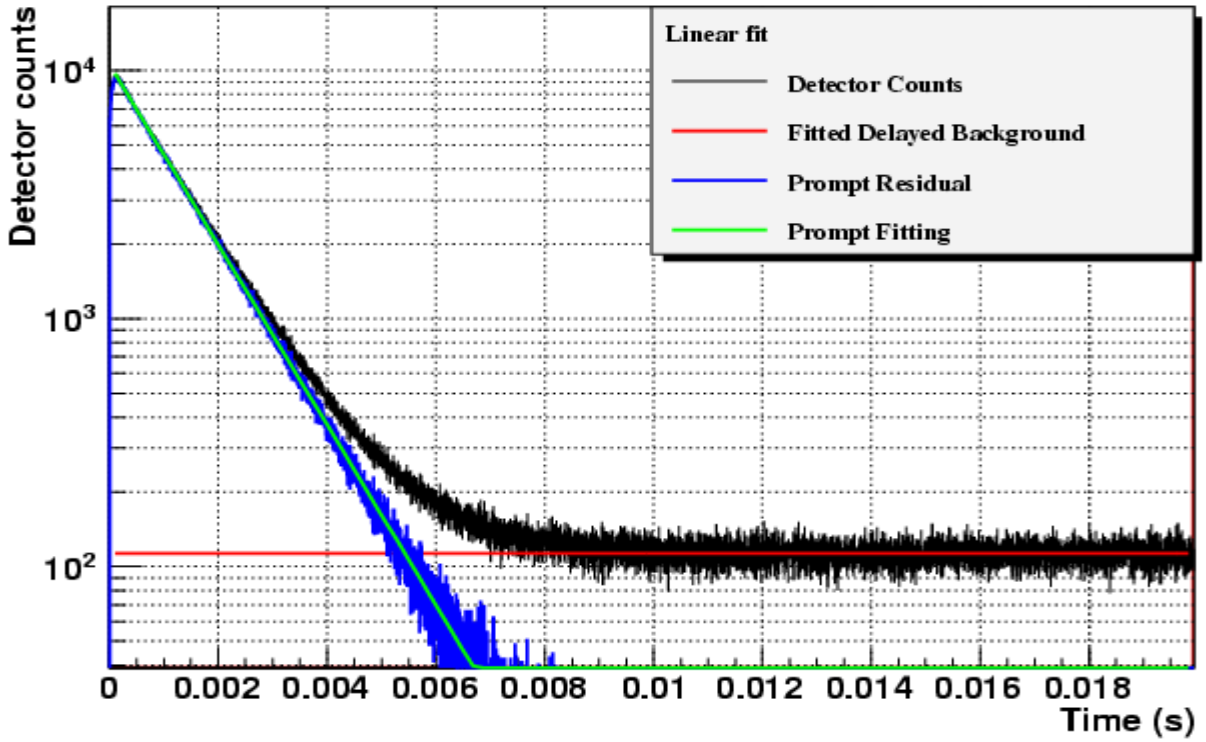

Figure 76. Linear fit of the pulsed neutron experiment recorded by MCS with long He-3 detector in EC6T channel of YALINA configuration with 21% enriched fuel in the fast zone and 1185 EK-10 fuel rods in the thermal zone in batch 0.2 in Dec-03-2009

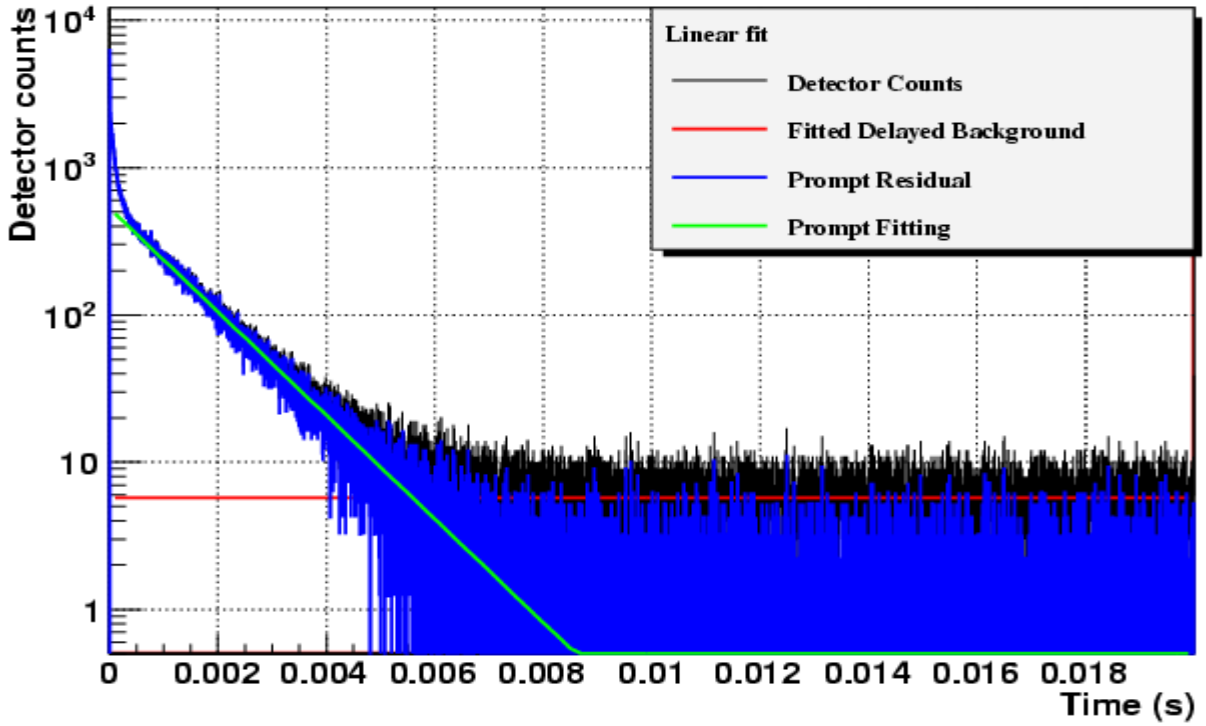

Figure 77. Linear fit of the pulsed neutron experiment recorded by DAQ system with long He-3 detector in EC3B channel of YALINA configuration with 21% enriched fuel in the fast zone and 1185 EK-10 fuel rods in the thermal zone in batch 0.3 in Dec-03-2009

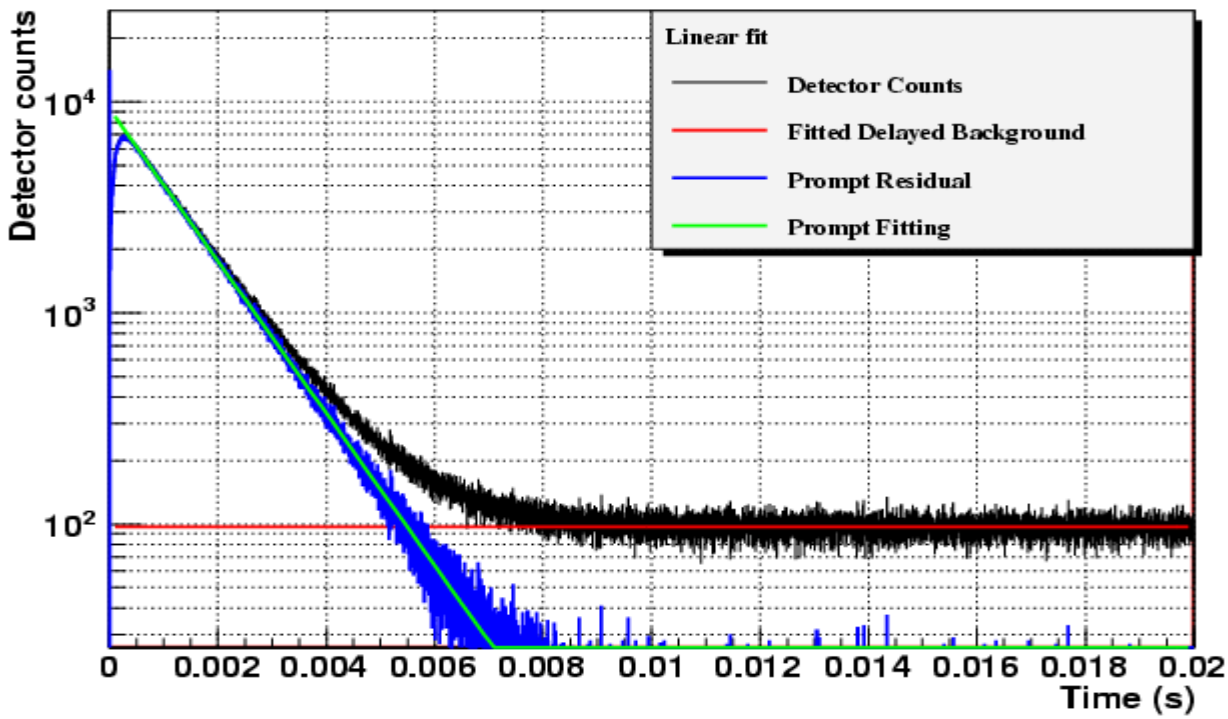

Figure 78. Linear fit of the pulsed neutron experiment recorded by DAQ system with long He-3 detector in EC7T channel of YALINA configuration with 21% enriched fuel in the fast zone and 1185 EK-10 fuel rods in the thermal zone in batch 0.3 in Dec-03-2009

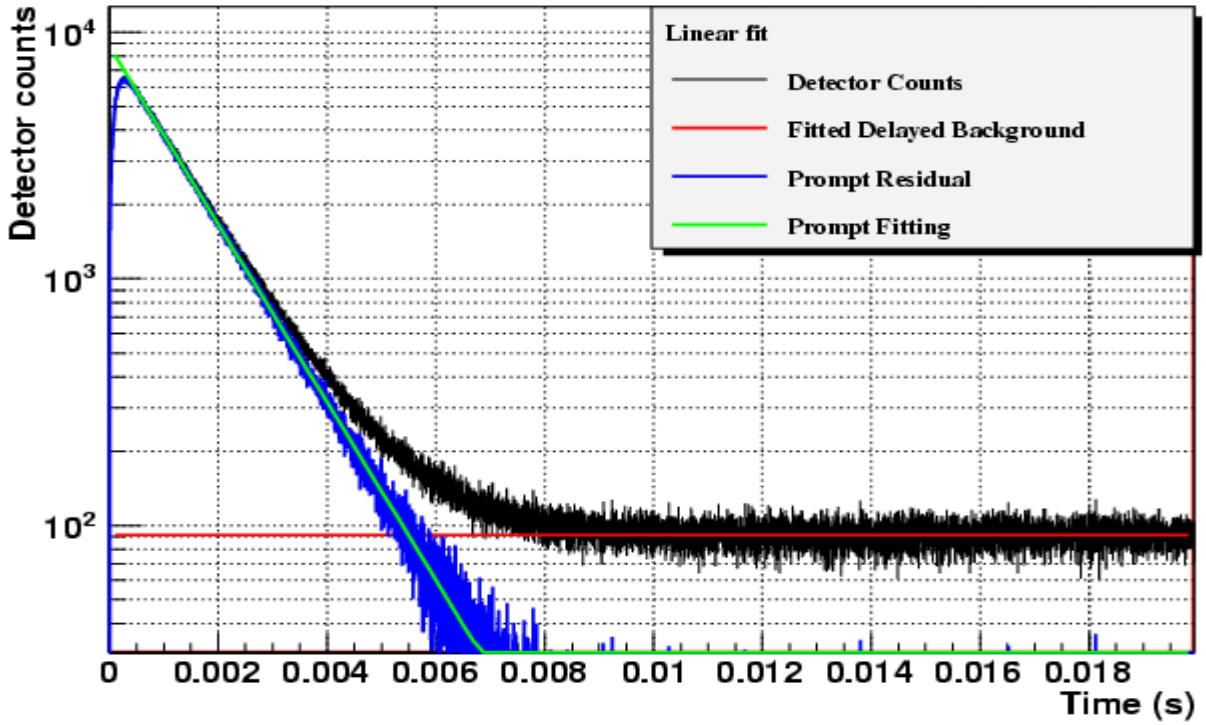

Figure 79. Linear fit of the pulsed neutron experiment recorded by MCS with long He-3 detector in EC7T channel of YALINA configuration with 21% enriched fuel in the fast zone and 1185 EK-10 fuel rods in the thermal zone in batch 0.3 in Dec-03-2009

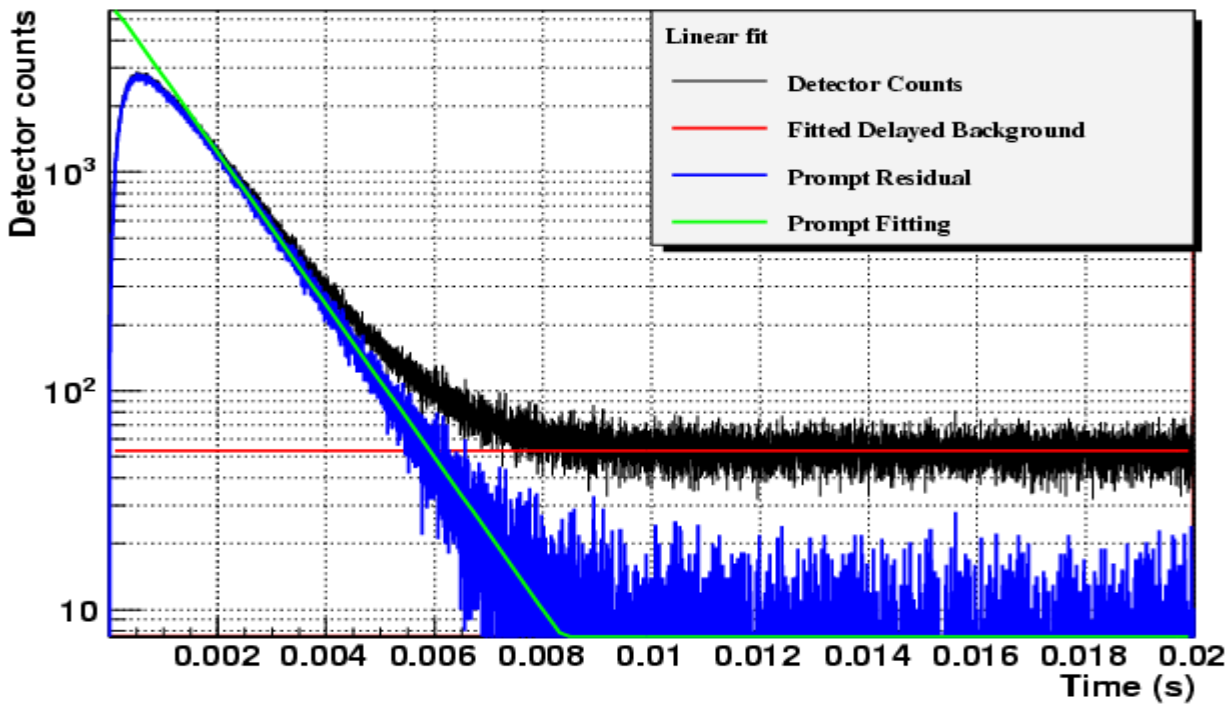

Figure 80. Linear fit of the pulsed neutron experiment recorded by DAQ system with long He-3 detector in EC8R channel of YALINA configuration with 21% enriched fuel in the fast zone and 1185 EK-10 fuel rods in the thermal zone in batch 0.4 in Dec-03-2009

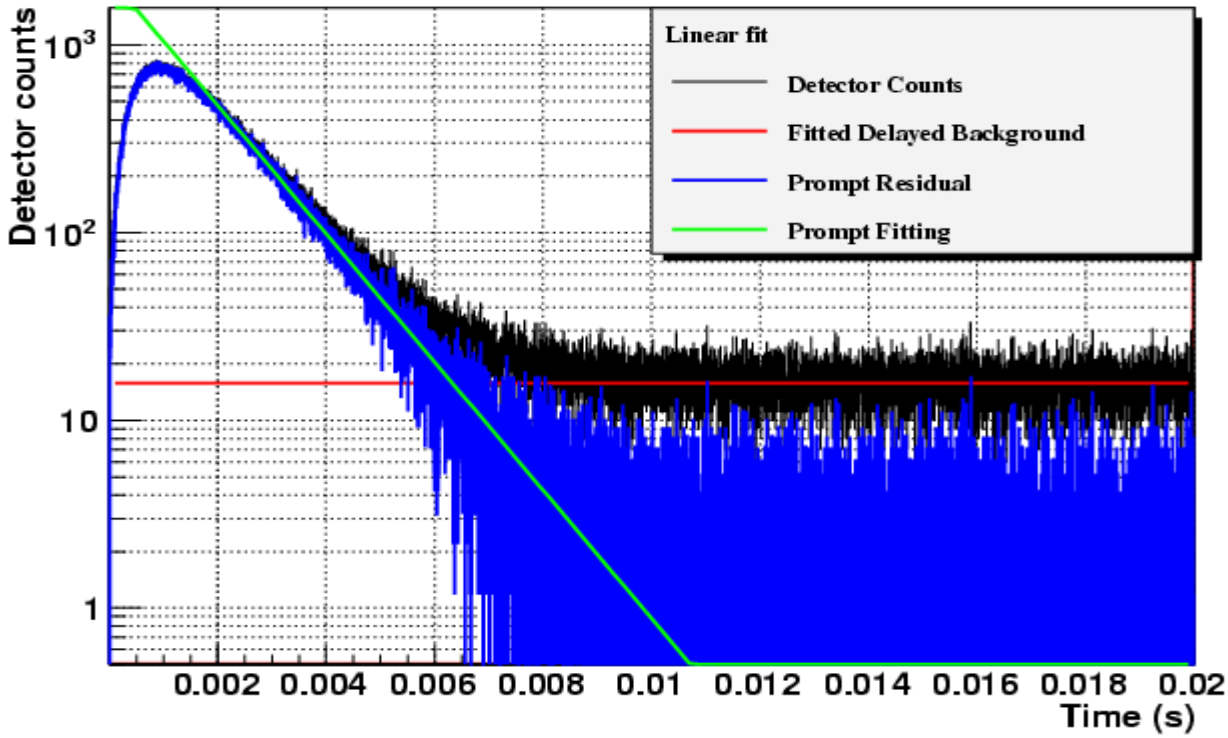

Figure 81. Linear fit of the pulsed neutron experiment recorded by DAQ system with long He-3 detector in EC9R channel of YALINA configuration with 21% enriched fuel in the fast zone and 1185 EK-10 fuel rods in the thermal zone in batch 0.4 in Dec-03-2009

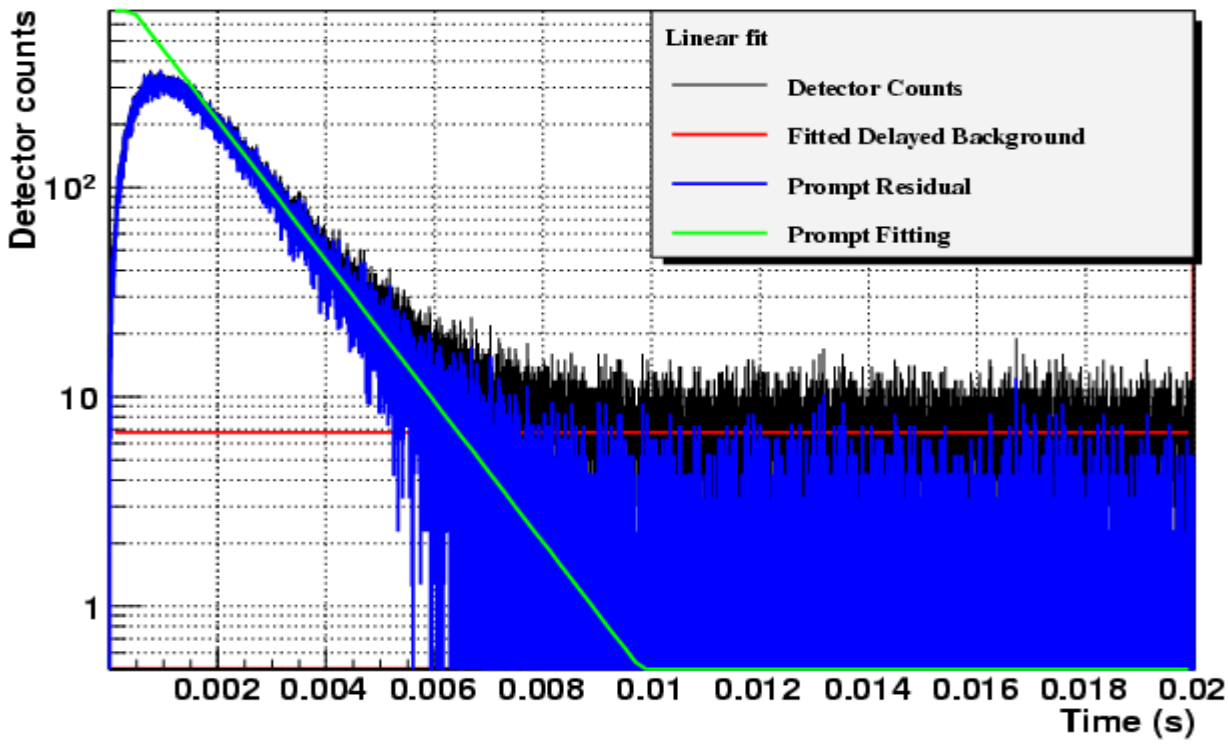

Figure 82. Linear fit of the pulsed neutron experiment recorded by DAQ system with long He-3 detector in MC3 channel of YALINA configuration with 21% enriched fuel in the fast zone and 1185 EK-10 fuel rods in the thermal zone in batch 0.5 in Dec-03-2009

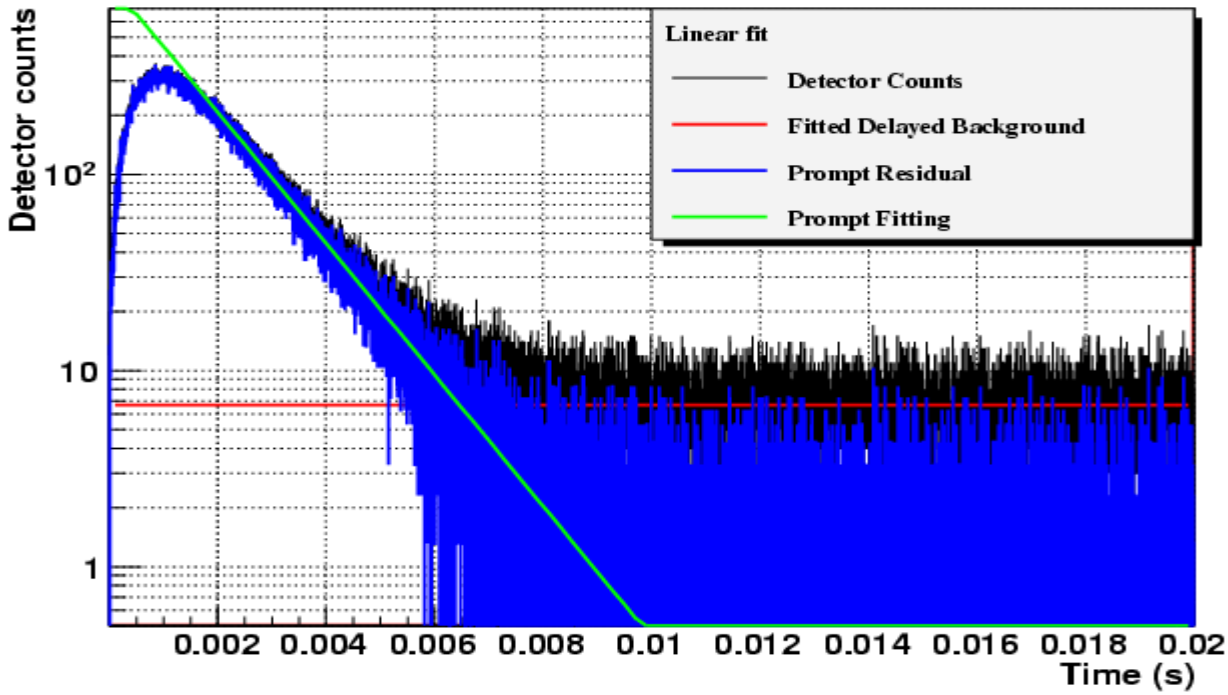

Figure 83. Linear fit of the pulsed neutron experiment recorded by DAQ system with long He-3 detector in MC4 channel of YALINA configuration with 21% enriched fuel in the fast zone and 1185 EK-10 fuel rods in the thermal zone in batch 0.5 in Dec-03-2009

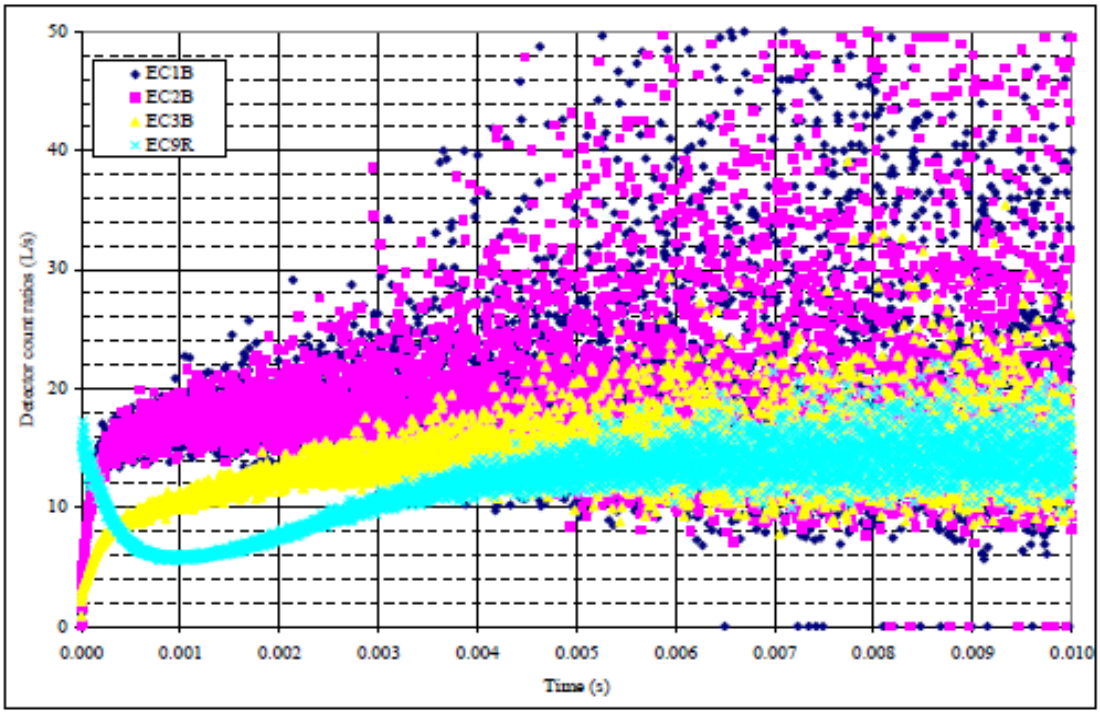

Figure 84. The detector count ratio of the He-3 long detector to the small detector at EC1B, EC2B, EC3B and EC9R positions in the YALINA configuration with 21% enriched fuel in the fast zone and 1185 EK-10 fuel rods in the thermal zone in Dec-17-2009

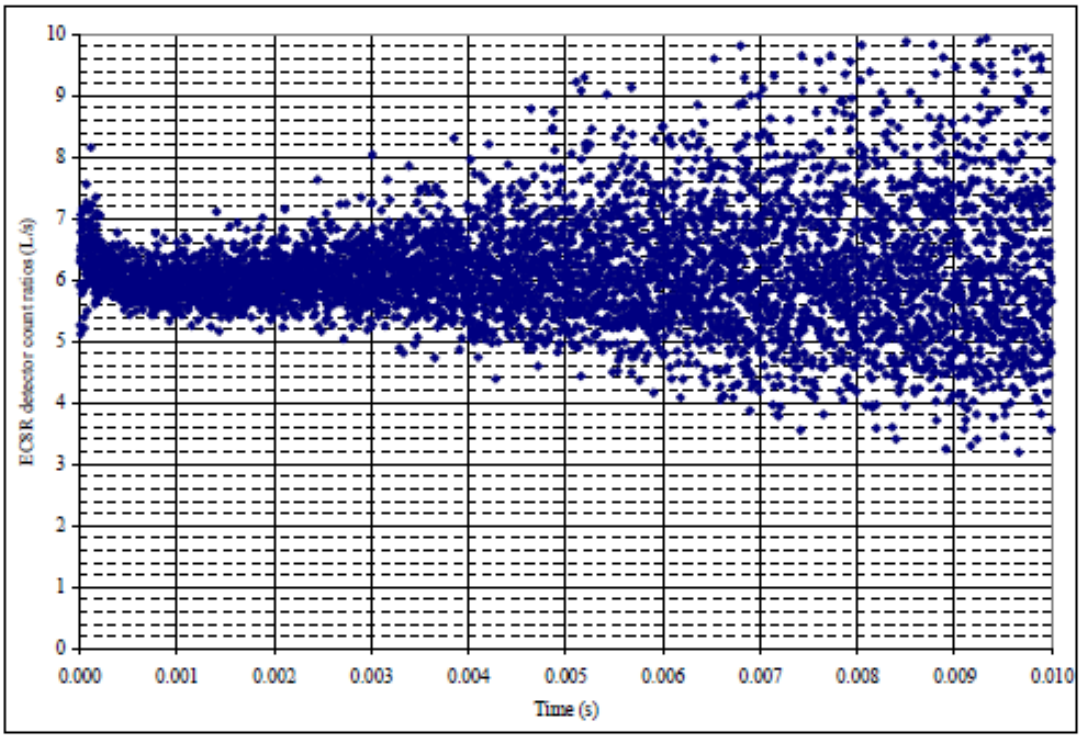

Figure 85. The detector count ratio of the He-3 long detector to the small detector at EC9R in the YALINA configuration with 36% enriched fuel in the fast zone and 1185 EK-10 in the thermal zone

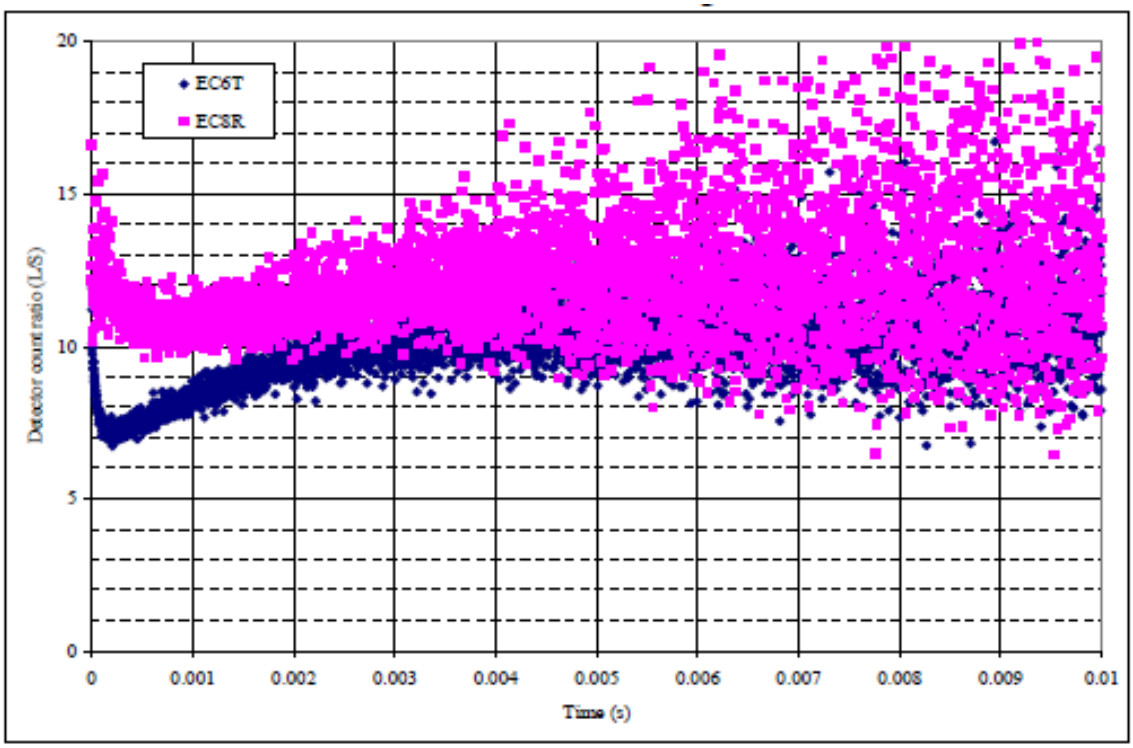

Figure 86. The detector count ratio of the He-3 long detector to the small detector at EC6T and EC8R in the YALINA configuration with 90% enriched fuel in the fast zone and 1141 EK-10 fuel rods in the thermal zone.

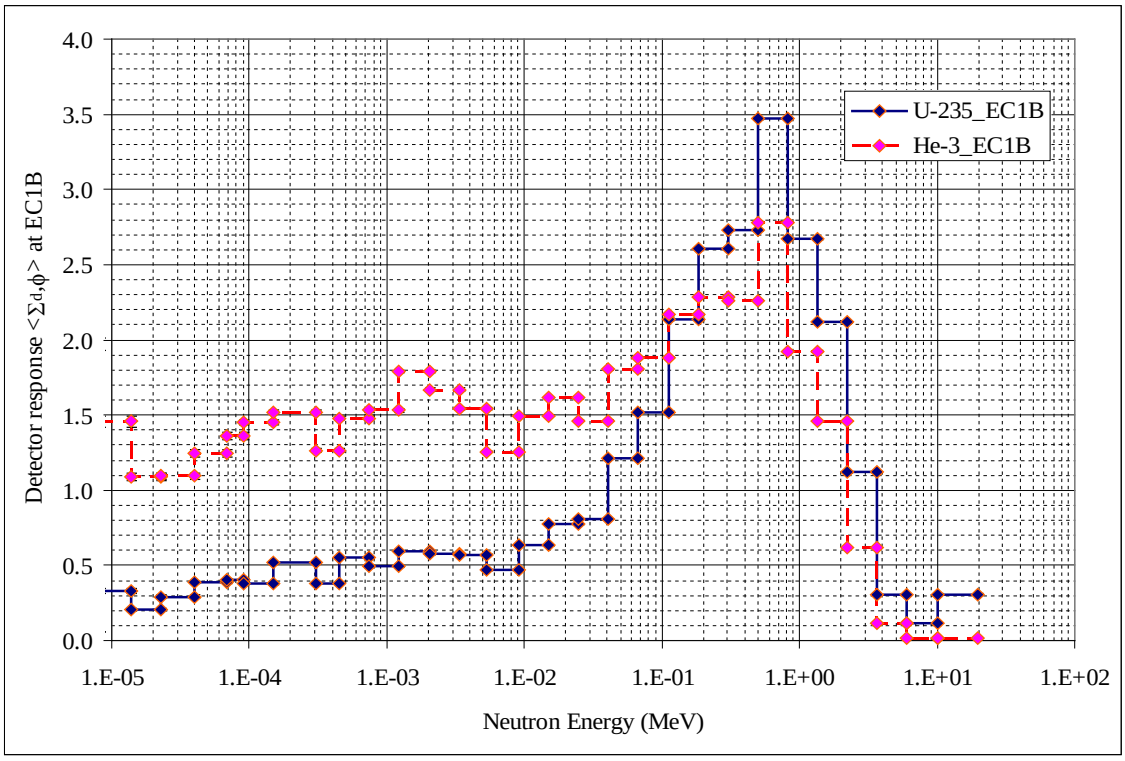

Figure 87. The Monte Carlo simulated detector responses of a U-235 long detector or a He-3 long detector at EC1B in the YALINA 1141 configuration

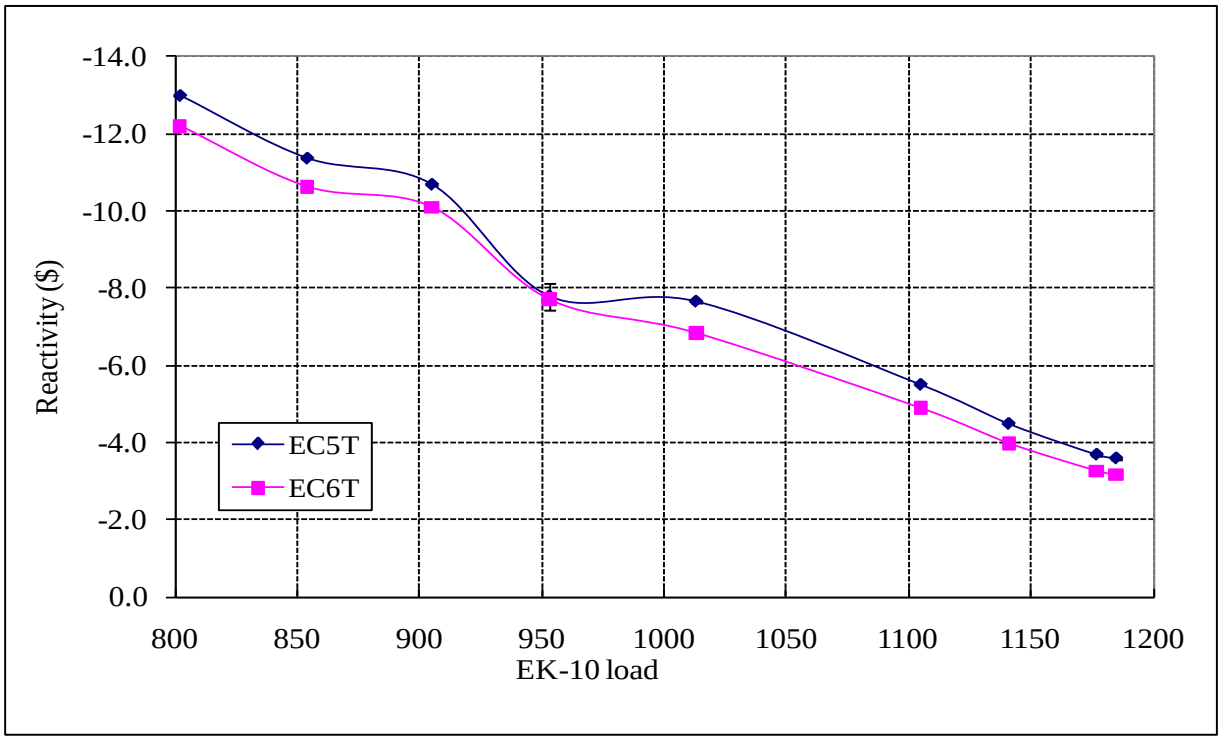

Figure 88. The reactivity obtained from the pulsed-neutron experiment for the YALINA configuration with 36% enriched uranium fuels in the fast zone and different EK-10 fuel rods in the thermal zone

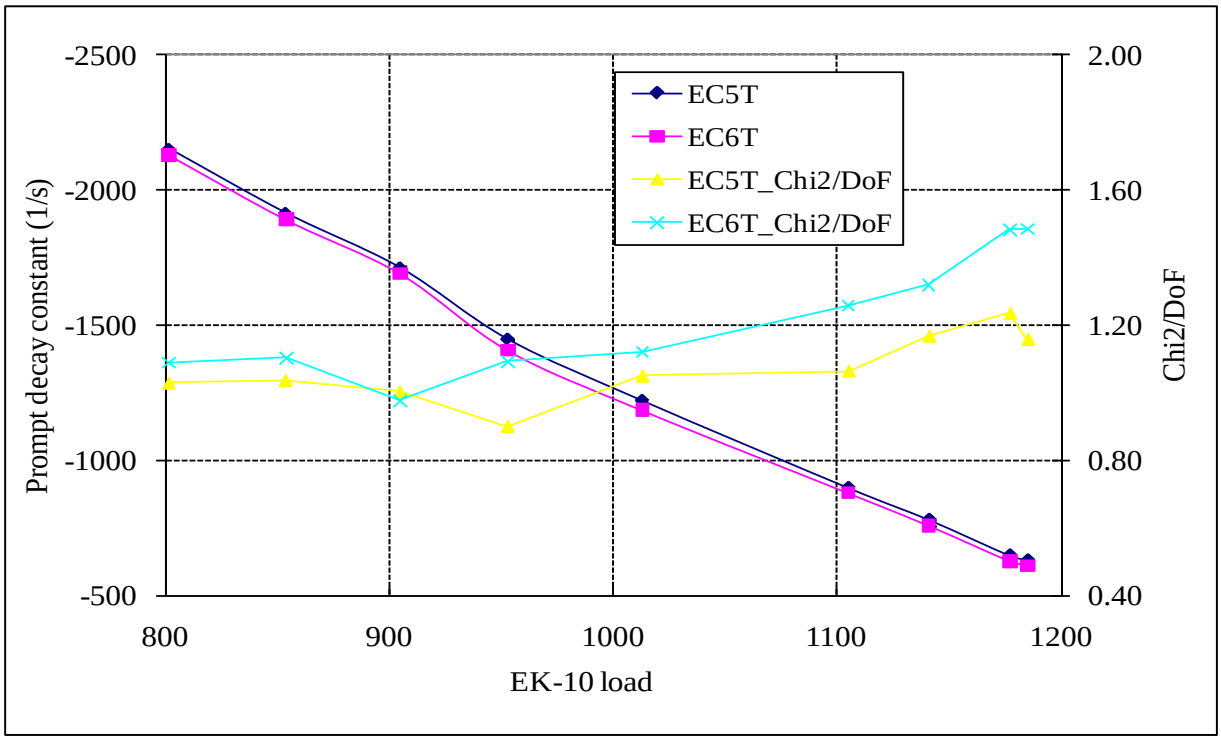

Figure 89. The prompt decay constants obtained from the pulsed-neutron experiment for the YALINA configuration with 36% enriched uranium fuels in the fast zone and different EK-10 fuel rods in the thermal zone

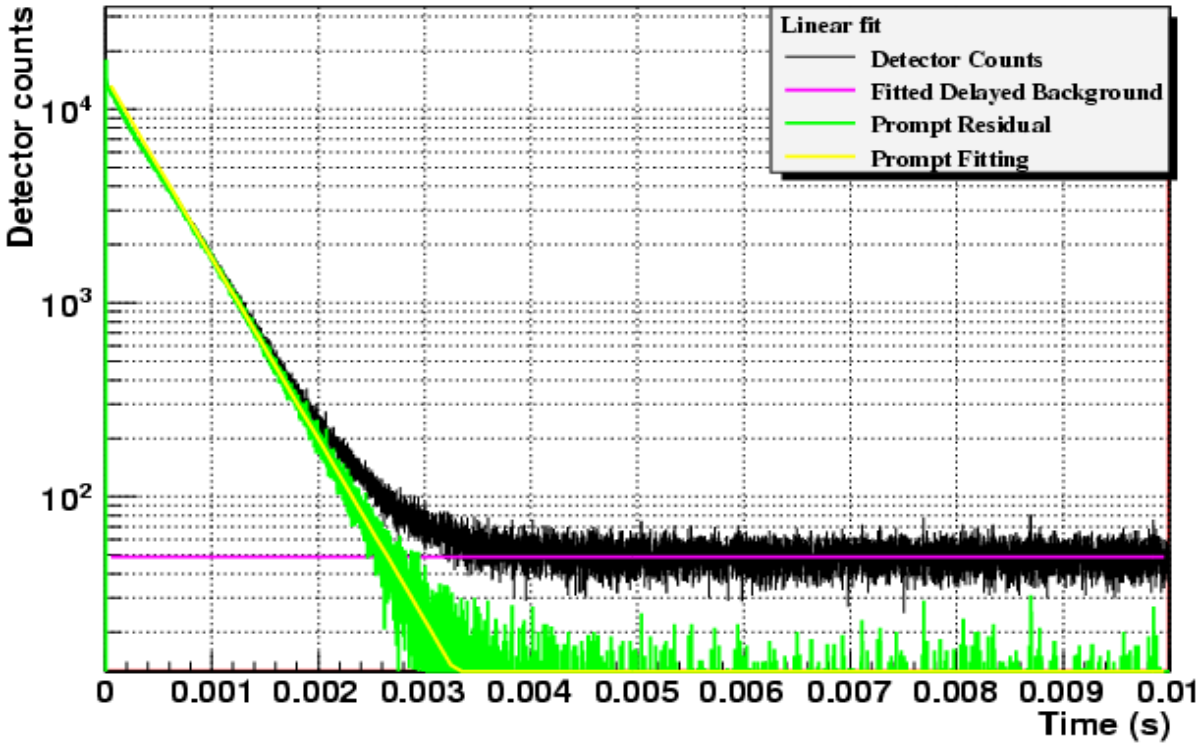

Figure 90. Linear fit of the pulsed neutron experiment recorded by small He-3 detector in EC5T channel of YALINA configuration with 36% enriched fuel in the fast zone and 802 EK-10 fuel rods in the thermal zone

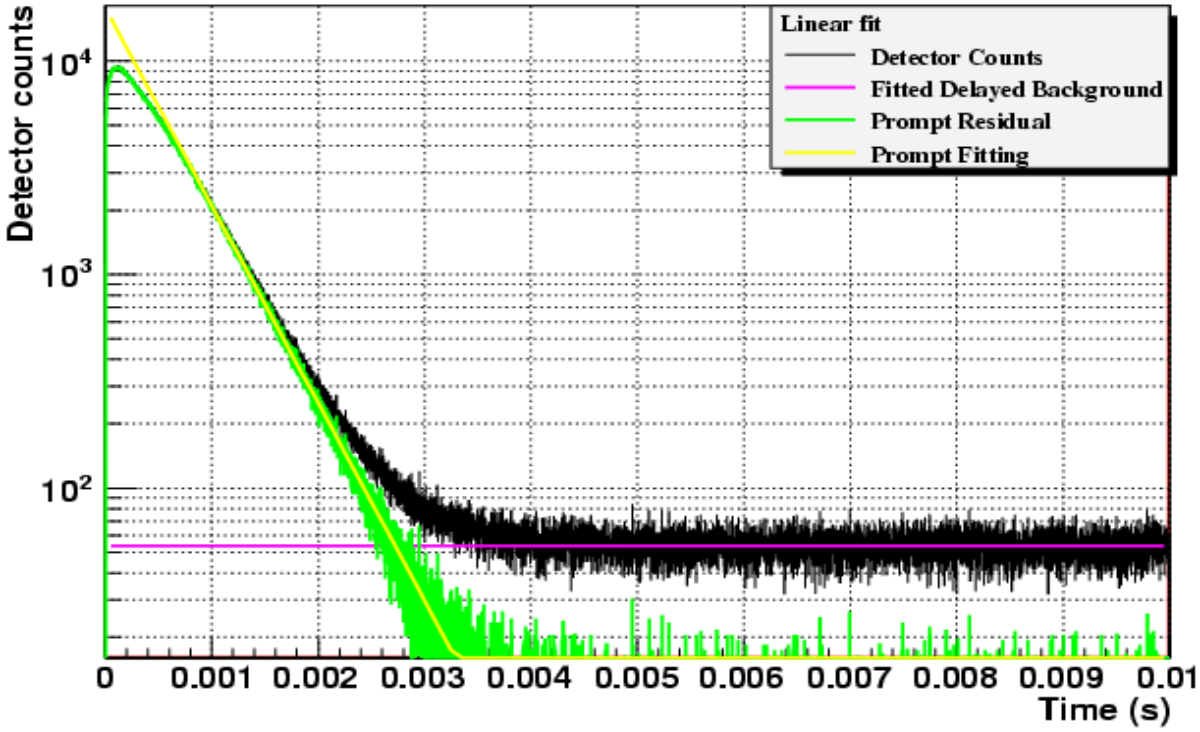

Figure 91. Linear fit of the pulsed neutron experiment recorded by small He-3 detector in EC6T channel of YALINA configuration with 36% enriched fuel in the fast zone and 802 EK-10 fuel rods in the thermal zone

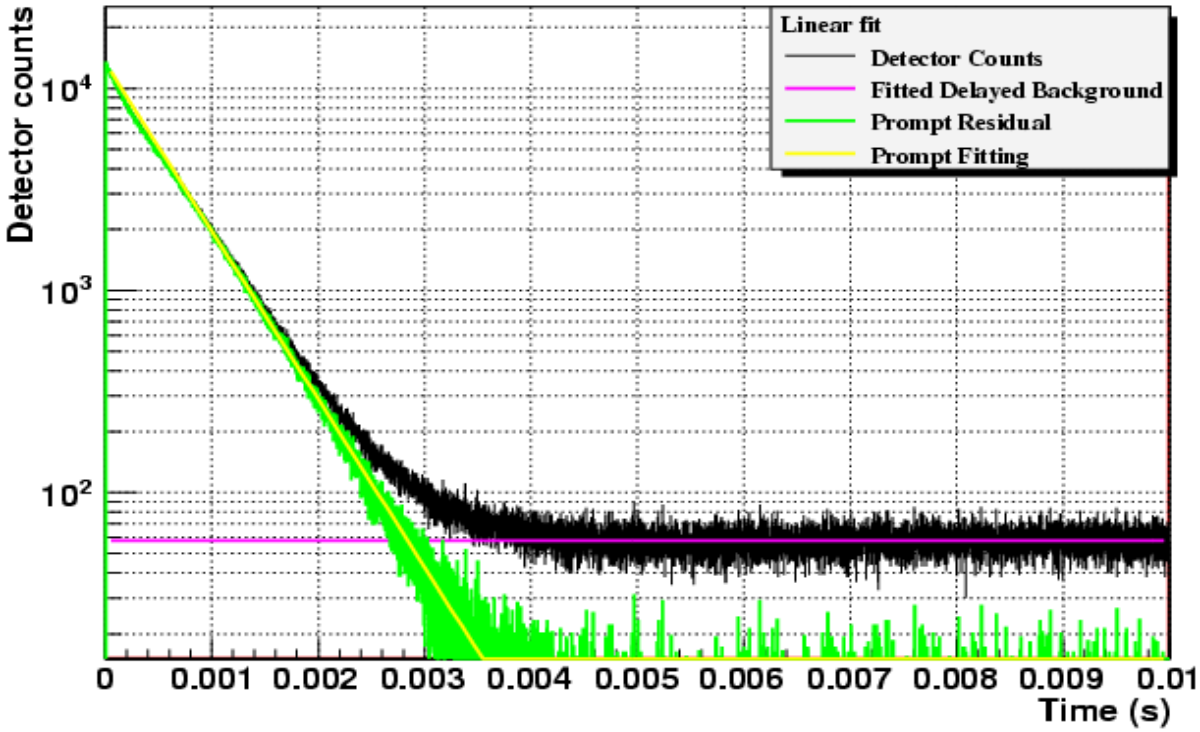

Figure 92. Linear fit of the pulsed neutron experiment recorded by small He-3 detector in EC5T channel of YALINA configuration with 36% enriched fuel in the fast zone and 854 EK-10 fuel rods in the thermal zone

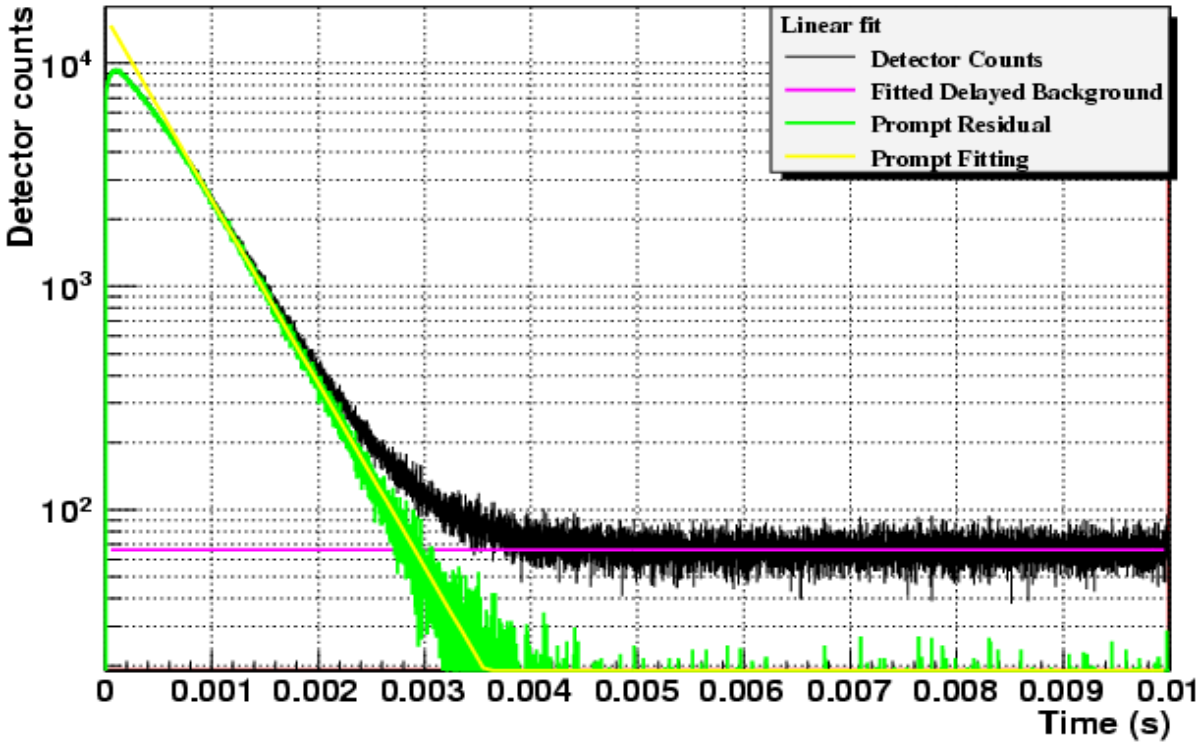

Figure 93. Linear fit of the pulsed neutron experiment recorded by small He-3 detector in EC6T channel of YALINA configuration with 36% enriched fuel in the fast zone and 854 EK-10 fuel rods in the thermal zone

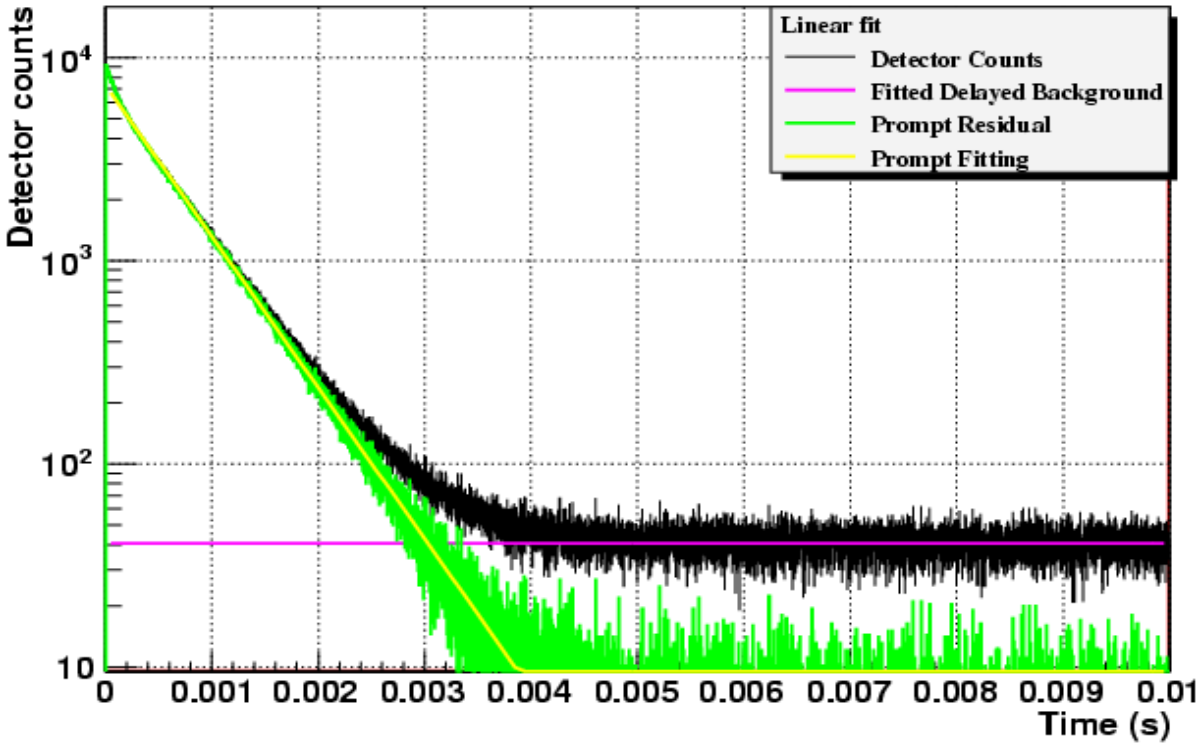

Figure 94. Linear fit of the pulsed neutron experiment recorded by small He-3 detector in EC5T channel of YALINA configuration with 36% enriched fuel in the fast zone and 905 EK-10 fuel rods in the thermal zone

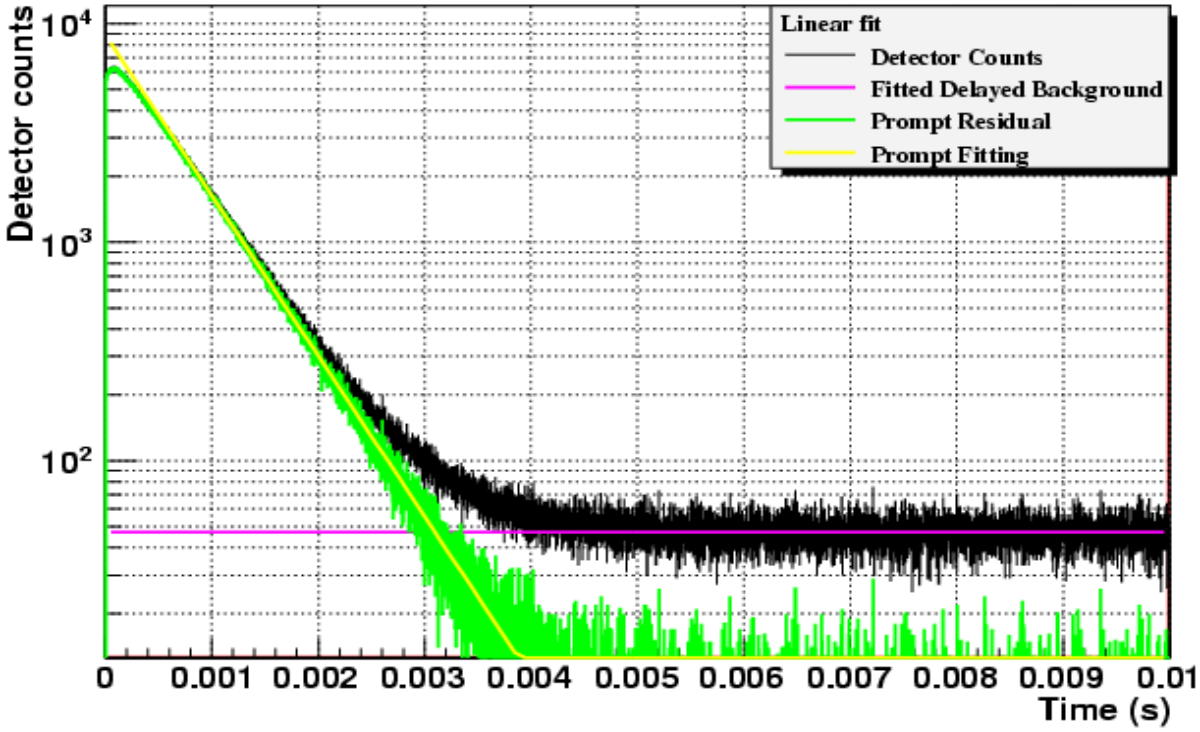

Figure 95. Linear fit of the pulsed neutron experiment recorded by small He-3 detector in EC6T channel of YALINA configuration with 36% enriched fuel in the fast zone and 905 EK-10 fuel rods in the thermal zone

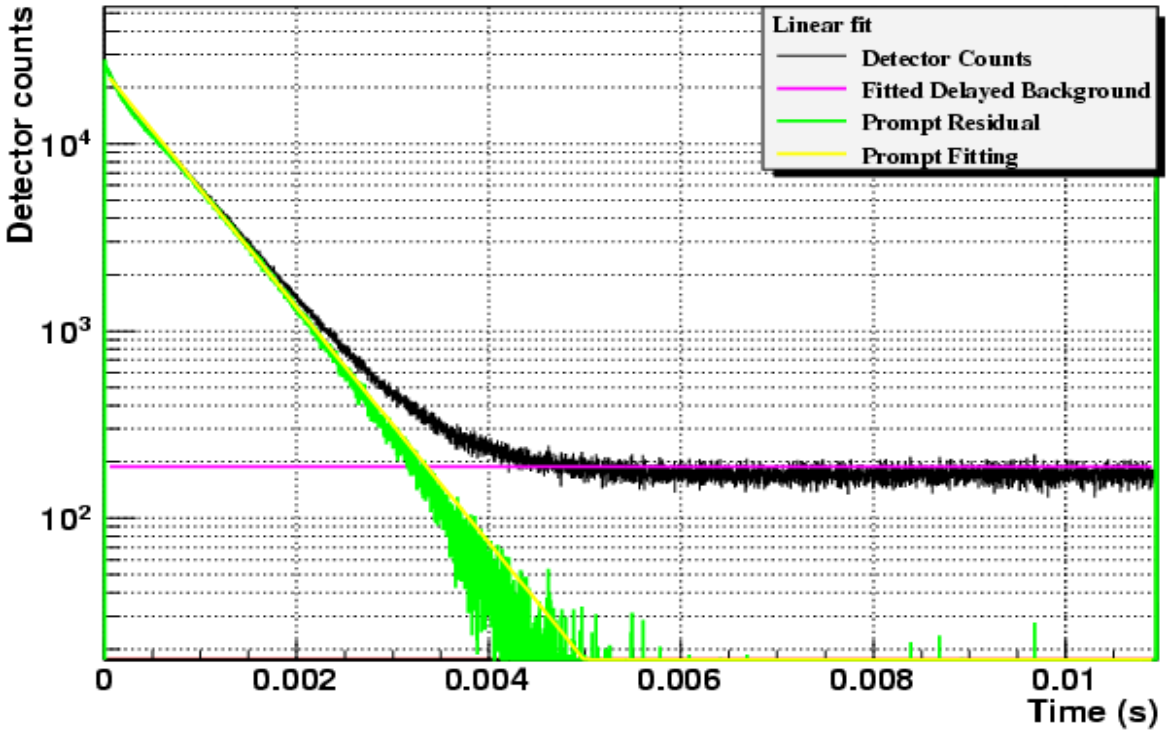

Figure 96. Linear fit of the pulsed neutron experiment recorded by small He-3 detector in EC5T channel of YALINA configuration with 36% enriched fuel in the fast zone and 953 EK-10 fuel rods in the thermal zone

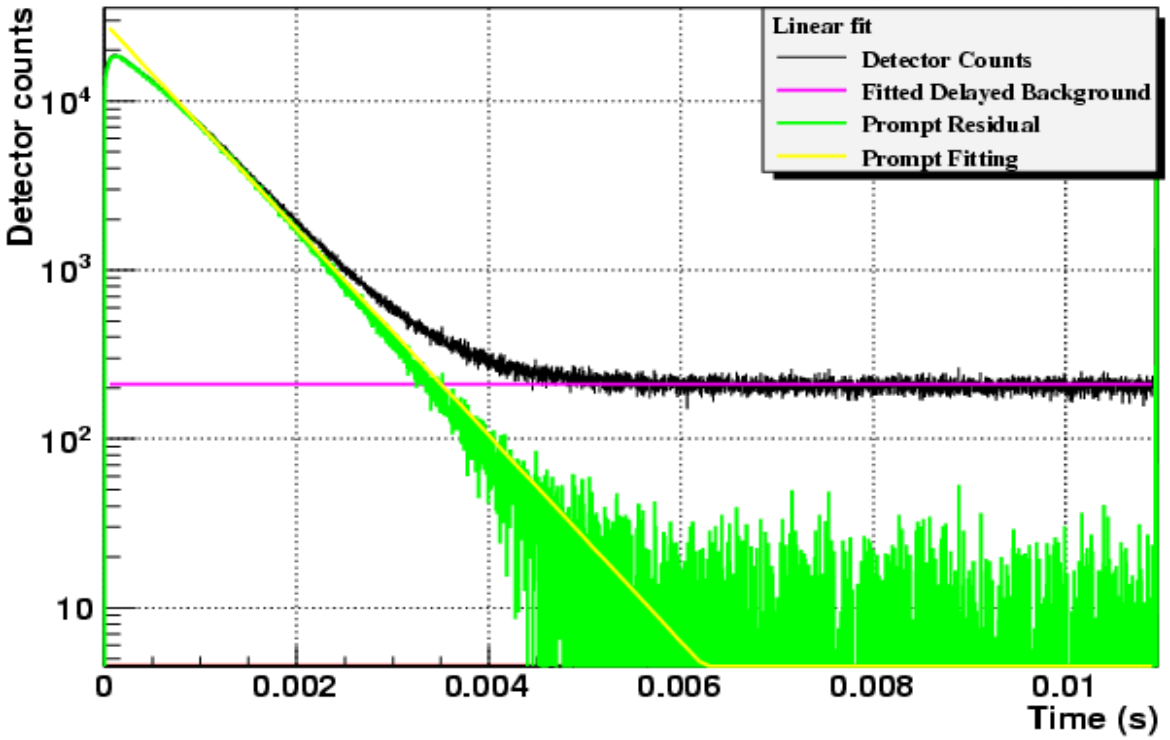

Figure 97. Linear fit of the pulsed neutron experiment recorded by small He-3 detector in EC6T channel of YALINA configuration with 36% enriched fuel in the fast zone and 953 EK-10 fuel rods in the thermal zone

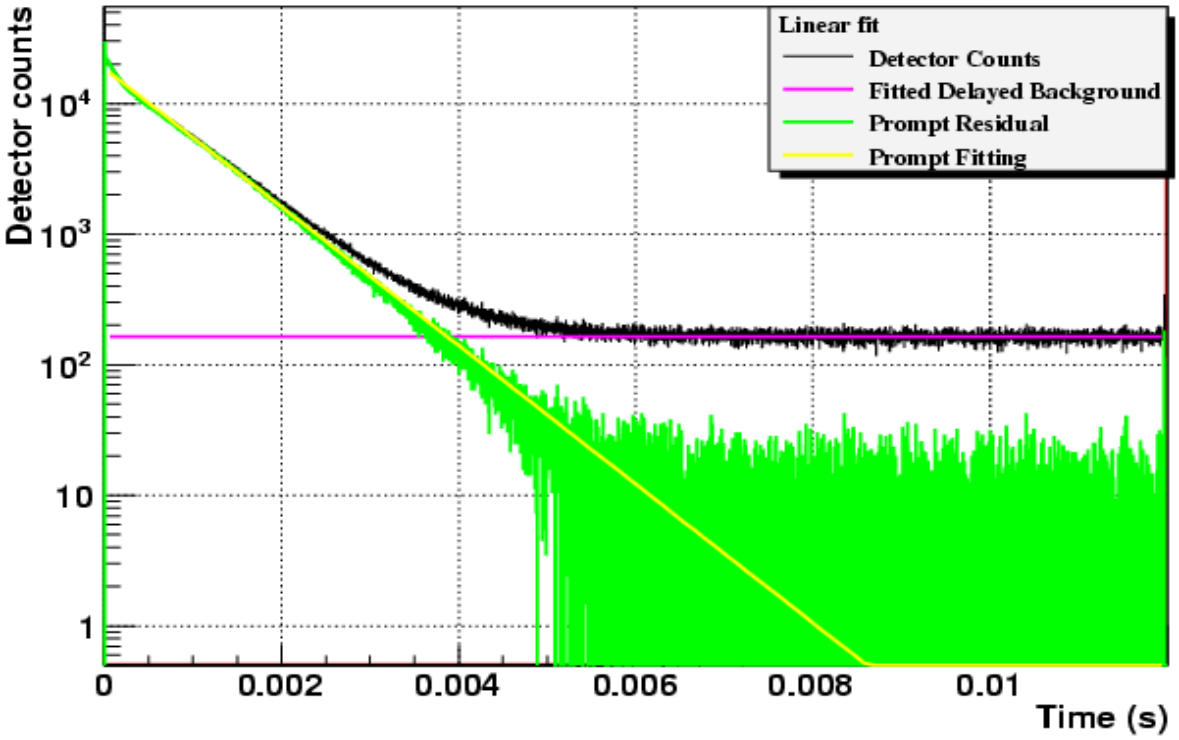

Figure 98. Linear fit of the pulsed neutron experiment recorded by small He-3 detector in EC5T channel of YALINA configuration with 36% enriched fuel in the fast zone and 1013 EK-10 fuel rods in the thermal zone

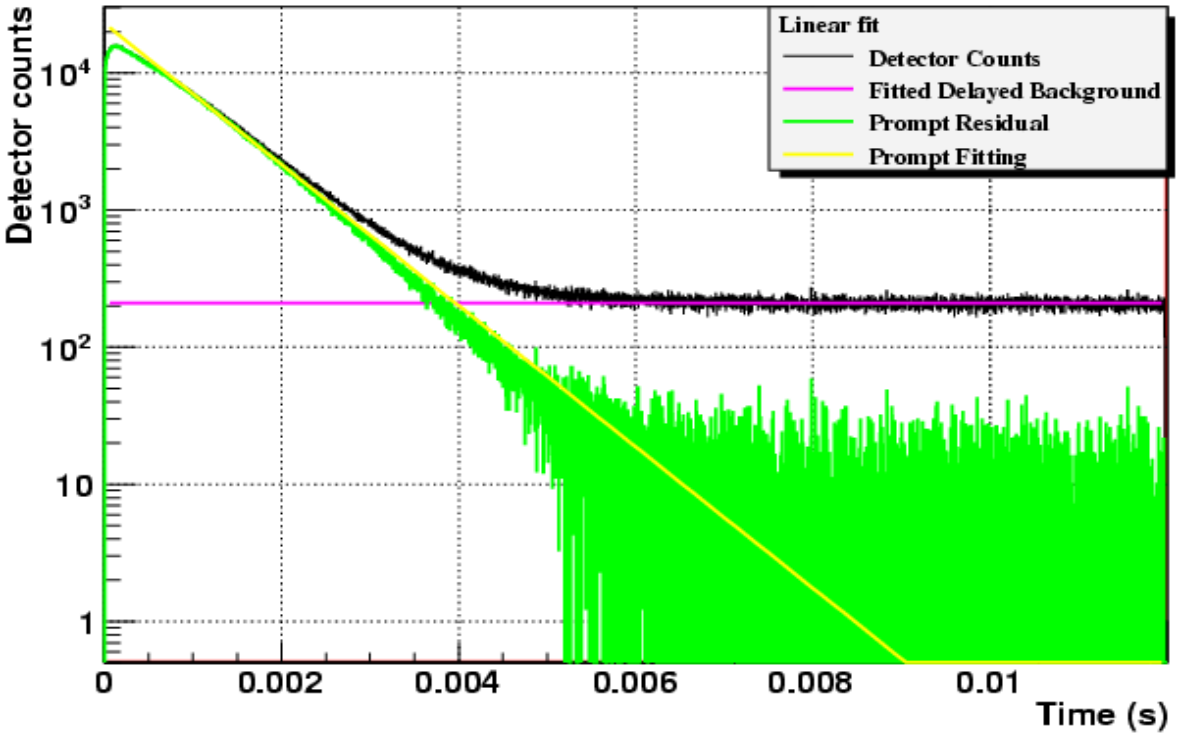

Figure 99. Linear fit of the pulsed neutron experiment recorded by small He-3 detector in EC6T channel of YALINA configuration with 36% enriched fuel in the fast zone and 1013 EK-10 fuel rods in the thermal zone

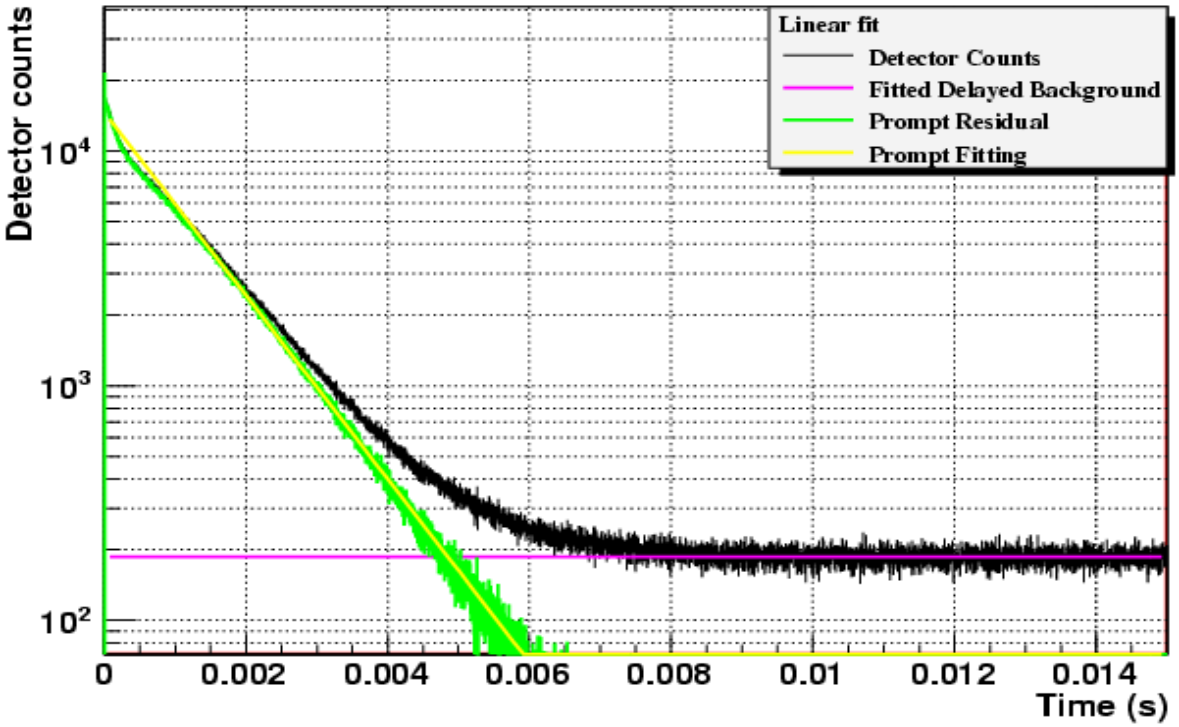

Figure 100. Linear fit of the pulsed neutron experiment recorded by small He-3 detector in EC5T channel of YALINA configuration with 36% enriched fuel in the fast zone and 1105 EK-10 fuel rods in the thermal zone

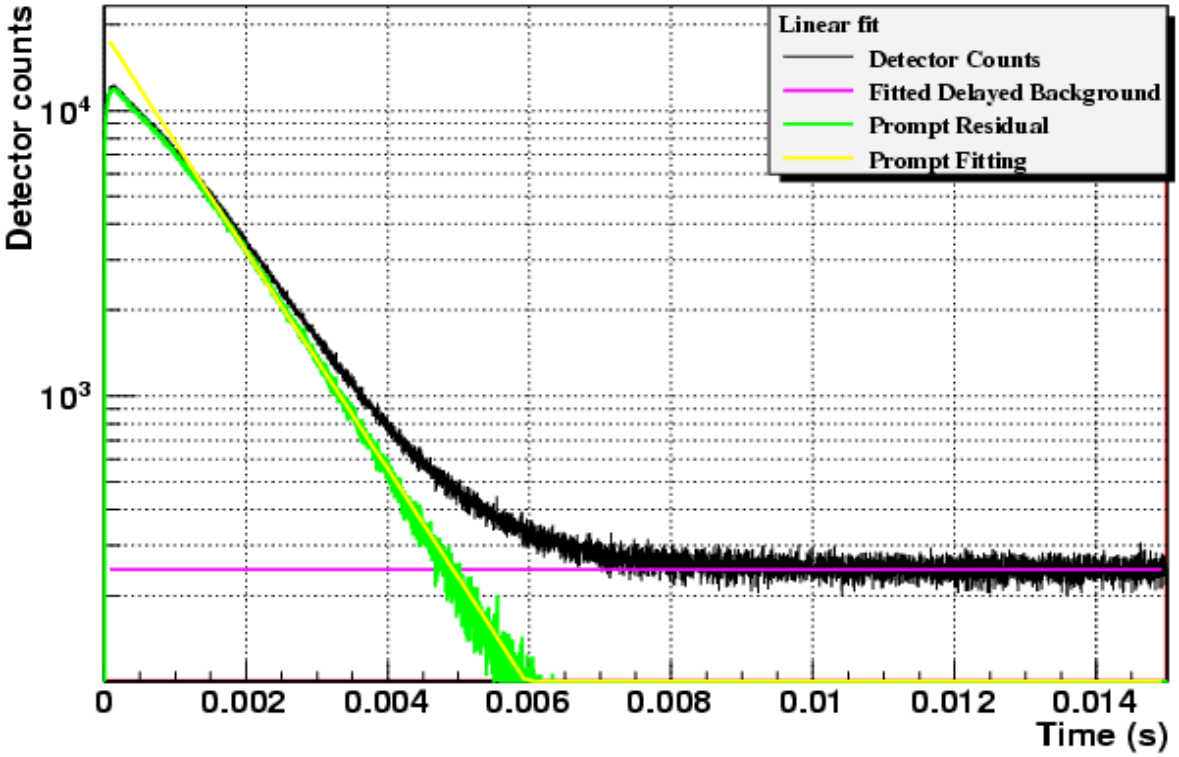

Figure 101. Linear fit of the pulsed neutron experiment recorded by small He-3 detector in EC6T channel of YALINA configuration with 36% enriched fuel in the fast zone and 1105 EK-10 fuel rods in the thermal zone

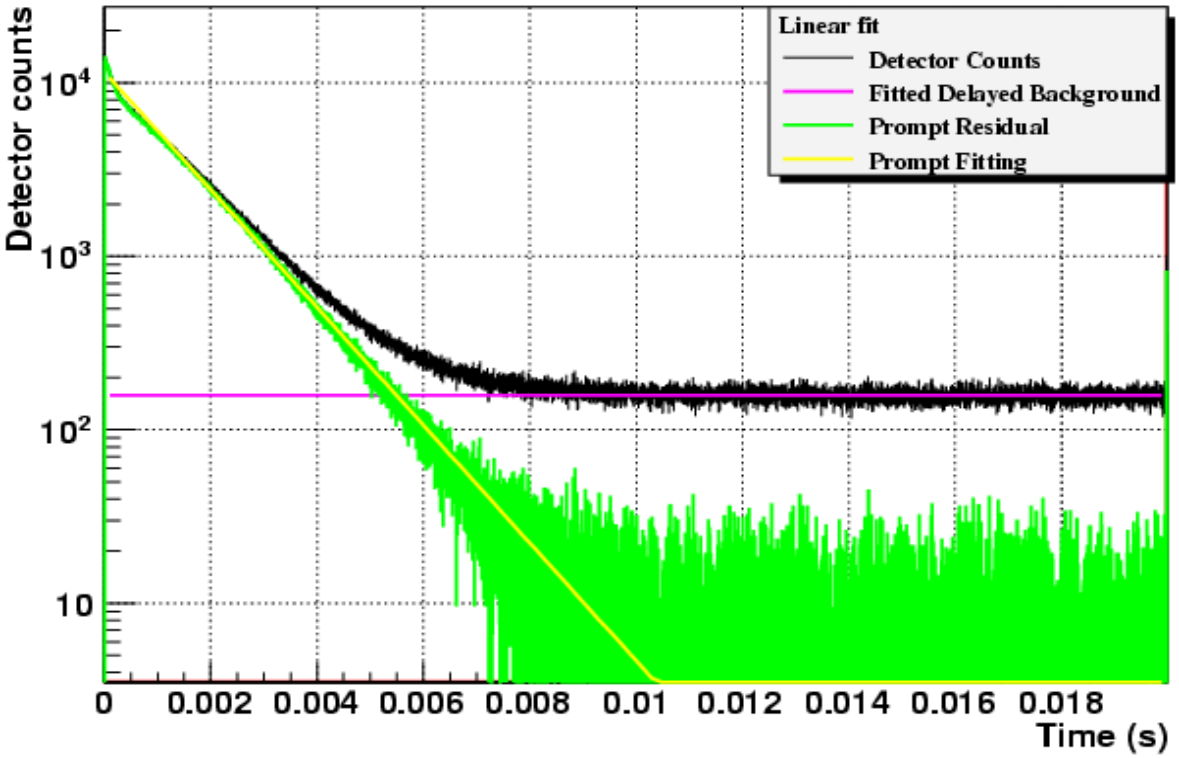

Figure 102. Linear fit of the pulsed neutron experiment recorded by small He-3 detector in EC5T channel of YALINA configuration with 36% enriched fuel in the fast zone and 1141 EK-10 fuel rods in the thermal zone

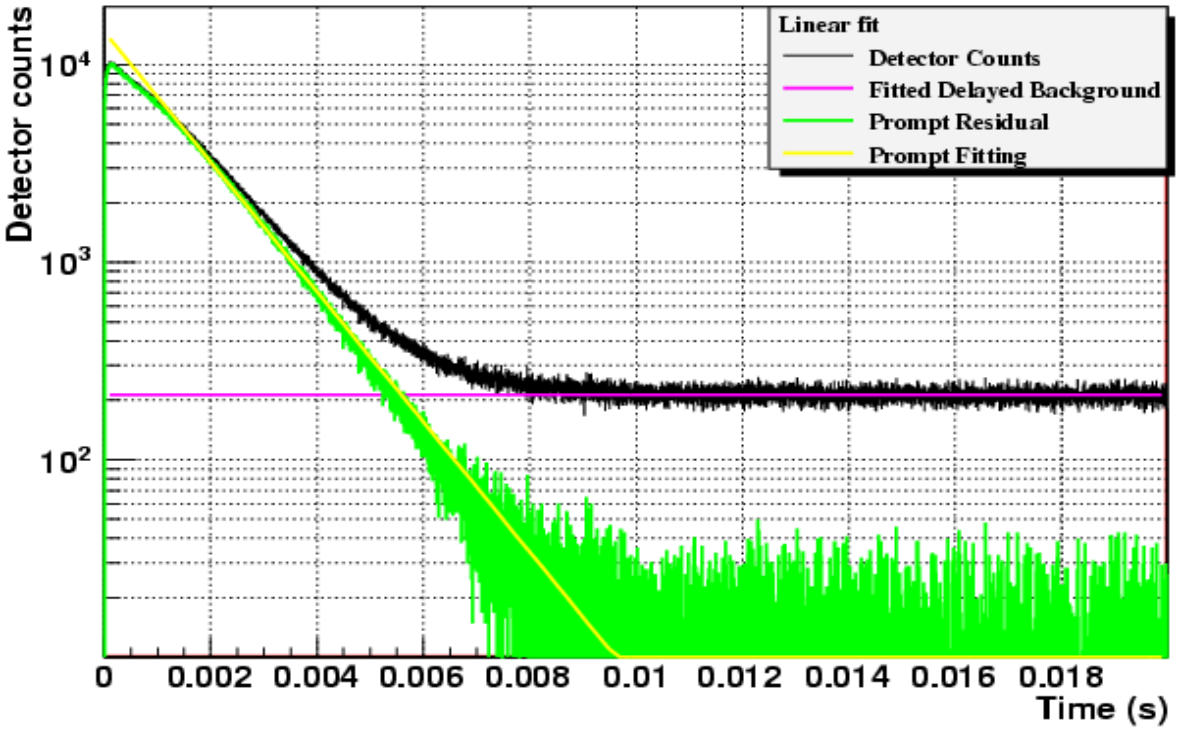

Figure 103. Linear fit of the pulsed neutron experiment recorded by small He-3 detector in EC6T channel of YALINA configuration with 36% enriched fuel in the fast zone and 1141 EK-10 fuel rods in the thermal zone

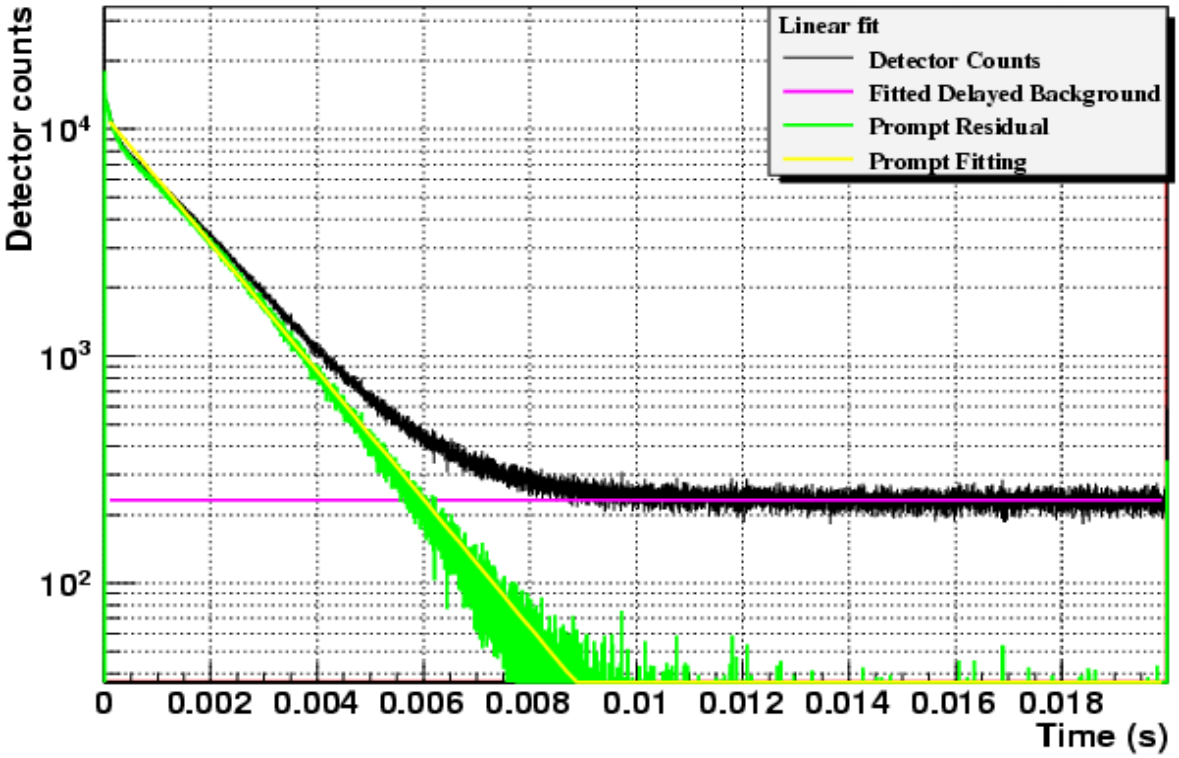

Figure 104. Linear fit of the pulsed neutron experiment recorded by small He-3 detector in EC5T channel of YALINA configuration with 36% enriched fuel in the fast zone and 1177 EK-10 fuel rods in the thermal zone

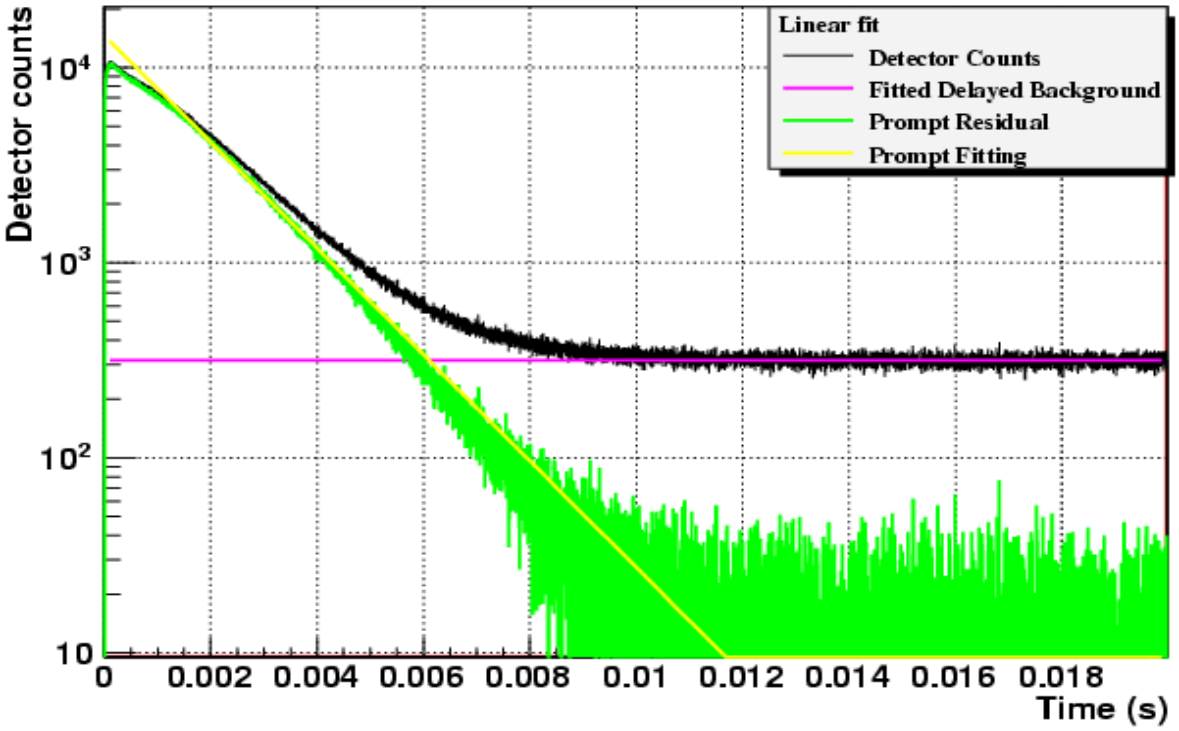

Figure 105. Linear fit of the pulsed neutron experiment recorded by small He-3 detector in EC6T channel of YALINA configuration with 36% enriched fuel in the fast zone and 1177 EK-10 fuel rods in the thermal zone

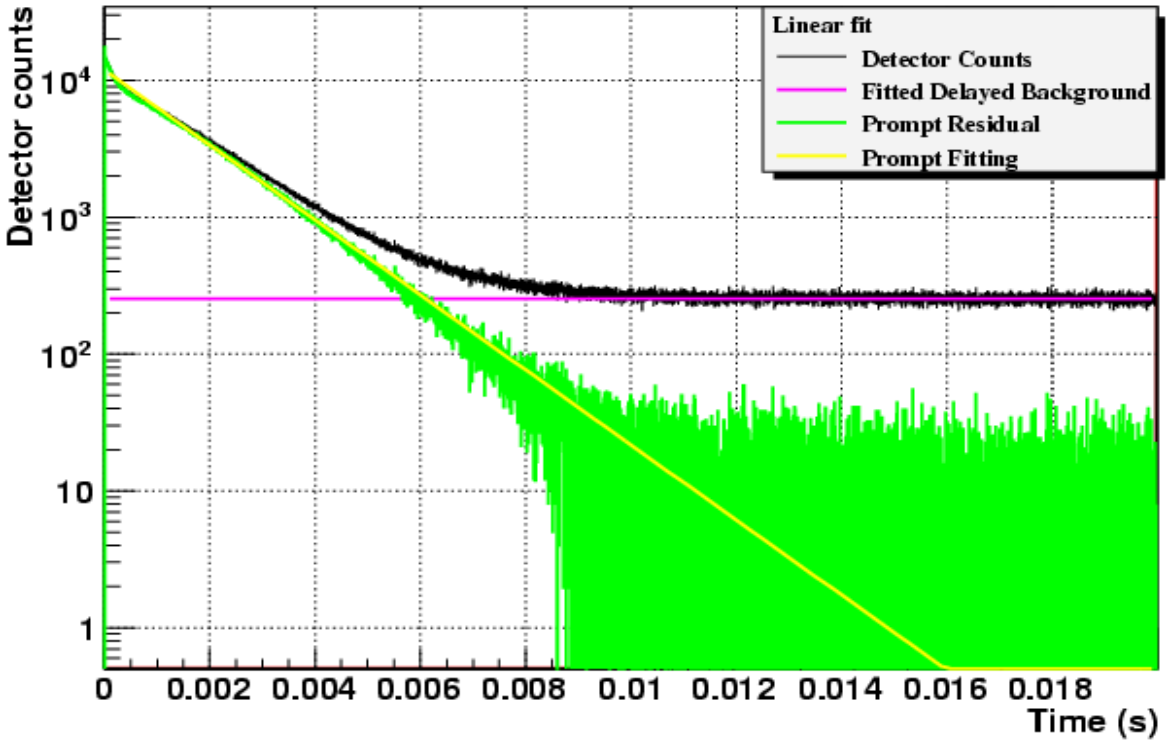

Figure 106. Linear fit of the pulsed neutron experiment recorded by small He-3 detector in EC5T channel of YALINA configuration with 36% enriched fuel in the fast zone and 1185 EK-10 fuel rods in the thermal zone

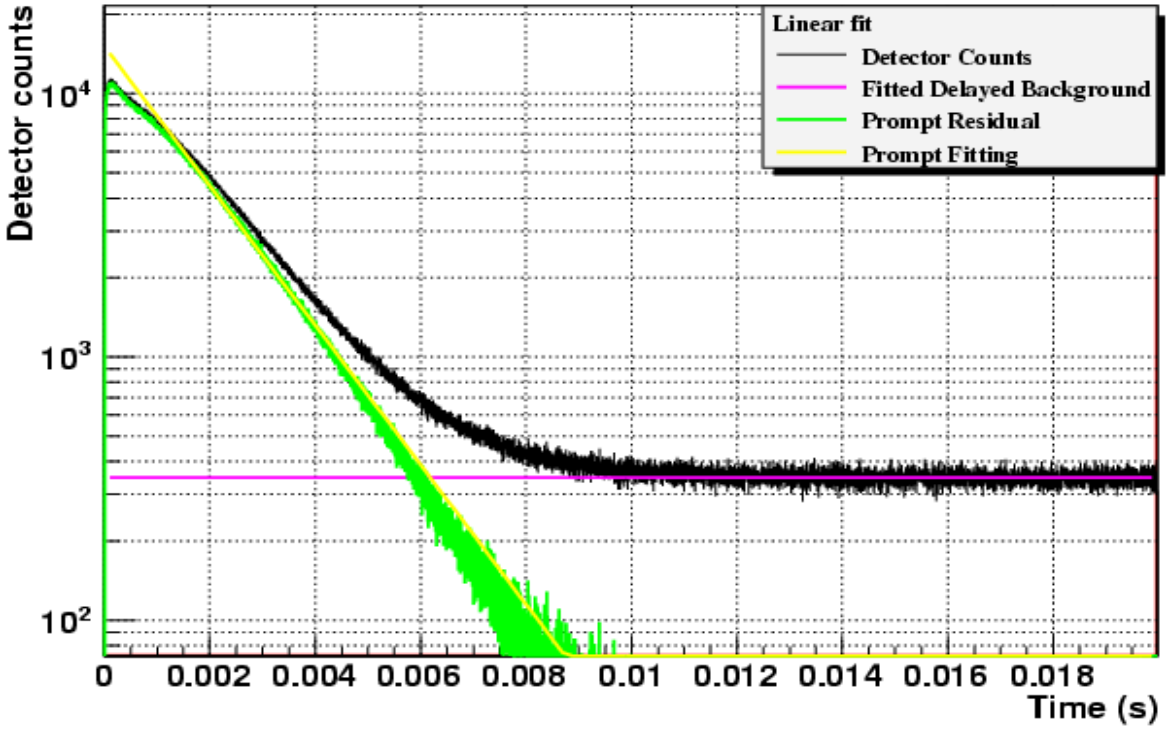

Figure 107. Linear fit of the pulsed neutron experiment recorded by small He-3 detector in EC6T channel of YALINA configuration with 36% enriched fuel in the fast zone and 1185 EK-10 fuel rods in the thermal zone

Nuclear Engineering Division
Argonne National Laboratory
9700 South Cass Avenue
Argonne, IL 60439

www.anl.gov

A U.S. Department of Energy laboratory
managed by UChicago Argonne, LLC